A STUDY OF MUONLESS EVENTS AND AN ATTEMPT TO IMPROVE THE HIERARCHY SENSITIVITY THROUGH NEURAL NETWORKS AT ICAL@INO

By

Ali Ajmi

Enrollment number: PHYS01201204001

Bhabha Atomic Research Centre, Mumbai.

A thesis submitted to the
Board of Studies in Physical Sciences

In partial fulfillment of the requirements

For the Degree of

DOCTOR OF PHILOSOPHY

of

HOMI BHABHA NATIONAL INSTITUTE

April 2016

Homi Bhabha National Institute

Recommendations of the Viva Voce Board

As members of the Viva Voce Board, we recommend that the dissertation prepared by **Ali Ajmi** entitled **"A study of muonless events and an attempt to improve the hierarchy sensitivity through neural networks at ICAL@INO"** may be accepted as fulfilling the dissertation requirement for the Degree of Doctor of Philosophy.

---------- **Date :**
Chairman : Prof. V M Datar

---------- **Date :**
Guide : Prof. S. Uma Sankar

---------- **Date :**
Member : Prof. Gobinda Majumder

---------- **Date :**
Member : Prof. Amol Dighe

---------- **Date :**
Member : Prof. Lalit Pant

---------- **Date :**
External Examiner :

Final approval and acceptance of this dissertation is contingent upon the candidate's submission of the final copies of the dissertation to HBNI.

I hereby certify that I have read this dissertation prepared under my direction and recommend that it may be accepted as fulfilling the dissertation requirement.

---------- **Date :**
Guide : Prof. S. Uma Sankar

STATEMENT BY AUTHOR

This dissertation has been submitted in partial fulfillment of requirements for an advanced degree at Homi Bhabha National Institute (HBNI) and is deposited in the library to be made available to borrowers under rules of the HBNI.

Brief quotations from this dissertation are allowable without special permission, provided that accurate acknowledgement of source is made. Requests for permission for extended quotation from or reproduction of this manuscript in whole or in part may be granted by the Competent Authority of HBNI when in his or her judgment the proposed use of the material is in the interests of scholarship. In all other instances, however, permission must be obtained from the author.

Ali Ajmi

DECLARATION

I, hereby declare that the investigation presented in the thesis has been carried out by me. The work is original and the work has not been submitted earlier as a whole or in part for a degree/diploma at this or any other Institution or University.

Ali Ajmi

ACKNOWLEDGEMENTS

I'm truly grateful to Prof. S. Uma Sankar, for not only being my PhD supervisor, but also the best guide and advisor, that a student can ever wish for. I must thank Prof. Gobinda Majumder for guiding me in the work on GENIE.

I thank Prof. Indumathi for invaluable suggestions during the progress of the work on muonless events. I thank Lakshmi S. Mohan for the useful discussions involving her work on separating ν_μCC events from the NC events. I thank Tarak Thakore for numerous discussions on Nuance and calculations of mass hierarchy χ^2. I thank Prof. Amol Dighe for several worthy discussions on the mass hierarchy contribution of the muonless events and the muon-containing events. I also thank Kolahal Bhattacharya for very helpful discussions.

I express my deep gratitude to Prof. Naba Mondal, Prof. Acharya, Prof. Sudeshna Bannerjee, Prof. Vivek Datar, Prof. Lalit Pant, Dr. Satyanarayana, Prof. Nita Sinha, Prof. Sandhya Choubey, Prof. Jasbinder Singh, Prof. Poonam Mehta, Prof. Naimuddin and all the co-members of the INO Collaboration. I specially thank Mr. P. Nagaraj and Mr. Pavan Vengala for ensuring the unfailing support of the computing facilities consistently. I thank Ravindra Shinde, Santosh Chawan and Vishal Gadholkar, for often enlightening me with the details of the ICAL electronics, efficient making of RPC units and various laboratory hands-on respectively. I also thank the Department of Atomic Energy (DAE) and the Department of Science and Technology, Government of India, for financial support.

I'm also fortunate to have cherished the good company of my fellow students and friends. Thank you, Mathimalar, Varchaswi, Nitali, Moonmoon, Neha D., Anushree, Raveendra, Rajesh, Sudeshna, Aman, Manas, Nizam, Apoorva, Neha, Abhijit, Suryanarayan, Pethuraj, and certainly thank you Abhik and Deepak.

Last but not the least, I owe it all to my parents, and thanking them will never be enough.

Contents

List of Figures

List of Tables

SYNOPSIS

Introduction

The INO is an upcoming experiment and my work involves simulations and their analysis to determine physics possibilities of the Iron CALorimeter detector. The ICAL aims to study the atmospheric neutrino interactions. The events at ICAL can be broadly classified into two types: the muon track containing events and the events with no muon tracks. The former basically refers to the vertical high energy ν_μ charged current (CC) interactions. The latter comprises of the neutrino neutral current (NC) interactions of all types, ν_eCC interactions and some ν_τCC interactions, and are referred as *muonless* events.

The thesis is based on the following topics: They are

1. *"Study of Muonless Events at ICAL"*. This in turn comprises of three subsections:
    - Obtaining an events sample rich in atmospheric ν_eCC events.
    - Their contribution to the determination of ν-mass hierarchy.
    - Estimating the Energy and Direction of the incident neutrinos in such muonless events.
2. Inclusion of GENIE as ν-Event Generator for INO
3. Improving the mass hierarchy determination using adaptive neural network for event selection.

Project I: Muonless Events at ICAL

The primary physics signal events in the ICAL at INO are the ν_μ charged current (CC) interactions with a well defined muon track. Apart from these events, the Iron Calorimeter can also detect other types of neutrino interactions, i.e. the electron neutrino charged

current interactions and the neutral current (NC) events. These interactions do not give clear muon tracks like the ν_μCC events. The low energy and horizontal ν_μCC events also do not give muon tracks. Therefore, apart from the muon track containing events, we should also focus on these "muonless" events, in order to extract maximum possible information from the ICAL detector.

We generated neutrino events by the Nuance neutrino generator [1], equivalent to 500 years of exposure. We then simulated these events using the ICAL detector geometry in GEANT4 [2].

Obtaining a ν_eCC rich events sample

It is possible to have a dataset containing mostly ν_eCC events, by imposing appropriate selection cuts on the events. The low- energy/horizontal ν_μCC events and the neutral current events (all 3 flavors) form the background to these events. The ν_τCC events (comprising a very small fraction of the total sample $\sim$0.5%) are also included.

We devised several selection criteria based on the hits ($\sim$#signals detected in an event) and layers. [The number of *hits* can be roughly interpreted as the number of signals in an event. The *layers* refer to the number of layers with one or more hits in an event.] The muon track containing events are mostly eliminated by choosing events confined to 5 layers. A lower threshold on the number of hits reject a significant fraction of the NC events as well as the low energy ν_μCC events.

Selection Criteria	**Total #events**	**#ν_eCC events**	**ν_eCC Purity**
hits>10	1006046	202838	20%
hits>10; layers$\leq$5	353874	163807	46%

Table 1: Event counts after the elementary selection cuts on the Geant output for the NH 500 years data in E_ν={0.1,100} GeV.

Additional selection cuts have been developed with the underlying logic that electrons/positrons produced give rise to electromagnetic showers. A few of them are mentioned here as follows:

- Most of the electrons/positrons are absorbed by thick iron layers. If the shower starts at the top/bottom of the iron layer, a sudden increment in number of hits in the following layer is expected. We look for sudden increase in the number of hits in the consecutive layer (calling it "max. hits difference").

- Based on the EM shower concept and the presence of iron layers, we seek for some pattern in the number of hits in adjacent layers . We select events with the majority of hits confined in one of the layers.

- The hits in different layers of ν_eCC events are non-uniform. The hits are mostly over concentrated in some layers, while entirely sparse in the rest (owing to the EM shower nature). This is reflected in a layerwise hits distribution. We put cuts on the parameters of the layerwise hits distribution in a ν-event. This exploits the fact that ν_μCC events have larger tails and the NC events have broader distributions than the ν_eCC events.

These criteria in combination with the elementary cuts (e.g. in Table 1) improve the ν_eCC purity in the selected sample. Effects of a few selection criteria are listed in Table 2. Each selection category accomodates a number of cuts in the parameters to obtain significant ν_eCC purity in each case [3]. One such example from each of the selection category is mentioned in Table 2.

It has also been noted that, with an increase in purity of the sample, the sample-size decreases, and so does the fraction of vertical events. So, an optimization is required between the purity and the sample size, depending on the physics we would like to extract.

Depending on the constraints used, one can obtain a neutrino data sample with the purity of ν_e events varying between 53% to 68% with 300 to 15 events per year respectively. Thus, with appropriate combinations of such cuts we can select an event sample of ν_eCC purity of $\sim 60\%$ in a sample size of ~ 100 events per year.

Application of the upper layer cut of 5 ensures that the information available from these muonless events is independent from that in the conventional analysis of ν_μCC

Selection Criteria	**Selected Sample size**	**ν_eCC Content**	**ν_eCC Purity**	**ν_eCC Net Selection Efficiency**
Maximum Hits diff.	156,000	82500	53%	50%
Overall Pattern: hits in layers	189,000	99814	56%	61%
Comparison: hits in layers	43,000	26006	60%	16%
Single layer hits	6,500	4420	68%	3%

Table 2: Examples of one of the cuts from each type of selection criteria on 500 years of NH data: Purity = ratio of ν_eCC content to selected sample size; Net Selection Efficiency = ratio of ν_eCC content in the selected sample to the same in the primary dataset i.e. with hits>10.

events. Events beyond this 5-layer range comprise mostly of ν_μCC events, with just 10% background due to the muonless events.

Contribution to the ν-mass hierarchy

The signature of matter efects are retained by the ν_eCC events in an ν_e-rich sample of these muonless events. The effect of muonless events in the mass hierarchy determination is also studied, with the hope of improving the hierarchy sensitivity of ICAL, even marginally. The neutrino oscillations have been applied using the normal and the inverted mass hierarchy parameters, which are denoted as NH and IH respectively. We used fixed oscillation parameters, and are as follows: $\Delta {m_{21}}^2 = 7.5 \times 10^{-5}$ eV^2, $\Delta {m_{31}}^2(NH) = 2.51 \times 10^{-3}$ eV^2, $\Delta {m_{31}}^2(IH) = -2.43 \times 10^{-3}$ eV^2, $\sin^2\theta_{12} = 0.31$, $\sin^2 2\theta_{13} = 0.09$, $\sin^2\theta_{23} = 0.5$ and $\delta_{CP} = 0$.

The data for NH is generated with three different seeds and similarly for IH. Calculating $\chi^2_{\text{true}} = \chi^2(NH1 - NH2)$, which will be approximately twice the number of bins, and $\chi^2_{\text{false}} = \chi^2(IH - NH)$, the average χ^2 is obtained as $< \Delta\chi^2 > = < \chi^2_{false} > - < \chi^2_{true} >$. This yields a value of 0.7. Considering the frequentist approach as described in [4], distributions of χ^2_{false} and χ^2_{true} calculated with 10 years of NH data and IH data are also observed (assuming NH ordering to be true). However, the statistical fluctuations are

too large to make any conclusive statement.

Apart from using the Nuance-oscillated sets, we generated the data without oscillation, and produced oscillated events sets for NH and IH using acceptance-rejection method. This ensures reduction in the effect of Monte Carlo fluctuations in the pair of datasets. For an ideal detector, the value of $< \Delta\chi^2 >$ saturates around 50 in 10 years. We found that in the ICAL detector, the contribution of these muonless events to the determination of ν-mass hierarchy is $\sim$1. The results stated donot include marginalisation of the neutrino oscillation parameters or the systematic errors.

Energy and Direction Estimation of the neutrinos in the muonless events

The NC events have an outgoing ν, that carries away a significant fraction of incident E_ν. The ν_eCC and the shower-like ν_μCC events also give no scope of "track-reconstruction". So, this project provides a solution to estimate the incident values of E_ν from the observable characteristics of such events.

A combination of *layers* and the *average hits per layer* gives a measure of the energy of the event. There is a direct correlation between the neutrino energy and the average hits per layer, when looked at events with particular number of layers hit. The energy distributions for different bins of these events are studied and the Landau distribution function is found to provide a good fit. The parameters of the fit can be associated to the energy of the neutrino. Calibration charts have been prepared to give an estimation of the energy of the incident neutrino in an NC event, ν_eCC event or the ν_μCC event, with an error $^{+150\%}_{-30\%}$. So, given the detector observables of an event, *i.e.* the number of *hits* and *layers*, we can tell the probable energy value of the incident neutrino for any of the three types of the muonless events.

Two kinematic variables based on the hit distribution are also defined and are used to determine the cosine of the polar angle of the neutrino direction ($\cos\theta$). The maximum horizontal spread of an event and a parameter called "MRatio" (derived from the layer-wise hits distribution) show significant correlation with the verticality and the up-down

direction of the incident neutrino respectively. Hence, an approximate estimation of the direction of the incident neutrino can also be obtained. We prepared a reference chart in 3-dimensions to estimate the possible $\cos\theta$ of the incident neutrino, by just observing the hit distribution of the muonless event in the detector.

Applying cuts on the MRatio, we can also select muonless samples rich in up-going ν's with $\sim$70% purity, and 25% efficiency. Cuts on the *maximum horizontal spread* can lead us to obtain a muonless sample rich in vertical ($\lesssim 65^o$) ν's to $\gtrsim$80% purity and 12% efficiency.

Project II: Inclusion of GENIE as ν-Event Generator for INO

This project primarily aimed at making an INO-user friendly version of the GENIE [5]. However, a number of significant and advantageous options have also been introduced in this process.

GENIE makes use of the ν-flux information in E_ν and $\cos\theta$ bins (*2D*). INO flux tables by HONDA show ϕ dependence also [6]. ICAL makes an angle $\sim 35^\circ$ w.r.t the geographical east direction. Therefore, GENIE@INO should include all such directional informations (*3D*). So, the GENIE source code is modified and a third option called FLUKA3D has been introduced. The 3D flux has been made easily accessible in GENIE, and hence makes us capable to modify the source code to accomodate any kind of flux-file formats in GENIE.

ICAL@INO is sensitive to ν's with energies greater than 0.5 GeV. Mass hierarchy discovery potential is large for events with energy of a few GeV. However, the flux at these energies is rather low. So, optional provision has been created for weighted atmospheric neutrino generation, which generates a larger number of events at higher energies.

GENIE gives the output in a standard inamicable ".root" format. It has provisions to convert to customized formats used by a few experiments, but INO requires its own format. So, a new option is made to get the GENIE output in an exclusive root format

for INO, which can be directly used for simulations.

So far, GENIE has been used to generate a fixed number of ν interactions. There was no effective provision to generate the atmospheric ν events for a certain exposure time. This provision has now been introduced. We can now generate the ν-interaction data for any length of exposure to the atmospheric neutrinos, using any detector geometry.

So, we have introduced the following 4 new options in the GENIE neutrino event generation, which are available at the GENIE@INO version:

- *FLUKA3D*: To include the 3D atmospheric neutrino flux information
- *-w <energy-weight>*: Option for weighted atmospheric event generation
- *nu_INOGEN_rootracker*: Command to get exclusive INO-customised output
- *-e <No. of years>*: To generate events for a desired exposure time of the detector.

Project III: Improving the neutrino mass hierarchy determination using neutral network

Studies of the hierarchy determination done so far in INO have been using generator level information. The detector simulations are used only to obtain the look up tables used for smearing the generator level event numbers [7, 8]. So, we now utilize complete detector simulation and reconstruction [9] to determine the expected results from the ICAL. We consider 500 years of ICAL data, generated by NUANCE in the energy range E_ν= {0.1,100}GeV, for all types of interactions (CC and NC) of all 3 neutrino flavours (ν_e, $\bar{\nu}_e$, ν_μ, $\bar{\nu}_\mu$, ν_τ, $\bar{\nu}_\tau$), followed by GEANT4 simulations. We use 5 different sets: 1 NOOSC (without oscillation), 3 NH with different seeds and 1 IH dataset. The oscillation parameters used are mentioned in chapter 6.

The signature for the neutrino mass hierarchy comes mostly from the high energy vertical neutrinos ("signal events"). An initial layer cut rules out most of the non-ν_μCC

background. The low energy and horizontal ν_μCC events still form a large fraction of the retained data sample. They result in adding spurious contribution to $\Delta\chi^2$. We employ methods of multi-variate analysis to select the signal events. We finally choose to use the adaptive neural network present in the ROOT, after optimisation of various methods and parameters.

This requires effective characterization of input variables for telling apart the signal from the background. We primarily define our signal events to be the ν_μCC events with $E_\nu > 4$ GeV and $|\cos\theta| > 0.5$, for the aid of choosing our selection parameters. After a thorough study of several variables, we choose the following observables.

- *Hits* or/and *layers* distinguish the low energy from the high energy range ν events.
- The *maximum horizontal spread* of the event distinguishes the horizontal high energy events from the rest.
- The high energy vertical ν_μCC events contain significantly larger number of *singlets* than the low energy or horizontal events. "Singlets" is the number of layers in an event with just one or single hit.
- A set of three consecutive layers in an event with a single hit is referred to as a *triplet*. A muon track containing event is expected to contain more triplets than a horizontal ν_μCC event.

Neural network analysis is employed with these parameters as inputs, to separate the signal events from all other events with good efficiency and good purity. The NOOSC set is used for the training of the neural network. The 3 NH and the 1 IH dataset are used for the analysis by applying the trained neural network on them. The trained neural network assigns a value or probability (0:bkg. $\longrightarrow$ 1:signal) to each of these events. The effect of the neural network application on one of the dataset is shown as follows. The signal and background event numbers of the NH dataset with seed 1 are listed in Table 3. The effect of application of the neural network is shown in Table 4.

Total signal events	Total bkg. events
$\sim 1.2\times10^5$	$\sim 6.3\times10^5$

Table 3: Signal and background events in 500 years of NH dataset (generated with seed 1) in E_ν={0.1,100} GeV, with the preliminary cut of Layers>5.

Probability >	**0.55**	**0.6**	**0.65**	**0.7**
#**signal-evts**	78880	74926	71202	67294
#**bkg-evts**	34196	27510	22010	17493
Efficiency %	66	62	59	56
Purity %	70	73	76	79

Table 4: Effect of the neural network probability cuts on the signal and background events of the NH dataset (generated with seed 1).

Putting a cut on the probability, we obtain a signal rich sample with optimum signal selection efficiency and signal purity. These selected events are binned in the reconstructed E_μ and $\cos\theta_\mu$ [10]. The $\Delta\chi^2$ is then calculated by a method similar to the one mentioned in Project I. We find that a binning scheme with different binwidths (optimized) extracts significant hierarchy information from the events.

Some hierarchy discrimination is present in the events with lower energy and smaller $|\cos\theta_\nu|$ than that of our initially defined "signal". So, we optimize over the definition of the "signal" events, so as to include all possible matter effects present in the data. We find that ν_μCC events with $E_\nu > 2$ GeV and $|\cos\theta| > 0.2$ give the highest hierarchy sensitivity. The hierarchy sensitivity, calculated from these selected events, reaches a 3σ level, with a $\Delta\chi^2$ of 9. The marginalisation and systematic errors are not included in this value.

This project aimed at the determination of the effective selection parameters, and the preliminary estimation of how the application of neural network will improve the mass hierarchy sensitivity of the ICAL detector. The effect of marginalisation of the neutrino oscillation parameters on the neural network selected sample has been checked as follows. We considered the events sample without oscillation and then subjected them to oscillation followed by accept-reject method [11] to produce the NH and IH sets of

data. The neutrino parameters for this calculations are chosen to be the same those in the INO white paper [11]. We chose $\sin^2\theta_{13} = 0.022$ ($\pm$ 5.3%), $\sin^2\theta_{23} = 0.5$ ($\pm$ 8.7%) and $|\Delta m^2_{eff}| = 2.47 \times 10^{-3}$ ($\pm$ 2.0%) eV^2. For fixed values of parameters, we obtain a $\Delta\chi^2$ of 10. We have chosen a thousand random sets of values for $\sin^2\theta_{13}$, $\sin^2\theta_{23}$ and $|\Delta m^2_{eff}|$ within their $\pm 3\sigma$ ranges to study the effect of marginalization. In computing the marginalized $\Delta\chi^2$ we have added the priors for each of the neutrino parameters. Marginalization has negligible effect on $\Delta\chi^2$, lowering it from 10 to 9, which becomes 10 again on addition of the prior. Inclusion of the errors due to systematic uncertainties reduces the $\Delta\chi^2$ from 10 to 8, but becomes 9.5 on addition of the prior.

Conclusion

The events containing muon tracks as well as the muonless events both comprise important sets of data available from the ICAL detector.

The muonless events can be processed to obtain a data sample rich in ν_eCC interactions. With the application of appropriate selection criteria of different types, the purity of the ν_eCC sample can vary from 56% (with a selection efficiency of 60%) to 68% (with a selection efficiency of 3%). The sample size and the fraction of vertical events decrease with increase in the purity of the sample. Therefore, the different selection criteria devised can be used to extract a ν_eCC events sample in accordance to one's priority/requirement of a better purity, a larger sample size, or a larger fraction of ν_eCC events in the vertical cone. The contribution of the muonless events to determining mass hierarchy has been found to be $\sim$1 in 10 years. We also produced calibration charts to estimate the energy and direction of the incident neutrinos in the ν_eCC interactions, the NC interactions or the low energy/horizontal ν_μCC events, i.e. all three types of the muonless events. This will aid an observer to tell the probable energy and direction of the neutrino seen at the ICAL, even though it contains no track.

The neutrino event generator is a vital component in the simulation studies of a

neutrino experiment. So far, Nuance has been used to generate neutrino interactions for INO simulations. However, Nuance being no more updated, INO has chosen to adopt GENIE as the neutrino event generator. This required us not only to make an INO-user friendly version of GENIE, but also led us to include four new options in the GENIE code, three of which may also be used for any other atmospheric neutrino experiments.

The events containing muon track are the primary signal events of ICAL. Major contribution to determining the neutrino mass hierarchy comes from these events. We employed the technique of neural network analysis to improve the hierarchy sensitivity of the ICAL. This not only gave us the ability to effectively choose ν_μCC events in the energy range >2 GeV in the vertical cone but also led to obtaining a 3σ hierarchy sensitivity, i.e. $\Delta\chi^2$ of 10 in 10 years at ICAL. This value reduces to 9.5, on including the marginalisation and the systematic uncertainties.

List of Publications:

Published Papers:

- **Muonless Events in ICAL @ INO**
  by Ali Ajmi and S. Uma Sankar: Published in JINST 10 (2015) 04, P04006, arXiv:1501.03252.

Other Papers:

- **Energy and Direction of neutrinos in muonless events at ICAL**
  by Ali Ajmi and S. Uma Sankar: arXiv:1505.07295.
- **Improving the hierarchy sensitivity of ICAL using neural network**
  by Ali Ajmi, Abhish Dev, Mohd. Nizam, Nitish Nayak, S.Uma Sankar: arXiv:1510.02350.

National and International Conference Presentations :

1. Oral Presentation on **Energy and Direction Estimation of neutrinos in muonless events at ICAL** by Ali Ajmi and S. Uma Sankar: Proceedings published in *Springer Proceedings in Physics, XXI DAE-BRNS High Energy Physics Symposium Proceedings, Guwahati, India, December 8 – 12, 2014 Editors: Bhuyan, Bipul (Ed.).*
2. Poster Presentation on **Inclusion of GENIE as ν-Event Generator for INO** by Ali Ajmi and Gobinda Majumder @ XXI DAE-BRNS High Energy Physics Symposium, Guwahati, India, December 8 – 12, 2014.
3. Poster Presentation on **Muonless Events in ICAL @ INO** by Ali Ajmi and S. Uma Sankar @ EPS-HEP Conference Vienna, Austria, 22-29 July, 2015: Proceedings published *in PoS (Proceedings of Science) EPS-HEP2015 (2015) 045, SISSA (2015-10-04).*

4. Oral Presentation on **Study of Muonless Events in ICAL @ INO** by Ali Ajmi and S. Uma Sankar @ NSPDI-15, IICHEP, Madurai, India, 27-31 March, 2015.

5. Poster Presentation on **Muonless Events in ICAL @ INO** by Ali Ajmi and S. Uma Sankar @ NNN15, Stony Brook University, New York, 28-31 October 2015.

1 Introduction

In this chapter, we like to remind the reader of some fundamental properties of the neutrino, and the experimental endeavour made so far to newly unravel and establish our understandings of this ellusive particle. We discuss the different types of interactions, the oscillation phenomenon, and how the neutrinos from various sources led us to determining the different parameters of the neutrino oscillation, concluded by a glance at the ongoing experiments.

1.1 Neutrinos

Neutrino, the light, weakly-interacting neutral spin-half particle was proposed by Wolfgang Pauli in 1930 to explain the continuous energy spectrum of electrons in beta decays. Experimental evidence for it was obtained by Reines and Cowan in 1956 [12]. They discovered the existence of neutrino by observing the reactor anti-neutrinos causing the inverse beta decay reaction $p + \bar{\nu}_e \rightarrow n + e^+$.

Neutrinos (ν), the second-most abundant particles in the universe after the photon, are so far known to exist in three species (or flavours) called the electron neutrino (ν_e), the muon neutrino (ν_μ) and the tau neutrino (ν_τ), and their corresponding antiparticles.

1.2 Neutrino Interactions

Neutrinos are weakly interacting particles, i.e. they interact only via $W^{\pm}$ and Z^0 bosons. Interactions involving the exchange of a Z^0 boson are called neutral current interactions and those with the $W^{\pm}$ boson exchange are called charged current interactions. The masses of the $W^{\pm}$ and the Z^0 being quite large 80 GeV and 91 GeV respectively, compared to other intermediating particles like photons or gluons, the "weak interactions" have a very small probability of occurence [13].

1.2.1 Charged Current Interactions

Charged current interactions (CC) are mediated by the charged boson. In neutrino-nucleon scattering, neutrinos exchange charge with the nucleon and turn into charged leptons. Figure 1.1 shows Feynman diagrams of the CC elastic and CC 1-π production reaction for ν_μ. In an experiment, CC interactions can be distinguished from NC interactions by finding charged leptons in the final state.

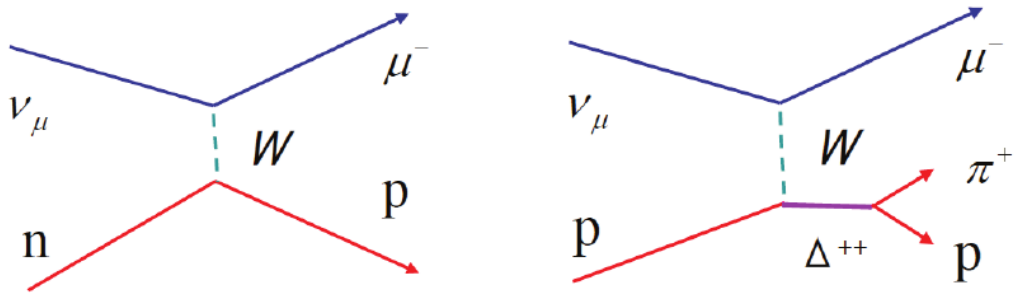

Figure 1.1: Feynman diagrams of CC quasi-elastic and CC 1-π production reaction for ν_μ [13].

1.2.2 Deep Inelastic Scattering

When a high energy neutrino interacts with the nucleons, the partons or the quarks interact too, to give rise to one or more hadrons as the product particles, apart from the lepton, as in figure 1.2. Interaction possibilities mediated by $W^{\pm}$ were known. The observation of absence of the charged lepton finally led to the possibility of the neutral current interactions [14, 15].

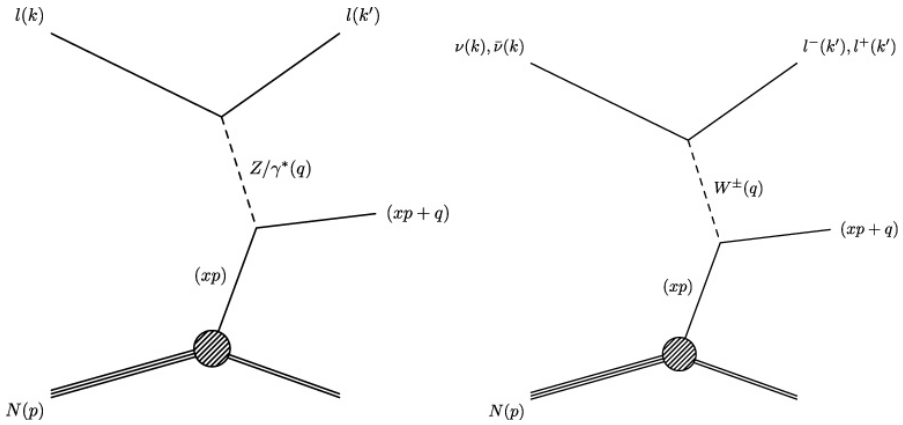

Figure 1.2: Feynman diagrams of Deep Inelastic Scattering of neutrinos [16].

1.2.3 Neutral Current Interactions

The existence of neutrino neutral current interaction (NC) was first observed in 1973 by the Gargamelle bubble chamber at CERN [17]. They observed NC deep-inelastic scattering $\nu + N \rightarrow \nu + X$. Later experiments also observed the electron elastic scattering $\nu + e^- \rightarrow \nu + e^-$ using ν_μ and $\bar{\nu}_\mu$ [18].

Unlike CC interactions, there is no charged lepton in final state. NC events have only hadrons or their decay particles in final state. Figure 1.3 shows Feynman diagrams of NC elastic and π^0 production via Δ^0 resonance [13].

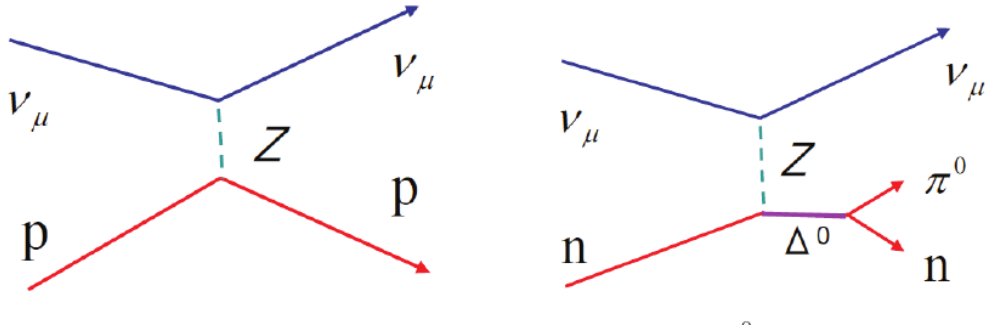

Figure 1.3: Feynman diagrams NC elastic and π^0 production via Δ^0 resonance [13].

1.3 Neutrino Mass and Oscillations

According to the Standard Model (SM), the masses of fermions result from the Higgs mechanism through the Yukawa coupling of the fermion fields with the Higgs doublet. In this regard, a fermion mass term must involve a coupling of the left-handed and the right-handed fields. So, the SM neutrinos are massless, because their fields do not have a right-handed component. However, if right handed neutrino field is introduced into the theory, it is possible for neutrinos to have mass through the Yukawa couplings to the Higgs doublet.

Nevertheless, neutrino experiments have firmly established the phenomenon of neutrino oscillations.

Neutrino oscillations is a phenomenon which occurs as a result of the mixing of neutrino flavour and mass states. The neutrinos can be looked upon as possessing two independent sets of eigenspaces: the mass eigenstates and the visible flavor or weak eigenstates (figure 1.4).

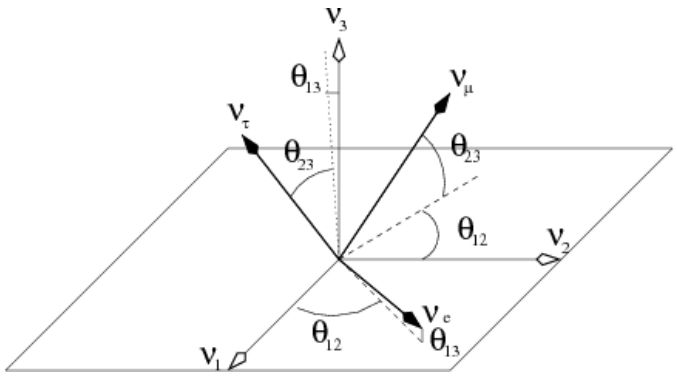

Figure 1.4: The three mixing angles that characterize the orientation of the flavor axes with respect to mass axes [19].

These two non-identical spaces are interrelated by the unitary mixing matrix U called the Pontecorvo-Maki-Nakagawa-Sakata matrix, U_{PMNS}, defined as follows.

$$\begin{bmatrix} \nu_e \\ \nu_\mu \\ \nu_\tau \end{bmatrix} = U_{PMNS} \begin{bmatrix} \nu_1 \\ \nu_2 \\ \nu_3 \end{bmatrix} \tag{1.1}$$

$$U_{PMNS} = \underbrace{\begin{bmatrix} 1 & 0 & 0 \\ 0 & c_{23} & s_{23} \\ 0 & -s_{23} & c_{23} \end{bmatrix}}_{Atmospheric(\theta_{23}\sim 45^\circ)} \underbrace{\begin{bmatrix} c_{13} & 0 & s_{13}e^{-i\delta_{CP}} \\ 0 & 1 & 0 \\ -s_{13}e^{i\delta_{CP}} & 0 & c_{13} \end{bmatrix}}_{Reactor(\theta_{13}\sim 9^\circ)} \underbrace{\begin{bmatrix} c_{12} & s_{12} & 0 \\ -s_{12} & c_{12} & 0 \\ 0 & 0 & 1 \end{bmatrix}}_{Solar(\theta_{12}\sim 33^\circ)} \tag{1.2}$$

where $c_{ij} = \cos\theta_{ij}$ and $s_{ij} = \sin\theta_{ij}$. Here, θ_{ij} refers to three mixing angles θ_{12}, θ_{13} and θ_{23}. δ_{CP} is the CP violating phase.

The mixing matrix of the 3-generations of the neutrinos is parametrized by 3 angles and 6 phases. As in Kobayashi-Maskawa mechanism [**?**], five of these phases can be pulled out and absorbed into fermion fields. They do not affect oscillation probabilities. Only the sixth imbedded phase δ_{CP} has a physical consequence and leads to CPV in

neutrino oscillation.

1.3.1 Oscillations In Vacuum

The theory of neutrino oscillations was first proposed by Pontecorvo, and the model of neutrino oscillations of the active flavors was built by Maki, Nakagawa and Sakata [20, 21]. We first discuss how this phenomenon of neutrino oscillation works in free space or in vacuum [22, 23].

As briefly stated above, the weak eigenstates or the flavor states are not pure mass eigenstates. As from eqn. 1.1, we can write,

$$|\nu_\alpha\rangle = \sum_i U_{\alpha i}|\nu_i\rangle. \tag{1.3}$$

The time evolution of the state is given by

$$|\nu_\alpha(t)\rangle = \sum_i U_{\alpha i} e^{-\mathrm{i}E_i t}|\nu_i\rangle, \tag{1.4}$$

where, E_i is the energy eigenvalue $E_i = \sqrt{p_i^2 + m_i^2}$, corresponding to the vacuum propagation hamiltonian H_0.

The amplitude of transition from one flavor state ν_α to ν_β is given by

$$A_{\nu_\alpha \to \nu_\beta}(t) = \langle \nu_\beta | \nu_\alpha(t)\rangle = \sum_i U_{\alpha i} U^*_{\beta i} e^{-\mathrm{i}E_i t}. \tag{1.5}$$

Hence the probability of oscillating from the flavour state ν_α to ν_β is

$$P_{\nu_\alpha \to \nu_\beta}(t) = |A_{\nu_\alpha \to \nu_\beta}(t)|^2 = \sum_{i,k} U_{\alpha i} U^*_{\beta i} U^*_{\alpha k} U_{\beta k} e^{-\mathrm{i}(E_i - E_k)t}. \tag{1.6}$$

Eqn. 1.6 is looked upon in two different ways: (i) if the flavour $\nu_\alpha = \nu_\beta$, then it is called the survival probability and (ii) if $\nu_\alpha \neq \nu_\beta$, then it is known as the oscillation probability.

Using the mixing matrix in eqn. 1.1, the oscillation probability can be written as follows

$$\begin{aligned} P_{\nu_\alpha \to \nu_\beta} = \delta_{\alpha\beta} \quad & -4 \sum_{i>k} Re\left[U_{\alpha i} U^*_{\beta i} U^*_{\alpha k} U_{\beta k}\right] \sin^2\left(\frac{\Delta m^2_{ik} L}{4E}\right) \\ & +2 \sum_{i>k} Im\left[U_{\alpha i} U^*_{\beta i} U^*_{\alpha k} U_{\beta k}\right] \sin\left(\frac{\Delta m^2_{ik} L}{2E}\right). \end{aligned} \tag{1.7}$$

Assuming CPT invariance, the oscillation probability expression for the anti-neutrinos is given by

$$\begin{aligned} P_{\bar{\nu}_\alpha \to \bar{\nu}_\beta} = \delta_{\alpha\beta} \quad & -4 \sum_{i>k} Re\left[U^*_{\alpha i} U_{\beta i} U_{\alpha k} U^*_{\beta k}\right] \sin^2\left(\frac{\Delta m^2_{ik} L}{4E}\right) \\ & +2 \sum_{i>k} Im\left[U^*_{\alpha i} U_{\beta i} U_{\alpha k} U^*_{\beta k}\right] \sin\left(\frac{\Delta m^2_{ik} L}{2E}\right). \end{aligned} \tag{1.8}$$

Transforming into natural units, we get

$$\frac{\Delta m^2_{ik} L}{4E} \approx 1.27 \Delta m^2_{ik}(eV^2) \frac{L(km)}{E(GeV)}. \tag{1.9}$$

The eqn.s 1.7 and 1.8 clearly show that the existence of neutrino oscillations must require non-zero and non-degenerate neutrino masses. Also, observing the oscillation phenomenon will fetch us only the neutrino mass squared difference, Δm^2_{ik}, and not the absolute neutrino mass, m_i. The eqn.s 1.7, 1.8 and 1.9 specify the sensitivity of an experiment, when it receives neutrinos with energy E (GeV) and of pathlength L (km) in the following vicinity of the neutrino mass squared difference:

$$\frac{\Delta m^2_{ik}(eV^2) L(km)}{E(GeV)} \simeq 1. \tag{1.10}$$

The real parts of eqn.s 1.7 and 1.8 are the CP invariant terms. But for the imaginary parts, the CP asymmetry can be read as:

$$P_{\nu_\alpha \to \nu_\beta} - P_{\bar{\nu}_\alpha \to \bar{\nu}_\beta} = 4 \sum_{i>k} Im[U^*_{\alpha i} U_{\beta i} U_{\alpha k} U^*_{\beta k}] \sin\left(\frac{\Delta m^2_{ik} L}{2E}\right). \tag{1.11}$$

To get an approximate picture of how the probability expressions look, we use one mass squared dominance (OMSD) approximation to simplify the above equations. The OMSD approximation is good enough for a reasonably large range of energies and baselines. Following eqn. 1.7, the probabilities $P_{\mu\mu}$ and $P_{\mu e}$ in vacuum are given by the following expressions [11, 24] .

$$\begin{aligned} P^{v}_{\mu\mu} = \; 1 \quad & - \sin^2\theta_{23}\sin^2 2\theta_{13}\sin^2\left(1.27\tfrac{\Delta m^2_{31}L}{E}\right) \\ & - \cos^4\theta_{13}\sin^2 2\theta_{23}\sin^2\left(1.27\tfrac{\Delta m^2_{31}L}{E}\right), \end{aligned} \tag{1.12}$$

$$P^{v}_{\mu e} = \sin^2\theta_{23}\sin^2 2\theta_{13}\sin^2\left(1.27\frac{\Delta m^2_{31}L}{E}\right). \tag{1.13}$$

1.3.2 Oscillations In Matter

When neutrinos propagate through matter, the probabilities can be modified significantly due to the so-called matter effect. The neutrinos undergo coherent forward scattering with the electrons, protons and neutrons, present in the matter [25]. The potential due to this scattering modifies the propagation hamiltonian term and hence affects the mixing of the neutrinos. Thus the oscillation probability gets modified in case of neutrinos propagating in matter compared to that in vacuum.

This phenomenon of altering the neutrino flavour while propagation in matter was formulated by Mikhaev, Smirnov and Wolfenstein (MSW) [26, 27]. The ν_es have both charged current and neutral current elastic scattering interactions with electrons. The ν_μ and the ν_τ have only neutral current interactions with electron.

So the Earth's matter potential must be considered due to the forward scattering amplitude of charged current ν_e interactions with electrons.

$$\nu_x + (e,p,n) \rightarrow \nu_x + (e,p,n) \;\; i.e.\; NC \;\; (x = e,\mu,\tau) \tag{1.14}$$

$$\nu_e + e^- \rightarrow \nu_e + e^- \quad i.e.\ CC\ and\ NC. \tag{1.15}$$

The additional CC interaction in eqn. 1.15 accounts for an extra potential V_{CC}. The potential V_{NC} due to the NC interactions is experienced by all three flavours. The effective potentials are,

$$V_{CC} = \sqrt{2} G_F n_e, \tag{1.16}$$

$$V_{NC} = -\frac{1}{\sqrt{2}} G_F n_n, \tag{1.17}$$

where n_e and n_n are the number densities of electrons and neutrons (or protons), respectively. G_F is the Fermi coupling constant. Therefore, the new hamiltonian is

$$H_m = H_0 + V_f \tag{1.18}$$

where V_f is

$$V_f = \begin{bmatrix} V_{CC} + V_{NC} & 0 & 0 \\ 0 & V_{NC} & 0 \\ 0 & 0 & V_{NC} \end{bmatrix}. \tag{1.19}$$

The matter Hamiltonian is diagonalized, and its normalized eigenvectors form the modified matter mixing matrix. We can thus compute the effective masses and mixing angles in matter. In OMSD approximation, the $(\Delta m^2_{31})^m$ and the $(\theta_{13})^m$ can be related to their vacuum equivalents as follows

$$(\Delta m^2_{31})^m = \sqrt{(\Delta m^2_{31} \cos 2\theta_{13} - A)^2 + (\Delta m^2_{31} \sin 2\theta_{13})^2}, \tag{1.20}$$

$$\sin 2\theta^m_{13} = \frac{\Delta m^2_{31} \sin 2\theta_{13}}{\sqrt{(\Delta m^2_{31} \cos 2\theta_{13} - A)^2 + (\Delta m^2_{31} \sin 2\theta_{13})^2}}. \tag{1.21}$$

where,

$$A = 2EV_{CC} = 0.76 \times 10^{-4} \rho(g/cc) E(GeV). \tag{1.22}$$

The probabilities $P_{\mu\mu}$ and $P_{\mu e}$ in matter are given by

$$\begin{aligned} P^m_{\mu\mu} = 1 \quad & -\cos^2\theta^m_{13}\sin^2 2\theta_{23} \quad \sin^2\left[1.27\left(\frac{\Delta m^2_{31} + A + \left(\Delta m^2_{31}\right)^m}{2}\right)\frac{L}{E}\right] \\ & -\sin^2\theta^m_{13}\sin^2 2\theta_{23} \quad \sin^2\left[1.27\left(\frac{\Delta m^2_{31} + A - \left(\Delta m^2_{31}\right)^m}{2}\right)\frac{L}{E}\right] \\ & -\sin^4\theta_{23}\sin^2 2\theta^m_{13} \quad \sin^2\left[1.27\left(\Delta m^2_{31}\right)^m\frac{L}{E}\right], \end{aligned} \tag{1.23}$$

$$P^m_{\mu e} = \sin^2\theta_{23}\sin^2\theta^m_{13}\sin^2\left[1.27\left(\Delta m^2_{31}\right)^m\frac{L}{E}\right]. \tag{1.24}$$

These expressions are insensitive to δ_{CP} as a consequence of OMSD. CP violations can be observed only in those experiments which are sensitive to oscillations driven by both Δm^2_{21} and Δm^2_{31}.

Taking negative sign for Δm^2_{31} gives the probabilities for the inverted neutrino mass hierarchy (to be discussed in section 1.4.3). Replacing $A \to -A$ in eqn. 1.23 and 1.24 gives the anti neutrino oscillation probabilities.

1.4 Neutrino Sources

The neutrinos come from a numerous different sources, both natural and artificial, with their energy varying over a wide range. The abundance of neutrinos can be estimated from the long list of its sources vs. the energy spectrum in figure 1.5.

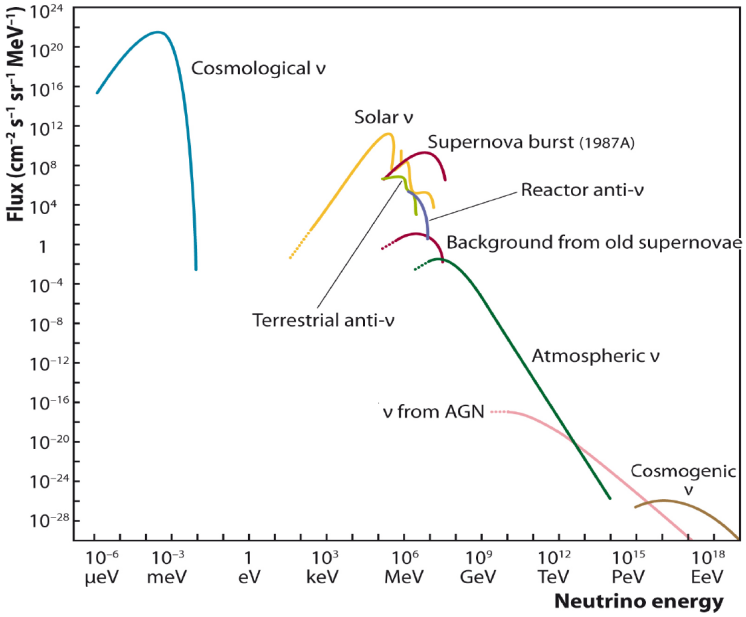

Figure 1.5: The neutrino energy spectrum from different sources [28].

The neutrinos in the energy range of μeV and meV are of cosmological origin, or the so-called "relic" neutrinos, having emanated from the big-bang nucleosynthesis [29]. The neutrinos from the sun [30], the supernovae, the nuclear reactors or the earth [31, 32] belong to the energy ranges of keV-MeV. The atmospheric neutrinos which are products of the cosmic ray interactions in the atmosphere cover the range of the MeV-TeVs. The neutrinos from the supernova remnants, Gamma Ray Bursts or Active Galactic Nuclei (AGN) or from interactions of ultra-energetic protons with the CMB [33] cover the higher ranges on the energy scale.

For energies less than TeV, neutrinos have very low cross section of interaction. Some of the sources being studied are discussed in the following subsections.

1.4.1 Solar Neutrinos

The sun is the most copious source of the electron neutrinos. The Standard Solar Model (SSM) predicts that most of the flux comes from the pp interaction neutrinos and the

CNO (Carbon Nitrogen Oxygen) cycle [34]. The underlying mechanism is basically the exothermal thermonuclear fusion reaction, shown below.

$$4p \rightarrow 4He + 2e^{+} + 2\nu_e. \tag{1.25}$$

There are other processes too as shown in figure 1.6. The electron neutrinos produced at the core of the sun and detected on earth serve as a direct telescope to observe the solar-core-phenomena.

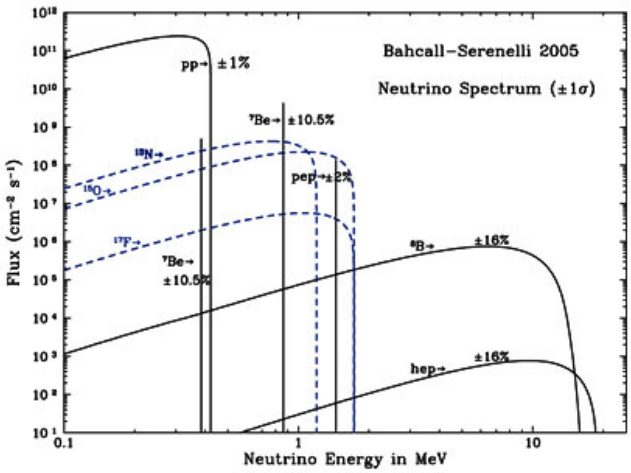

Figure 1.6: The various reaction channels for solar neutrinos [35].

Ray Davis' Homestake experiment [36] was the first to observe the solar neutrinos through the Chlorine-Argon interaction.

$$\nu_e + {}^{37}Cl \rightarrow {}^{37}Ar + e^{-}. \tag{1.26}$$

However, they saw only one-third of the solar ν_es predicted by the SSM. This discrepancy was known as the Solar Neutrino Problem. They had no directional or energy information. The three gallium solar neutrino experiments: GALLEX/GNO [37, 38, 39]

and SAGE [40, 41] detected solar neutrinos through the following reaction,

$$\nu_e + {}^{71}Ga \rightarrow {}^{71}Ge + e^-. \tag{1.27}$$

Owing to the lower energy threshold solar neutrinos from all the sources of SSM were detected. The solar neutrino anomaly showed its persistence in all three of them. The Super-Kamiokande and SNO experiments provided important information about the solar neutrinos in the higher energy part.

The Super-Kamiokande [42] could reconstruct the approximate direction of the electron, and confirmed the above discrepancy in solar data.

The anomaly was finally settled, when SNO [43] detected the solar neutrinos in multiple neutrino interaction channels. SNO was able to detect neutrinos via three different interactions: ES (elastic scattering), CC and NC. The count of the neutral current interactions was the most important one to establish the neutrino oscillation from the ν_e to ν_μ/ν_τ flavor.

The solar neutrino experiments and the KamLAND [44] found the θ_{12} to be $\sim$33° and $|\Delta m^2_{21}| \sim 7.9\times10^{-5}\text{eV}^2$.[1]

1.4.2 Atmospheric Neutrinos

The atmosphere is perpetually exposed to a shower of cosmic rays. Primary cosmic rays are high energy particles arriving on the earth from galactic and extragalactic sources. These are composed of protons ($\sim$87%), alpha particles ($\sim$11%) and heavier nuclei ($\sim$2%). When cosmic rays enter the atmosphere, interactions with the nuclei in the air molecules produce secondary particles [45]. Mostly pions are produced, but kaons are also observed in the higher energy range. The energy spectrum follows the following power law:

$$N(E)dE \propto E^{-\gamma}dE, \tag{1.28}$$

[1] For the current updated/accepted values of the oscillation parameters with the uncertainties on their central values, please refer to table 1.1.

where $\gamma \simeq 2.7$ for sub-TeV range and 3 beyond it. The atmospheric neutrinos are created during the decay of the produced pions and kaons and the following muons during flight, as given by the following interactions,

$$\pi^{+(-)} \rightarrow \mu^{+(-)} + \bar{\nu}_\mu(\nu_\mu), \tag{1.29}$$

$$\mu^+(\mu^-) \rightarrow e^{+(-)} + \nu_e + \bar{\nu}_\mu(\nu_\mu). \tag{1.30}$$

Kaon also decays in a similar fashion and gives the two neutrino types, but their contribution to the atmospheric neutrino flux (in the range of $\sim$ few GeV) is small compared to the pions. Thus the fluxes of atmospheric ν_e and ν_μ are produced. Production of ν_τ requires mesons with heavier quark masses and hence their numbers are too small and can be neglected.

The neutrino fluxes on the earth's surface thus follows the ratio:

$$R = \frac{\Phi(\nu_\mu) + \Phi(\bar{\nu}_\mu)}{\Phi(\nu_e) + \Phi(\bar{\nu}_e)} \approx 2,$$

where Φ is the flux of neutrinos. The value of the ratio increases with energy, as muons at high energies reach the surface of the earth, before decaying.

The detector acceptance for electrons and muons being different, this ratio R cannot be directly measured. So, experiments quote this aspect in terms of the double-ratio R_0 defined as,

$$R_0 = \frac{(N_\mu/N_e)_{data}}{(N_\mu/N_e)_{expected}}$$

The flux normalisation uncertainties which is about 20% and the detector systematics can thus be done away with. R_0 will be unity if the experiment observes the same flavor composition as predicted. Thus, any deviation of this value from unity predicts the unknown neutrino interactions.

The atmospheric neutrino flux is symmetric about a given direction on the surface of

the Earth, that is

$$\Phi_\nu(E, \cos\theta) = \Phi_\nu(E, -\cos\theta)$$

where θ is the zenith angle. At energy ranges lower than 3 GeV, the geomagnetic effects result in deviations from this equality. At higher energies, any asymmetry in the fluxes of the upgoing and downgoing neutrinos is attributed to the neutrino oscillation. Large deviations at lower energies, are also caused by the neutrino oscillations. Hence, this up-down asymmetry is also an evidence of atmospheric neutrino oscillations.

The Irvine-Michigan-Brookhaven (IMB) [46, 47] and the Kamiokande [48, 49] observed this ratio R_0 in the atmospheric neutrinos to be less than one. They were water Cherenkov detectors, which initially aimed to study proton decay, but soon found their so-called "main background", the atmospheric neutrinos taking the front-dias. This *Atmospheric Neutrino Anomaly* thus invited several other atmospheric neutrino experiments. The iron calorimeters at NUSEX [50] and Frejus [51] could not see this anomaly, as they collected a very small data sample. However, Soudan2 [52, 53] which also used the iron tracking calorimeter, recorded the flavor ratio to be less than one. The Super Kamiokande [42] finally collected the data with a very large statistics with 92 kton-yr exposure, in about 2 yrs. The significant disappearance of the muon neutrinos at the Super-Kamiokande finally confirmed the existence of neutrino oscillations, $\nu_\mu \rightarrow \nu_\tau$ dominantly [54, 55]. The asymmetry in the zenith angle distributions were also noted by the Kamiokande, Soudan2 and the liquid scintillators at MACRO [56]. The allowed region of Δm^2 and $\sin^2 2\theta$ is shown in figure 1.7. Two long-baseline accelerator neutrino experiments, the K2K [57, 58] and the MINOS [59] also confirmed the results from the atmospheric neutrino experiments.

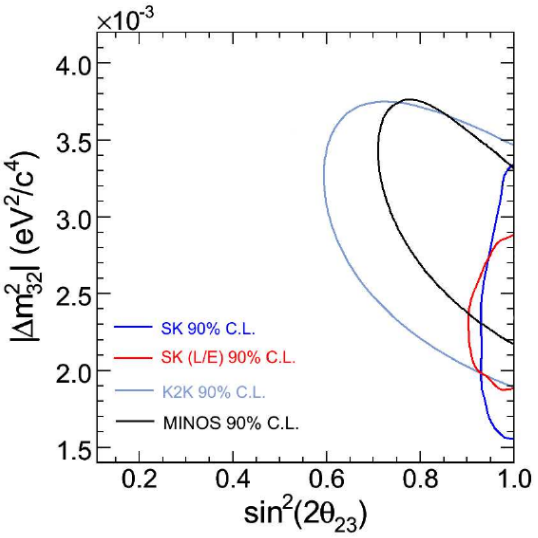

Figure 1.7: The allowed regions of Δm^2 and $\sin^2 2\theta$ shown for the $\nu_\mu \rightarrow \nu_\tau$ channel [55, 57, 59, 60].

1.4.3 Accelerator Neutrinos

Large scale neutrino interactions, which can be obtained by man-made neutrino sources provide for detailed investigations of the neutrino oscillation phenomenon. A number of long-baseline accelerator-based experiments were launched to confirm the ν_μ-disappearance and the ν_τ-appearance. The latter is subjected to lower statistics, owing to the τ production threshold of 3.5 GeV and its detection efficiency.

When high energy proton beams strike the heavy nuclear target in the accelerators, beams of pions and kaons are produced, which eventually decay to give rise to the neutrinos. An approximate control is obtained on the neutrino energy and type, by selecting and manipulating the kinematic properties of the π/K beams. Such neutrino sources are used at the Brookhaven, CERN, Fermilab etc.

Typically ν_μs or $\bar{\nu}_\mu$s are produced at the accelerators. However, the beam gets contaminated due to a certain fraction of the kaons decaying into ν_e and $\bar{\nu}_e$. There are long shields to absorb the non-decaying mesons and the charged muons, to let the neutrino

beam emerge. A near detector or the short-baseline experiment mainly normalises the flux of the neutrinos, while the farther one or the long-baseline experiment inspects the oscillation characteristics. The K2K [61] was the first long-baseline accelerator based neutrino experiment using a neutrino beam of an average energy of 1.4 GeV, peaking at 1 GeV. Thus, it observed the $\nu_\mu \rightarrow \nu_e$ appearance too, in addition to the general ν_μ disappearance. The MINOS [59] experiment uses an almost pure ν_μ beam produced by hadron decays. The ICARUS [62, 63] and the OPERA [64, 65] experiments at the Gran Sasso Laboratory, searched for oscillation in the neutrinos from the CERN, i.e. the CNGS neutrino beam.

The values of θ_{23} and $|\Delta m^2_{32}|$ measured by the atmospheric [66] and the long-baseline accelerator [67, 68] experiments are consistent with each other and indicate maximal mixing. They found the mixing angle $\theta_{23} \sim 45°$ and the mass squared difference $|\Delta m^2_{32}|$ to be $\sim 2.6 \times 10^{-3}\text{eV}^2$. [2]

As explained in the earlier sections, the three flavours mix to form three non-degenerate mass eigenstates with masses m_1, m_2 and m_3. We get two independent mass-squared differences $\Delta m^2_{21} = m^2_2 - m^2_1 = \Delta m^2_{\text{solar}}$ and $\Delta m^2_{31} = m^2_3 - m^2_1 = \Delta m^2_{\text{atm}}$. Solar and atmospheric neutrino data indicate that $\Delta m^2_{\text{solar}} \sim 0.03 \Delta m^2_{\text{atm}}$. Hence the third mass-squared difference $\Delta m^2_{32} = \Delta m^2_{31} - \Delta m^2_{21}$ is approximately equal to Δm^2_{31}. The energy dependence of the solar neutrino survival probability requires Δm^2_{21} to be positive but there is no experimental information on the sign of Δm^2_{31}. Thus two very different patterns of neutrino masses are allowed: $m_1 < m_2 < m_3$ called normal hierarchy (NH) and $m_3 < m_1 < m_2$ called the inverted hierarchy (IH), shown in figure 1.8.

[2] For the current updated/accepted values of the oscillation parameters with the uncertainties on their central values, please refer to table 1.1.

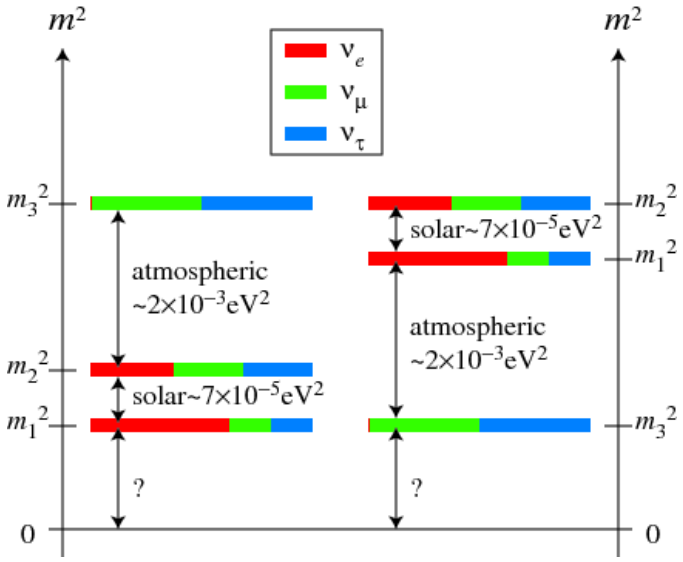

Figure 1.8: The neutrino mass hierarchy: normal ordering and the inverted ordering [19].

1.4.4 Reactor Neutrinos

The importance of reactor neutrinos dates back to the discovery of Reines and Cowan.The fission reactions of the neutron rich heavy nuclei like the ^{235}U, ^{238}U, ^{239}Pu, ^{241}Pu, etc. comprise of β-decays, which produce anti-neutrinos ($\bar{\nu}_e$). Neutrinos produced in the nuclear reactors derive their energy from these fission reactions. The energy of these $\bar{\nu}_e$s should thus vary in the range of a few MeVs, mostly around 2-3 MeV but with significant tail till about 8 MeV. A typical power reactor core bears about 3GWth of thermal power and the typical $\bar{\nu}_e$ flux generated is ~6×10^{20} per core per second [69]. Nuclear reactors provide an excellent scope to observe the appearance and disappearance of the $\bar{\nu}_e$ and thus study their oscillation.

The KamLAND experiment [70, 71, 72] in the 2000s showed the oscillation property in the reactor neutrinos at a baseline of ~180km.

Two reactor experiments with their baselines ~1km, CHOOZ [73] and PALO VERDE [74] were constructed in the 1990s to measure θ_{13}. The CHOOZ was built 1050m away from the two reactors at the CHOOZ power plant. PALO VERDE had its detectors at

750, 890 and 890m away from the reactors of Palo Verde Nuclear Generating Station. Both their data could only set an upper limit on the value of θ_{13}.

So, there was a need for the second generation of experiments to measure the θ_{13}. This next generation of reactor experiments, Daya Bay [75], RENO [76] and Double Chooz [77, 78] finally measured the value of θ_{13} to be $\sim$8.9°. This high (with respect to the expectations of the physics community) value of the "reactor mixing angle" enhances the ability to determine the neutrino mass hierarchy and restores the hope of measuring δ_{CP} too.

1.5 Study of the atmospheric neutrinos

An atmospheric neutrino detector is placed on (or just below) the Earth's surface. Distances travelled by the neutrinos detected in these experiments thus vary from 15 km for the downgoing neutrinos to $\sim$12,000 km for neutrinos travelling through the earth, after being produced in the atmospheric interactions. The atmospheric neutrino flux spans a wide energy range from hundreds of MeV to TeV and beyond. This enables us to study neutrinos with widely varying pathlengths, or L/E.

Till the present day, there have been effectively two types of atmospheric neutrino detectors - water Cerenkov detectors and tracking calorimeters. This research work relates to the latter type, as in Iron Calorimeter detector, described in chapter 2.

1.6 Current Research in Neutrino physics

A systematic program of experiments with both natural [41, 39, 42, 43] and man made sources [44, 59, 78, 75, 76, 79, 80] have led to a wealth of data on neutrino oscillation parameters. A three flavour oscillation fit to all the data gives the following values for these parameters, as in table 1.1.

ν-oscillation parameters	Best fit values	3σ-range
Δm^2_{21} in 10^{-5}eV^2	7.60	7.11-8.18
Δm^2_{31} (NH) in 10^{-3}eV^2	2.48	2.30-2.65
Δm^2_{31} (IH) in 10^{-3}eV^2	2.38	2.20-2.54
$\sin^2\theta_{12}$	0.323	0.278-0.375
$\sin^2\theta_{23}$ (NH)	0.567	0.392-0.643
$\sin^2\theta_{23}$ (IH)	0.573	0.403-0.640
$\sin^2\theta_{13}$ (NH)	0.0234	0.0177-0.0294
$\sin^2\theta_{13}$ (IH)	0.0240	0.0183-0.0297
$\delta_{\rm CP}/\pi$ (NH)	1.34	0.0-2.0
$\delta_{\rm CP}/\pi$ (IH)	1.48	0.0-2.0

Table 1.1: Best fit results and the 3σ-range of the global 3ν oscillations, as from the reference [81]

The following questions still remain unanswered in the neutrino oscillation studies:

- What is the pattern of neutrino masses? Is the true hierarchy normal or inverted?
- What is the octant of the angle θ_{23}? Is it $< 45°$ or $> 45°$?
- Most importantly, is there CP violation in the neutrino sector?

A number of experiments are currently running [79, 80, 82] or being planned [83, 84, 85, 86, 87, 88] to address these issues. Among the current experiments, NOνA experiment can determine the hierarchy for the following two favorable combinations: (i) the hierarchy is normal and δ_{CP} is in the lower half-plane or (ii) the hierarchy is inverted and δ_{CP} is in the upper half-plane. If nature chooses one of the other two combinations, then NOνA has no hierarchy sensitivity [89, 90]. Present data shows a slight preference for normal hierarchy and δ_{CP} in the lower half-plane [79, 91].

1.7 Organisation of this report

The research works in this report involve the study of atmospheric neutrino interactions in the ICAL detector at the India-based Neutrino Observatory (INO). So, we give a short description of the detector in chapter 2 and attempt to give a brief outline of the different softwares used for this study in chapter 3. The actual research work done is contained in the following 3 chapters.

There have been three major project topics covered in my research, and are:

- "Study of muonless[3] events in ICAL@INO": This comprises of three sub-projects, which are as follows,
  - Obtaining a ν_eCC rich events sample
  - Contribution of the muonless events in determining neutrino mass hierarchy
  - Energy and direction estimation of the incident neutrinos in the muonless events
- Incorporation of GENIE as the neutrino event generator for ICAL
- Improving the mass hierarchy sensitivity of ICAL using neural network analysis

Finally, chapter 7 summarises the entire research work done.

[3] *muonless* event can be roughly understood as *trackless* event or a shower-like event.

2

The ICAL@INO

The Iron-CALorimeter or the ICAL is the main detector to be set up at INO (India-based Neutrino Observatory). It is a giant magnetized neutrino detector for studying the atmospheric neutrino interactions.The present study is based on the ICAL detector. So, it is necessary for the reader to have a clear picture about the structure and the various salient features of the detector. This chapter aims to describe the complete structure of the ICAL detector, starting from the details of the active detector element, the implementation of the magnetic field, and includes brief description of the electronic readouts and the gas compostion in the detector.

2.1 The India-based Neutrino Observatory

India-based Neutrino Observatory or the INO, is an upcoming experimental facility in the Theni district of the state of Tamilnadu in Southern India. The Observatory will be set up under Bodi West Hills (figure 2.1), ensuring ∼1 km of rock covering in all directions. This reduces the background due to the cosmic ray muons for the experiments. A comparison of this background reduction with respect to other underground experiments is shown in figure 2.2.

Figure 2.1: The Bodi Hills in Theni. [11]

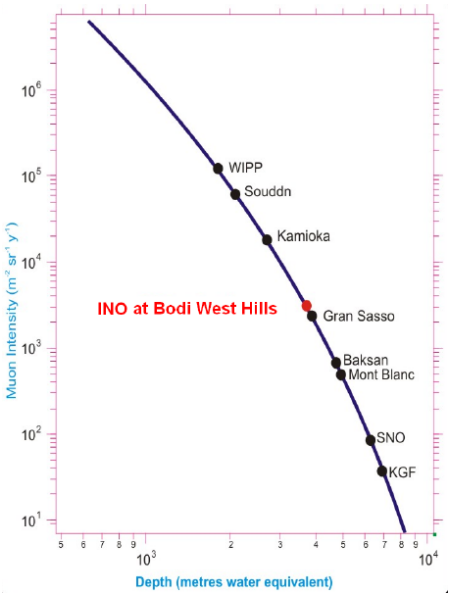

Figure 2.2: Atmospheric muon background as a function of depth. [11]

The INO cavern will be accessible through a ∼1.9 km long tunnel. One large and three small laboratory caverns are to be built. The important component of INO will be the Iron Calorimeter (ICAL). However, INO will also facilitate experiments like the Neutrino-less Double Beta Decay (NDBD), direct dark matter search experiments, low energy neutrino spectroscopy, etc. The largest cavern, that will house the main iron calorimeter detector (ICAL), is 132 m (L)×26 m (W)×32.5 m (H). This cavern is called "UG-Lab 1", as shown in the schematic sketch in figure 2.3.

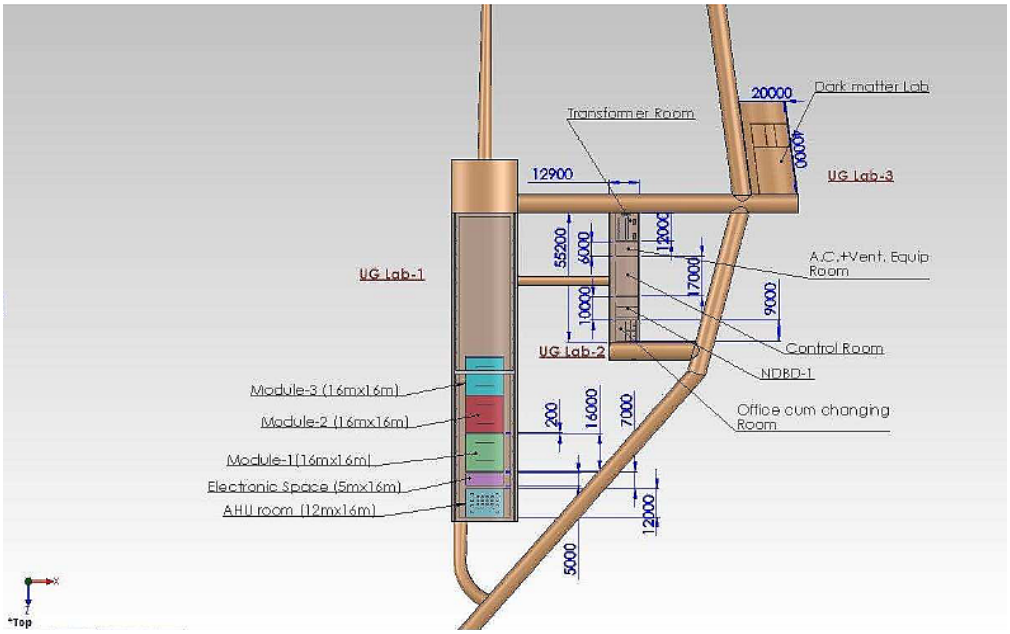

Figure 2.3: A Schematic Sketch of the INO cavern. [11]

2.2 Physics Prospects of the ICAL@INO

ICAL is mainly equipped to study the tracks of the muons from the charged current interactions of the $\nu_\mu/\bar{\nu}_\mu$s. The ability of the ICAL to tell apart the μ^+ and the μ^-, i.e. the ν_μ and the $\bar{\nu}_\mu$ gives it the advantage of studying the matter effects on the atmospheric neutrinos. Therefore it is most well suited to determine the neutrino mass ordering. ICAL can observe neutrinos with varying baselines from ∼10-10000 km. So, ICAL will be able to observe the oscillation pattern and measure the atmospheric oscillation parameters quite precisely.

2.3 The ICAL Detector

ICAL comprises of three modules, with ∼30,000 RPCs, and 151 iron layers weighing about 50 ktons in total. A sketch of ICAL is shown in figure 2.4. Each module contains 8 × 8 RPCs in a layer, each of which spans a surface of 1.84 m × 1.84 m and is 2.5 cm

in width (height) [10]. The ICAL detector will have a total dimension 48 m × 16 m× 16 m. The iron plates will be 5.6 cm thick. The iron layers are set apart from one another by 4 cm gaps. The active detector elements, i.e. the resistive plate chambers (RPCs) [92, 93, 94] are placed in these gaps. The steel structures placed every 2 m on both X and Y sides, support the iron plates and the RPCs.

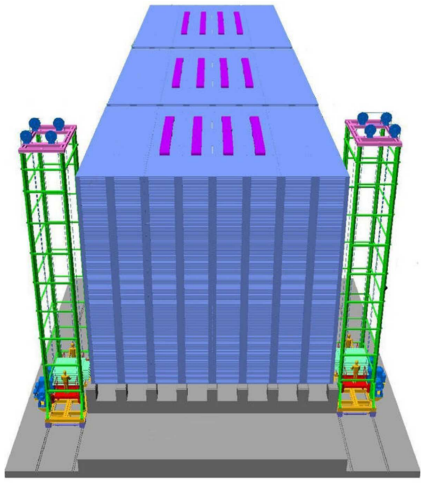

Figure 2.4: A Schematic Sketch of the INO Detector. [83]

2.3.1 Resistive Plate Chambers or RPCs

RPCs have a good charged particle detection efficiency of ∼ 90–95%. This allows the determination of the X and Y coordinates of the track of the charged particles passing through the RPC. The layer number of the RPC gives the Z coordinate. RPCs give a time resolution of ∼1 ns. This helps to distinguish between the upward and the downward-going particles.

Every RPC unit (figure 2.5) is made up of a pair of 3 mm thick glass plates of area around 2 m × 2 m. The glass plates of an RPC are held apart by 2 mm spacers. The glass plates are coated with graphite (mixed with an adhesive) on the outer side. A high voltage of about 10 kV is applied across the two faces of the chamber and operated in avalanche mode. Copper strips are placed on either sides of the RPC, orthogonal to

each other. Any charged particle, passing through the RPCs, will ionise the gas in the chamber and these signals will be picked up by the X and Y copper strips as shown in figure 2.6.

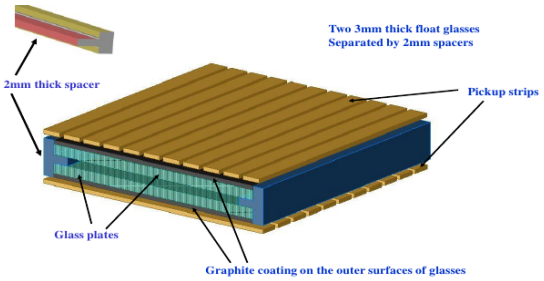

Figure 2.5: Structure of an RPC. [83]

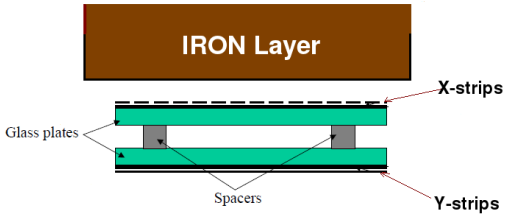

Figure 2.6: A Schematic diagram of the detector unit: RPC and an iron layer.

2.3.2 The ICAL magnet

The iron layers not only serve as the heavy target for the neutrinos but also carry the solenoidal magnetic field in the detector [95]. The neutrinos produce charged/neutral particles during interactions, which propagate through the detector. The iron layers are magnetised to ∼1.3 T. The simulated mapping of the horizontal projection of the magnetic field and in the vertical plane are shown in figures 2.7 and 2.8 respectively.

There will be two vertical slots cut into the module for the winding of the current-carrying copper coils as shown in figure 2.7 [95]. The bending of charged particles not only helps in the identification of their charge, but also in measuring the momenta of the particles. The μ^-/μ^+ tracks can thus be identified and reconstructed to get the muon momenta, besides identifying a ν_μ event from a $\bar{\nu}_\mu$ event.

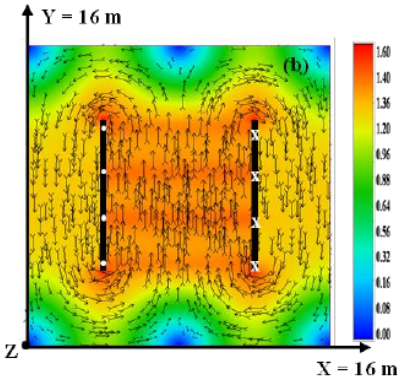

Figure 2.7: Horizontal projection of the magnetic field.[95]

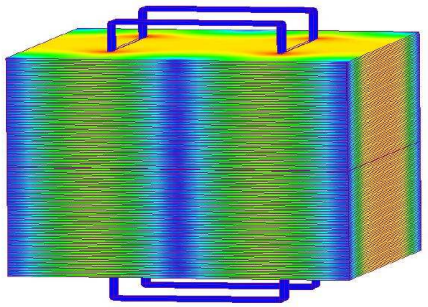

Figure 2.8: Magnetic map of a single module.[95]

2.3.3 The ICAL electronic readouts

The X-Y signal strips map the points of interactions in a RPC detector. The aim is to generate a trigger signal according to hits on the pick-up strips, to record the pattern of hits, the timing etc. i.e. to receive and convert the detector signals into our useful or readable information. The DAQ system includes the Front end electronics, the Back end electronics and finally the computer-interface.

The typical signal range on the strips across a 50Ω load is 0.5 - 2 mV. They have a rise time of about 1 ns and hence need a high speed, low noise pre-amplification before these RPC strip signals can be further processed by the front-end electronics.

The preamplified RPC strip signals are fed to Analog Front End (AFE) boards. One of the main functions of the AFE board is to convert these amplified analog RPC pulses into logic signals by using low threshold discriminator circuits. The AFE boards also incorporate a primitive trigger logic on board, where discriminator outputs of four channels are shaped to 50 ns pulses and logically ORed to generate level-0 trigger signals.

The discriminator signals from the AFE boards are further processed by Digital Front End (DFE) electronics, which mainly consists of three sections - event data readout, monitoring and level-1 trigger generation.

The trigger signal is produced as a result of the combination of the number of strips fired, the number of layers receiving the signal in coincidence, out of a certain number of consecutive layers [96, 97]. The data is latched and is fed to the data acquisition system via the signal routers.

2.3.4 The ICAL gas system

The gas system basically has the following components built in.

1. Purifier Column: It contains Molecular sieve used to absorb moisture and purify it.
2. Mixing Unit : This receives the gas from MFCs (Mass Flow Controllers)
3. Distribution Panel: The RPC's can be connected in parallel (or cascade), which is achieved by "Flow resistors" viz. Capillaries.
4. Safety Bubblers: This is to take care of the back pressure exerted and protect the RPCs from over pressurizing.
5. Isolation Bubblers prevent back diffusion of air into the RPC and also indicate the flow of gas.
6. Exhaust Manifold: All the gas to be vented is collected in this manifold and a single output is provided to either vent the used gas into the atmosphere (open system) or feed it back after analysing its composition (closed system). This manifold has a pressure sensor to indicate the pressure of this gas with respect to room pressure.

The choice of the gas in the RPC largely depends on the following factors: low working voltage, high gain, high rate capability and good proportionality. Freon (R134A) is used, which is a prime requirement for an elelectronegative gas. The gas is ionised by the passing charged particle. Recombination of ions in the mixture produces ultraviolet photons. These should be extinguished as they might generate spurious pulses at other parts of the detector. For this a quenching gas is required which absorbs the photons.

Halogens and hydrocarbons are usually used. In this case Isobutane is being used. SF_6 (Sulphur-hexafluoride) is used for absorbing the excess avalanche electrons. The gases are mixed in the following ratio, R134A : Isobutane : SF_6 = 95.2 : 4.5 : 0.3 %.

3

Simulation and Software Tools

This chapter aims to give a light update to the reader, about the various software packages to be used for the present study or work. One should in principle understand the working of the software in every bit of detail, before implementing them in one's phenomenological studies. We have used the Nuance, the GENIE, the GEANT4, the ROOT and the TMVA for our analysis. So, we attempt to give a quick overview of the functioning of each of these software tools.

3.1 Monte Carlo Neutrino Event Generators

Monte Carlo neutrino generators are programs that use random number generators explicitly in order to simulate the interaction of neutrinos with matter, while taking into account the physics laws and models.

A neutrino of a particular flavor (if not specified by the user) with a 4-vector momentum and a target nucleus are chosen by these generators [98]. The possible product particles are decided in reference to the physics lists in their libraries and kinematically simulated to get the final state particles in the given detector geometry.

The most commonly used primary neutrino interactions in the generators are usually categorized as follows [99]:

- (Quasi-)elastic scattering ($\nu\ N\ \rightarrow\ l\ N'$),
- meson productions via resonance ($\nu\ N\ \rightarrow\ l\ N'\ m$),
- coherent pion production ($\nu\ X\ \rightarrow\ l\ \pi\ X$) [100],
- Deep inelastic scattering ($\nu\ N\ \rightarrow\ l\ N'\ hadrons$),

where $N,\ l,\ m,\ X$ denote nucleon, lepton, meson and nucleus, respectively.

Simulating neutrino interactions within the energy range of interest to the current and near-future experiments poses significant challenges. To cover this broad energy range, one requires bridging between the perturbative and non-perturbative pictures of the nucleon. Inclusion of a variety of scattering mechanisms is also important. There are several aspects involved , which include elementary cross-sections, hadronization models and nuclear physics. Each model has to be considered in its corresponding range of validity and then included to make whole the picture. Only then, one can generate events over the entire desired phase space. This inevitably introduces challenges in merging and tuning models, in making sure that double counting and discontinuities are avoided. In addition there are kinematic regimes which are outside the stated range of validity of all available models, in which case one is left with the challenge of developing our own models or deciding which model best extrapolates into this region. The actual implementations of the models are different in the generators [99]. Therefore, the results may be different between the generators even if they use the same model. This is why it is also important to compare various kinematical distributions from different generators.

The neutrino generators are hence the access points of a neutrino experiment to the theory inputs required for retrieving the physics information from the data. There are several neutrino event generators available, such as ANIS [101], GENIE [5], GiBUU [102, 103], NEGN [104], NEUT [105], NUANCE [1], the FLUKA routines [106], NUNDIS/NUNRES [107], and NuWRO [108].

Neutrino physics is an evolving topic, with the neutrino experiments in full swing,

which are studying neutrinos from numerous sources, such as reactors, accelerators, the atmosphere and astrophysical sources, thus spanning a wide range of energies from MeV to TeV. Our emphasis would be on the range of few-GeV for atmospheric neutrinos. We have used Nuance and GENIE for generating atmospheric neutrino data for our present study. They are briefly discussed in the following subsections.

Several neutrino generators have been devised so far, depending on the varied needs of various neutrino experiments.

GENEVE [109] has been the Monte Carlo neutrino generator for the ICARUS Collaboration, well suited to study the atmospheric neutrino interactions. It was developed during the late 1990s and mostly depends on the interaction models from the 70's.

NEUT is the Monte carlo generator built for the simulations in Super-Kamiokande and the K2K experiments, well suited for neutrino interactions with protons and oxygen [105].

NeuGEN is the neutrino generator [110] in the mid 1980's for the Soudan 2 experiment, to understand the backgrounds due to neutrinos in the proton decay.

The NuWro Monte Carlo generator [126] of neutrino interactions has been developed during ∼2006-12 by the Wroclaw group, to study neutrino interactions. NuWro simulates neutrino-nucleon and neutrino-nucleus reactions for energies till TeV. NuWro provides choices for the description of the target nucleus. The NuWro has also been implemented as a tool in analysing MiniBooNE CCQE data [127]

GIBUU aims to provide an unified transport framework in energy ranges from MeV to GeV for reactions on nuclei, like electron-nucleus, photon-nucleus, hadron-nucleus, heavy ion and neutrino-nucleus collisions [128, 129]. It simulates particle transportation in nucleus including nuclear effects with uptodate models.

3.1.1 Nuance

The Nuance software package for generating neutrino interactions was developed by Dave Casper [1], with the advent of the Super Kamiokande experiment.

It is a FORTRAN based program, which we shall use to generate neutrino events, with atmospheric neutrino flux impinging on a simple detector geometry. The detector geometry must be specified by the user, along with the constituent target materials.

It first retrieves the list of cross sections from its libraries, sums the cross-sections and the rates of all the known interaction channels. The deep-inelastic scattering is also considered, within appropriate energy bars. Thus the total cross-section and event rate is obtained. The number of events to be generated is either specified by the user or calculated from the exposure time specified, with the help of the event rate. The neutrino events are then generated and the information saved in ascii format.

The models of final state interaction with the nucleus, used in this program was originally developed for the IMB experiment.

The Monte Carlo neutrino generator of Nuance also accommodates the option of generating neutrinos with varied oscillation parameters. The oscillation of neutrinos during propagation through earth is done by assuming the earth's sphere in 25 concentric shells of varying density.

3.1.2 GENIE

GENIE "Generates Events for Neutrino Interaction Experiments" is a ROOT-based universal, object-oriented/C++ neutrino MC Generator. GENIE is updated consistently and it aims to become a "canonical" Monte Carlo neutrino event generator with wide applicability [5]. The origins of the code come from the Soudan experiment [130] and later, MINOS [59] has been primary applicant.

Current neutrino experiments have complicated detectors composed of many elements and the neutrinos are present in different flavors over a wide energy spectrum (from 1 MeV to 1 PeV).

It encompasses and supersedes Fortran neutrino MC generators, such as GENEVE [109], NEUT, NeuGEN [110] and NUX [111] used in many previous and current neutrino experiments.

Neutrino interaction physics models in GENIE: The neutrino–nucleus interaction involves a large variety of processes, all of which must be modeled to get an accurate description of the experimental signature of any detector and its many components. Since most theoretical models describe a small subset of these processes, GENIE must include several such models. The list of physics models include nuclear, cross-sectional, quasi-elastic scattering, elastic neutral current scattering, baryon resonance production, coherent neutrino-nucleus scattering, non-resonance inelastic scattering, quasi-elastic charm production, deep-inelastic charm production, inclusive inverse muon decay and neutrino–electron elastic scattering. GENIE also takes care of modeling the transition region, total cross section and the neutrino-induced hadronic multiparticle production modeling, where it uses the AGKY hadronization model [**?**] which was developed for the MINOS experiment.

The Monte Carlo method: It is a numerical solution to a problem that models objects interacting with other objects or their environment, attempting to model nature through direct simulation of the essential dynamics of the system in question. It gives a solution to a macroscopic system through simulation of its microscopic interactions.

GENIE the neutrino event generator for experimental physics uses the PRNG MT19937. It is a random number generator based on the Mersenne Twister [112].

GENIE has already been adopted by many neutrino experiments, including those using neutrino beamlines, and will be an important physics tool for the worldwide accelerator neutrino program.

3.2 GEANT4

Geant4 [113] is a package of programs in c++, for simulating the passage of particles. It involes certain characteristics which are as follows:

- The detector geometry explicitly described, no matter how complicated,

- The elements or materials comprising the system specified,
- Identify the particles of interest, like the incident particle, the target particle on its way etc.,
- Generate an event or interaction,
- Tracking of the particles through the system, even in presence of electromagnetic fields,
- Calling the corresponding physics processes to govern the particle interactions from the incorporated physics-list,
- Keeping track of the responses from the sensitive detector components,
- Converting these responses into observables of the detector, which may involve digitisation,
- Option for independent generation of events,
- Recording the information of events and tracks,
- Visualizing the detector and the trajectories of the propagating particles, and
- Options to store (for analysis) the simulated data at different levels.

Thus it incorporates multiple functions like tracking, geometry, physics models and hits or detector responses, all in one go. The physics processes include electromagnetic, hadronic and optical processes, covering a a wide energy range from <1 keV to the TeV.

The toolkit has been the product of the joint endeavour of physicists and software engineers round the world collaborating with each other. To add to its success, GEANT4 has not only been used in particle physics but also nuclear physics, accelerator design, space engineering and medical physics.

3.3 TMVA

ROOT [114] is very commonly used by most high energy physicists for analysing data. TMVA or Tools for Multi Variate Analysis [115] is a collection of classifiers built in the ROOT environment and is a better way to analyse the data than just implementing a random classifying technique in isolation. Thus TMVA gives one common platform / interface for high-end multivariate classifiers. A trial of all the methods using common data pre-processing capabilities is obtained at ease. All the classifiers are trained and tested on the same data and evaluated consistently.

There are several optional classifiers and regression methods available in the TMVA, such as follows.

- Rectangular cut optimisation
- Projective and multidimensional likelihood estimators
- k-Nearest Neighbor algorithm
- Fisher, Linear and H-Matrix discriminants
- Function discriminants
- Artificial neural networks
- Boosted decision trees
- RuleFit
- Support Vector Machine

Some of the above classifiers are discussed in chapter 6. A number of preprocessing methods like the decorrelation, principal value decomposition, gaussianisation etc. or combination methods like boosting, categorisation etc. are applied on the parameters used for better discrimination.

3.3.1 Working Principle

A schematic flowchart in figure 3.1 shows the working principle of the TMVA.

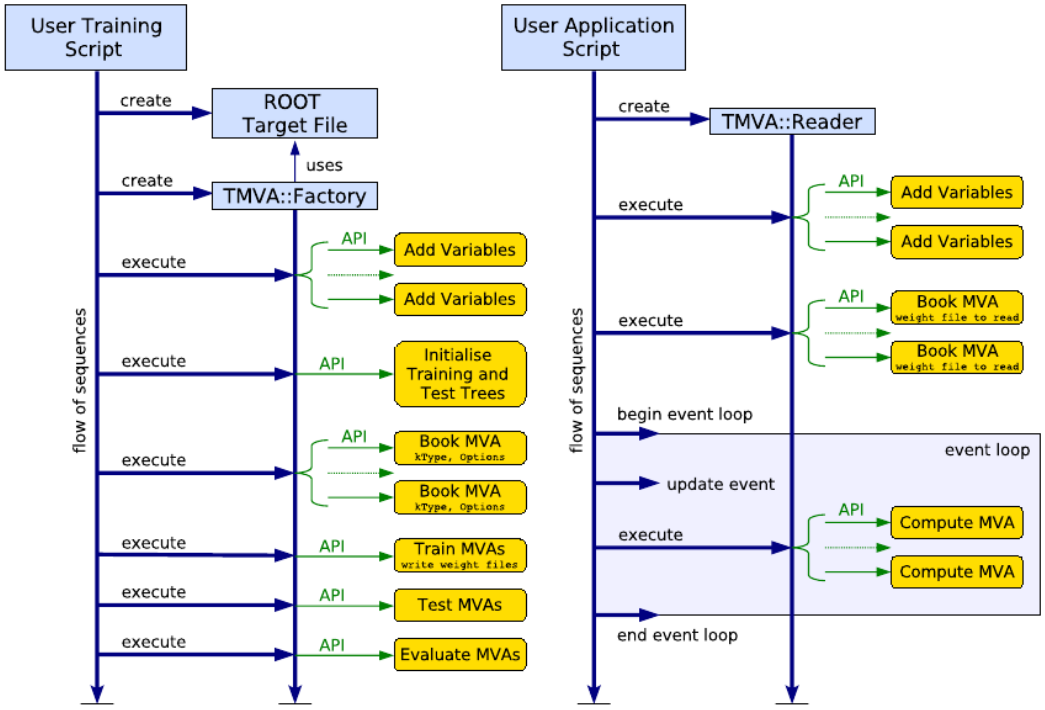

Figure 3.1: Left: Flow (top to bottom) of a typical TMVA training application. Right: Flow (top to bottom) of a typical TMVA analysis application. [115]

The main program of the user, which calls for the TMVA, is mostly a ROOT macro or a C++ executable script. The TMVA can access to a ROOT file. The "signal" events and the "background" events are clearly demarcated in the file used for the training and testing purpose. This is done by a class called "TMVA Factory". Firstly, the discriminating variables are stored in the training trees, as certain functions. There are several MVA methods available, and the user selects the ones, as per one's requirement. The configuration options are also specified by the user. The TMVA then undergoes training, testing and evaluates the performance as a certain probability value. These results or

the so-called *weights* of the training methods are stored in an XML format, which will be used for analysing any new dataset.

Another class called the "TMVA Reader" reads this information, corresponding to whichever of the trained methods the user has chosen during analysis. For every event now, the variables are stored in assigned memory addresses and the response values are calculated. This output value tells the user, to the extent the TMVA can observe signal-like characteristics or background-like characteristics in an event.

3.3.2 Salient Features

The use of Monte Carlo sampling, Genetic Algorithm, Simulated Annealing [115] in TMVA accounts for huge speed of volume search by sorting events in binary tree.

The discrimination of signal from background may be required at different stages of the data analysis, as for example:

- Event level (Higgs searches, ...)
- Cone level (Tau-vs-jet reconstruction, ...)
- Track level (particle identification, ...)
- Lifetime and flavour tagging (b-tagging, ...)

Depending on the level at which the classification is needed, the input variables to be fed into the TMVA are decided in such accordance. Here are a few examples from some standard HEP analyses.

- Event properties (jet/lepton multiplicity, sum of charges, ...)
- Kinematic variables (masses, momenta, decay angles, ...)
- Event shape (sphericity, Fox-Wolfram moments, ...)
- Detector response (silicon hits, dE/dx, Cherenkov angle, shower profiles, muon hits, ...)

The variables used in our research work have been explained in chapter 6 with the required justifications.

3.4 Conclusion

The above mentioned software packages, be it a neutrino event generator, an interaction simulator, or a comaparative analyser that feeds on the variables of an event, are very important and crucial for an experiment to design, record and analyse the data correctly and most efficiently. Therefore, they must be understood well and implemented appropriately in any experimental study.

4

Muonless Events in ICAL@INO - I

This chapter explains how we can obtain a data sample rich in electron neutrino charged current interactions in the ICAL. We first give the reader an initial picture of the entire data to be collected by ICAL. We then devise several selection criteria to distinguish between the ν_eCC events from the rest of the *muonless* events. Each of these variables is discussed in detail, including how the putting (even manually) of cuts on these variables yield us an enriched sample. We then use this selected sample to extract the hierarchy information from these ν_eCC events.

4.1 Introduction

The neutrinos and anti-neutrinos undergo two types of interactions, depending on the mediating particle. The charged current (CC) interactions are mediated by the $W^{\pm}$ particles and the neutral current (NC) interactions by the Z^0. The CC events are different for each flavour and can be distinguished by the charged lepton in the final state. If the charge of this lepton can be determined, then they can be distinguished from the anti-neutrino interactions also. The NC events appear the same for neutrinos/antineutrinos of all flavors due to the absence of any charged lepton in the final state.

ICAL is mainly designed to observe the CC events of ν_μ and $\overline{\nu}_\mu$, from the tracks

given by μ^- and μ^+ respectively. The magnetised iron layers of ICAL help to identify the charge of the particles, such as muons, passing through many layers. The CC events of ν_e ($\overline{\nu}_e$) produce electrons (positrons) which create a shower in the detector. This shower is mostly absorbed in the iron layers. Hence, the CC events of ν_e or $\overline{\nu}_e$ look very similar to the NC events in the ICAL detector.

The present chapter focuses on muonless events in ICAL, which excludes the identified ν_μCC events. Any event, that does not show a distinguishable muon track, is referred to as a "muonless" event.

4.2 Objective and Motivation

There are some anomalies noticed in the low energy range of the LSND and the Mini-BooNE data. The existence of sterile neutrinos (ν_s) is proposed to account for it. The ν_s do not couple with Z^0, i.e. they do not have NC interactions. Therefore, if there are any oscillations taking place from the active flavours to the sterile flavours, then there should be a deficit noted in the count of NC interactions. So, recognizing the sample of NC events is an essential necessity in this regard.

The muonless events include the ν_eCC events too. The ν_τCC also contribute to muonless events, though their numbers are very small. Identifying the sample of ν_eCC events is always advantageous and welcome. Accessability of another sample of charged current ν-interactions apart from the ν_μ will certainly further add to the physics information at ICAL. Additional contribution to determining the neutrino mass hierarchy is one of them.

4.3 Data Generation and Simulation

It must be remembered that besides the above mentioned ν_μ and ν_e NC events, the ν_τ events (both CC and NC) and the low energy or near horizontal ν_μCC events are likely to appear as muonless events in the detector and form an important background. So,

one must include the ν_τCC, all the NC and the ν_μCC events too.

The data for the following study is generated by Nuance, using normal hierarchy parameters. Simulations with inverted hierarchy parameters are also made, but not mentioned here, to avoid repetition. They are denoted as NH and IH (if required) respectively. It is preferable to use 500 years of data, and then scale down later, to avoid the uncertainty due to the statistical fluctuations.

Therefore, 500 years of data including all such types of events are generated by Nuance v3 [1]. The events are then simulated in the ICAL detector using the GEANT4 ICAL code inoical0_v111102_1 [2]. The oscillation parameters used in generating the events are: Δm^2_{21}=7.5e$^{-5}eV^2$, $|\Delta {m^2_{eff}}^2|$=2.47e$^{-3}eV^2$, $\sin^2\theta_{12}$ =0.31, $\sin^2 2\theta_{13}$ =0.09 and δ_{CP}=0, $\sin^2\theta_{23}$ =0.5.

4.3.1 Signal-Detection

Charged particles produced by the neutrino interactions pass through one or more RPCs and generate *hits*. These hits are our primary signals. The layer number of RPC gives the z-coordinate of the hit. The x and y-coordinates are given by the copper-strips of the pick-up panels which are orthogonally oriented at the top and the bottom of the RPCs. The number of strips in x-direction, with a signal, gives x-strips and similarly in y-direction gives y-strips. The maximum of the number of x-strips or y-strips is defined to be the number of "strips-hit" in that layer. This number of strips-hit in a layer, when summed over all the layers which have received hits in that event, gives the number of strips-hit in that event. The hits distribution mentioned hereafter refers to this value.

In the following study, we assume an ideal detector with no noise and any event registering a single hit is considered a detectable event.

4.3.2 Flavor-Ratio of the data sample

The 500 years of data from Nuance, in the energy range E_ν={0.8,20} GeV (which is to be fed into the Geant4 INO ICAL code) gives the following flavour distribution of events

in table 4.1.

Event type	**No Osc.**	**NH**	**IH**
ν_e**CC**	671289	676014	671399
ν_e**NC**	241070	241502	242157
ν_μ**CC**	1513637	1103263	1103667
ν_μ**NC**	563427	409638	409132
ν_τ**CC**	-	17741	17952
ν_τ**NC**	-	151973	152360

Table 4.1: Flavour distribution of events in the 500 years Nuance data

However, all of the above events do not leave hits in the detector. The detectable events are those which leave some hits and we are interested in only those. Since, we are to deal with events that donot have distinguishable muon tracks, we shall count the events under the following mentioned categories. Apart from the ν_eCC, the ν_μCC are kept as a separate account. Henceforth, all the NC events and the ν_τCC events are grouped as the "others".

	# ν_e**CC events**	**#NC events**	# ν_τ**CC events**	# ν_μ**CC events**
NO OSC.	644356	662286	-	1491317
NH	649487	661109	17481	1087709
IH	644926	661849	17714	1088032

Table 4.2: Counts of observable events without applying any selection cut on the Geant output of the Nuance data files, i.e., events with non-zero hits at the ICAL@INO detector.

4.4 Obtaining a ν_eCC pure data sample

The muonless events sample contains the ν_eCC events, the only (significant) type of charged current interactions besides the muon-track containing ν_μCC events. Obtaining such a sample with minimum possible contamination will give us a sample of atmospheric ν_es, i.e. with energy of few GeV, which is a new domain for understanding.

4.4.1 Types of events and their signatures

Vertical and high energy muons travel through large number of layers before stopping/decaying. Therefore, the ν_μs which have high energy and are incident mostly along the vertical direction give hits in large number of layers, in case of CC interactions. In fact, the muons thus produced, form clear tracks in the detector and their momentum can be reconstructed. The curvature induced along the muon path due to the magnetic field, leads to the charge identification. On the contrary, the ν_μs which have lower energy or are incident mostly along the horizontal direction [116] are confined to a smaller number of layers. They can hardly be distinguished from the hadron showers which also emanate from the event vertex.

The ν_eCC events produce electrons which can give rise to em showers, but no track can be seen. The NC events have no charged lepton in the final state and hence have lower number of hits. In these events, only the final state hadrons are visible in the detector. They are indistinguishable from ν_eCC events [18, 17].

Therefore, to make a final judgement of the effectiveness of the selection criteria which are to be described in the following subsection, we consider the neutrinos in the entire energy range of 0.1 to 100 GeV. So, in such a scenario, our signal strength is as shown in table 4.3.

Selection Criteria	**Total #events**	**#ν_eCC events**	**ν_eCC Purity**
hits>0 (all detectable events)	3840083	1106742	29%

Table 4.3: Event counts of the original data sample from the Geant output for the NH 500 years data in E_ν={0.1,100} GeV.

4.4.2 Selection Criteria and their underlying principle

We devise certain conditions to ensure that the selected event sample contains mostly ν_eCC events, with minimum possible background of ν_μCC and NC events.

The total number of hits created by the produced particles in the detector and the number of layers with hits are first studied.

In order to understand the behaviour of the different neutrino events in the detector, we first look at the hits distributions of all the three event types: the NC, the ν_eCC and the ν_μCC, in different energy ranges of the incident neutrinos in figure 4.1.

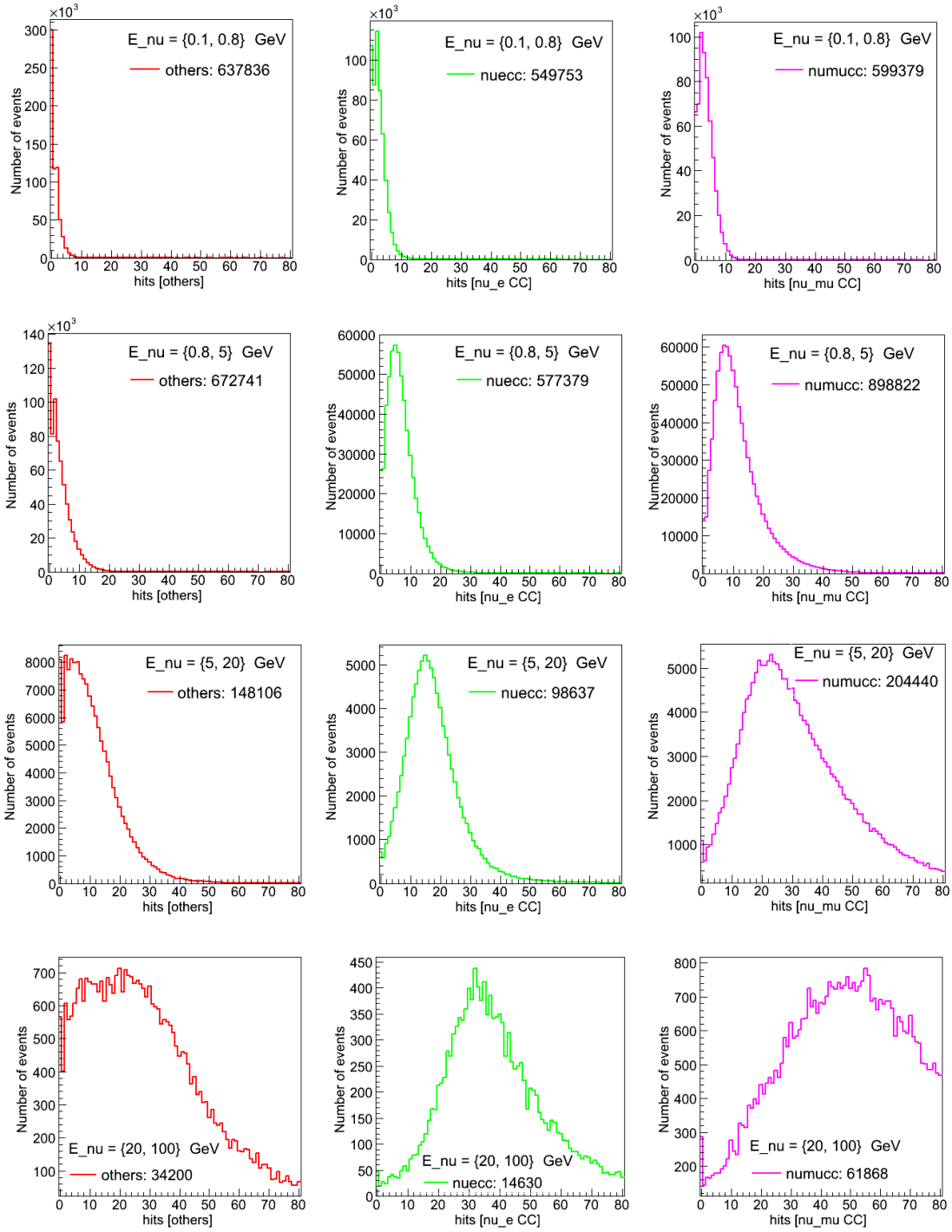

Figure 4.1: Hits distribution in the neutrino energy bins (from top to bottom in order): E_ν={0.1,0.8} GeV; E_ν={0.8,5.0} GeV; E_ν={5.0,20.0} GeV; E_ν={20.0,100.0} GeV, in case of the three types of neutrino events (from left to right in each row): others (all NC +ν_τCC); ν_eCC; ν_μCC events.The x-axis gives the number of hits, and the y-axis the events count.

The distributions in figure 4.1 show that, for ν_μCC events, the number of hits increases with the energy of the incoming neutrino. This increase is much less for ν_eCC events and hardly exists in case of the NC events. The figure also clearly suggests a lower threshold of $\sim$10 hits to suppress a large fraction of NC events and low energy ν_e, ν_μCC events. With this cut, 12% of the total NC events are retained. The survival fraction for ν_eCC events is about 18%. So, out of the total set of survived ν_eCC and NC, more than 60% are ν_eCC events, as seen in Table 4.4. The events containing high energy muons can be separated by restricting the number of layers or by identifying the muon track in ICAL.

4.4.3 Hits and Layers

The electrons/positrons, in general, travel a shorter distance than the hadrons. On the other extreme, the muons of the ν_μCC events travel through several layers. A primary observation of the layer distribution shows that a cut on the number of layers hit in an event is an effective criterion. Here the "layers" refer to the number of layers which receive one or more hits in an event. However, the layer cut is a very sensitive cut, owing to the thick iron layer in between two RPC layers.

As mentioned earlier, ν_μCC events either with low energy muons and/or in horizontal direction, do not have any identifiable muon track. Such events have been found to be a significant fraction in the selected events sample. So, a separate count is maintained for them. The rest of the backgrounds, i.e. the ν_eNC, ν_μNC, ν_τCC and NC are all contained in the "others". The ν_τCC events being pretty small in number, are not separately counted.

We implement a lower threshold on the number of hits (here, 10 at least). This suppresses the NC background and also the spurious events generated purely out of noise.

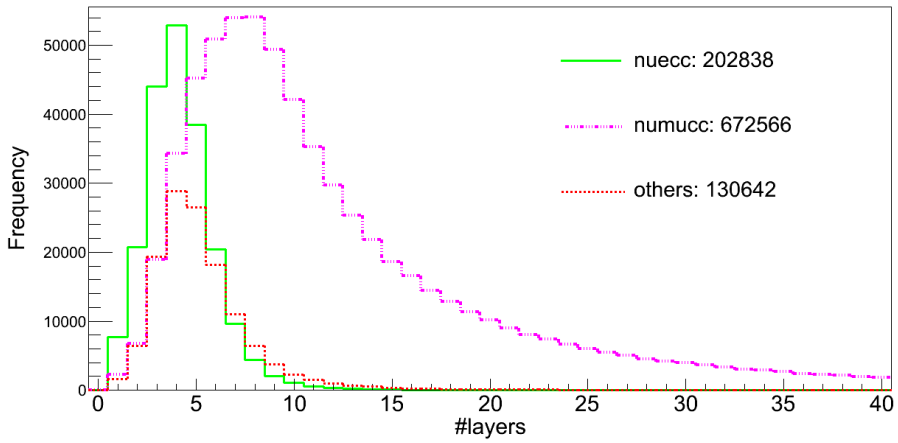

Figure 4.2: Distribution of number of layers for all events with more than 10 hits, for the 500 years NH data in E_ν= {0.1,100} GeV.

The ν_eCC events layer distribution, after a minimal hits cut (typically 10), peaks around 5 while that of the ν_μCC events peaks around 10, as seen in figure 4.2. So, by selecting events which are confined in 5 layers or less, we can reject ν_μCC events which are energetic and/or vertical. However, low energy ν_μCC events, especially those in the horizontal direction, do pass this cut and give rise to the events listed below. Various cuts on the number of hits and layers have been imposed on the set of events E_ν={0.1,100} GeV. A few significant ones among them are listed in Table 4.4.

Selection Criteria	ν_e**CC**	**others**	ν_μ**CC**
hits>0	1106742	1050814	1682527
hits>10 (only)	202838	130642	672566
hits>15 (only)	97535	69340	445977
hits>20 (only)	52398	42476	314597
hits>15; layers≤4	47711	19390	19875
hits>15; layers≤5	68702	32953	36211
hits>15; layers≤7	89614	52550	76194
hits>10; layers≤4	125321	56177	62113
hits>10; layers≤5	163807	82717	107350

Table 4.4: Events counts after applying the selection cuts on the Geant output for the NH 500 years data in E_ν={0.1,100} GeV.

As shown in Table 4.4, requiring the number of layers with hits in the event to be below cut value, leads to a reduction in the fraction of ν_μCC events in the sample.

The average number of hits per layer has been studied as a mean to eliminate events containing tracks. The muon tracks give mostly 2-3 hits in a layer. So, applying a lower cut on the average hits per layer (hpl) seems to be quite reasonable in rejecting most ν_μCC events. The hits per layer cut is useful in studying vertical, high energy muon events. Here, given that the number of layers is constrained to be smaller than or equal to 5, it is not very effective. The addition of this cut leads only to a marginal improvement. The effect of this cut added to those in table 4.4 is demonstrated in table 4.5.

Selection Criteria	ν_e**CC**	**others**	ν_μ**CC**
h>15; L≤4	47711	19390	19875
h>15; L≤4; hpl≥4.0	47711	19390	19875
h>15; L≤5	68702	32953	36211
h>15; L≤5; hpl≥3.5	63911	29831	31512
h>15; L≤5; hpl≥4.0	60187	27496	28429
h>10; L≤4	125321	56177	62113
h>10; L≤4; hpl≥2.5	125321	56177	62113

Table 4.5: Checking the effect of the cuts on average hits per layer added to the above selection criteria on the Geant output of the NH 500 years data in E_ν={0.1,100} GeV. [**"h"**=#**hits; "L"**=#**Layers; "hpl"=hits/layer**]

Applying the above or similar cuts, it is seen that the fraction of ν_eCC events in the sample increases, but at the cost of sample size and fraction of vertical events. Hence, an optimized set of criteria needs to be chosen.

Distribution pattern of the hits in the layers: The cuts on the basis of hits and layers are indeed the simplest and very effective selection criteria. However, a number of various other parameters have also been studied, to ensure how much they can contribute to improve the purity of the ν_eCC events in the sample. The purity of the ν_eCC events in a sample is the ratio of the number of ν_eCC events to the total number of events in the selected sample.

The behaviour of a ν_e-interaction is certainly different from the other two types of interactions, as far as our physics knowledge is concerned. The presence of the electron/positron makes it stand apart from the NC interactions. The way electrons/positrons lose their energies in the detector is different from the way μ^+/μ^- do. The challenge is to utilize these characteristics in distinguishing ν_e events from ν_μ events in the data from

the ICAL detector.

4.4.4 Maximum Hits Difference

The ν_eCC events contain electromagnetic (EM) showers. They should generate a huge number of hits, but most of them are absorbed by the thick iron layers. However, in some events the shower may start at the edge of the iron layer. In such cases, a sudden and significant increment in the number of hits in the following layer is expected. A schematic diagram of this principle is presented in figure 4.3.

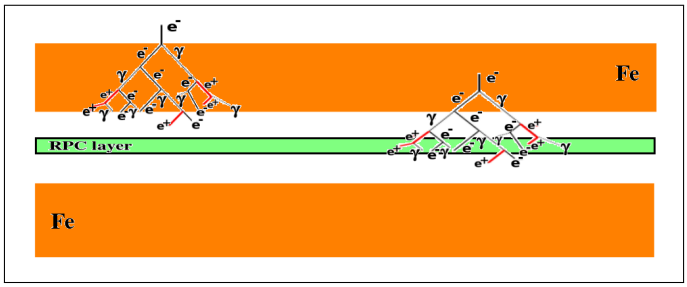

Figure 4.3: Schematic diagram of EM shower in a ν_eCC interaction at the edge of the iron layer.

The difference in the number of hits in two adjacent layers in an event is calculated. This difference is maximized over all such pairs in that event. The value of the maximum difference in hits thus obtained forms our present selection criteria. The distribution is shown in the figure 4.4. The effect of this cut is shown in Table 4.6.

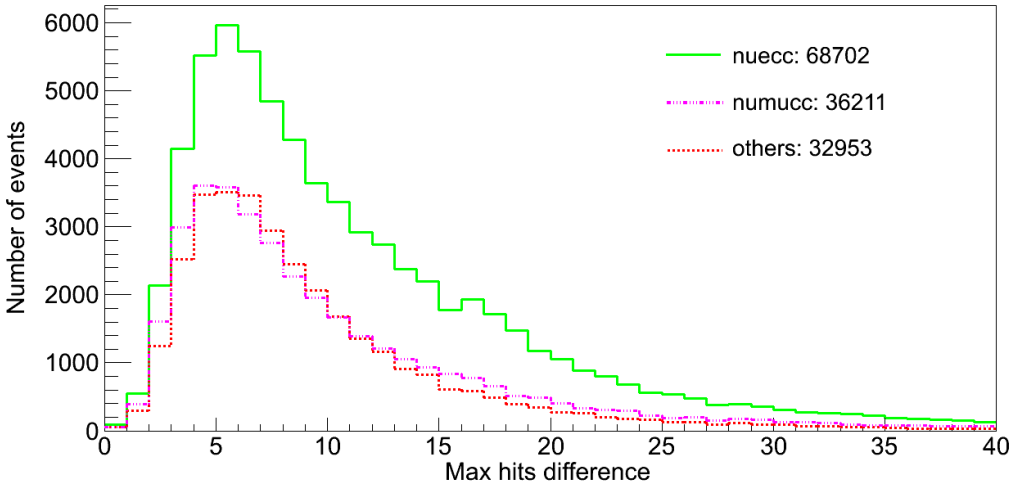

Figure 4.4: Distribution of maximum difference in the number of hits in adjacent layers for events with more than 15 hists in a maximum of 5 layers, for the 500 years NH data. E_ν={0.1,100} GeV.

Selection Criteria	ν_e**CC**	**others**	ν_μ**CC**
h>10; L≤5;	163807	82717	107350
h>10; L≤5; max hits diff.>5	82500	34701	38824
h>15; L≤5;	68702	32953	36211
h>15; L≤5; max hits diff.>5	50295	21844	23991

Table 4.6: Events counts after applying the hits-layers selection criteria and adding the cut on maximum difference in the number of hits in adjacent layers. (500 years NH data in E_ν={0.1,100} GeV.)[**"h"**=#**hits; "L"**=#**Layers**]

This selection criteria helps in improving the ν_eCC events ratio by about 3-4%. However, a simultaneous study of the Nuance MC information shows that the larger hits difference is given by mostly horizontal ν_eCC events.

4.4.5 Comparing the hits in each layer

The number of hits in every individual layer in an event is studied. This criterion, in a way seeks a pattern in the number of hits in adjacent layers. A variety of patterns are assumed and checked with the set of events. Two of them are stated below. The underlying logic still rests on the concept of the EM shower.

Additional hits in the next layer: One of the layers hit is chosen and additional 5 or 6 hits are demanded in the very next layer. All the layers in the event are checked. The event to be selected must have at least one such pair of layers. A lower threshold of 2 layers thus becomes an inherent constraint.

Majority of hits in one layer: One can call this criterion a modified version of the earlier one. According to this criteria, the event must contain 50% or 60% of the total number of hits in a single layer. Therefore, no lower cut on the number of layers is required here.

The effect of the selection cuts are shown in Table 4.7.

Selection Criteria	ν_e**CC**	**others**	ν_μ**CC**	ν_eCC purity %
hits>15; layers≤5;	68702	32953	36211	50
hits>15; layers≤5; $h_L > h_{L\pm1}+5$	47009	21191	22934	52
hits>15; layers≤5; h_L >50% hits	38479	13745	16934	56
hits>15; layers≤5; h_L >60% hits	29123	9038	11948	58
hits>15; layers≤4;	47711	19390	19875	55
hits>15; layers≤4; $h_L > h_{L\pm1}+5$	34399	13308	13868	56
hits>15; layers≤4; h_L >50% hits	32737	10931	12679	58
hits>15; layers≤4; h_L >60% hits	26006	7735	9690	60

Table 4.7: Events counts after applying the hits-layers selection criterion and demanding (i) 5 additional hits in adjacent layers (h_L, $h_{L\pm1}$); (ii) 50-60% of total number of hits in one layer. (500 years NH data in E_ν={0.1,100} GeV.) [**"hits"=total #hits; "h_L"=hits in any of the layers, say the L^{th} layer.**]

The following statement must be remembered for this current section and in those of relevance: If the statistical errors are considered for the event counts, then the corresponding variations in the calculated values of the purity are far less than 1%.

4.4.6 The Overall Distribution Pattern of Hits among the layers

The hits in different layers of the ν_eCC events are non-uniform. The hits are mostly over concentrated in some layers, while entirely sparse in the rest. Although the muonless

events all look like shower, the muon containing low energy ν_μCC events tend to spread out less in the horizontal direction than the ν_eCC events.

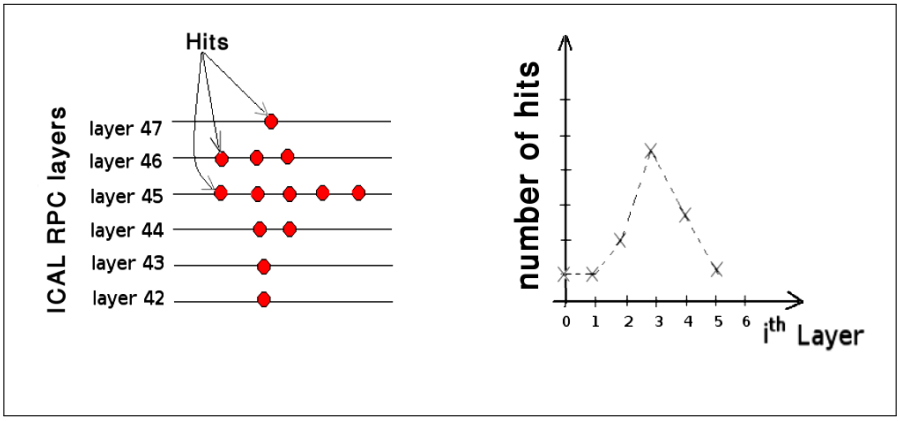

Figure 4.5: Schematic Diagram of hits in the RPC layers

Figure 4.5 shows the hit pattern among various layers in an event (left panel) and the number of hits vs layer number (right panel). For the plot in the right panel, the lowest layer hit is labelled to be **0**, the next **1** and so on. In such a plot, the ν_μCC gives a broader peak than the ν_eCC / NC. Hence, events selected with such sharper peaks should reduce the fraction of ν_μCC events in our sample. This property can be parametrized as either the mean or RMS value of the layerwise hits distribution of each event. However, having studied both the quantities, the cut on the RMS value appeared comparatively more effective. A distribution of the "RMS" values for the data sample with a minimum threshold of 10 hits as shown in figure 4.6.

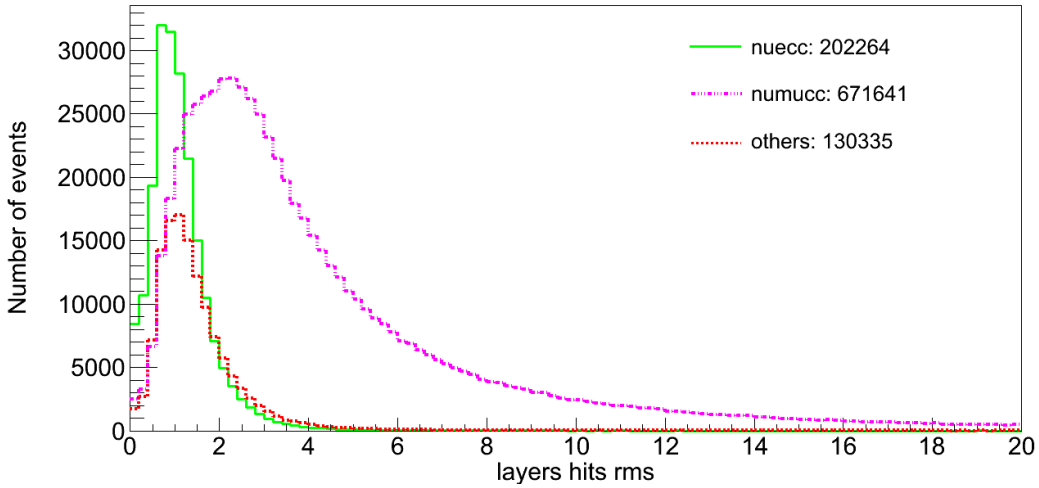

Figure 4.6: Distribution of RMS values for events with more than 10 hits, for the 500 years NH data. E_ν={0.1,100} GeV.

The distributions of the mean values also look similar, and not shown here. Cuts applied on this RMS value possesses tremendous capability to select the ν_eCC events. Some of the results are shown in table 4.8. The cut on the RMS value can even override the so-long-used layers-cut too, as seen in the table 4.8. In fact, even if we implement a lower threshold of minimum 3 layers on our dataset, we can fetch 48% of purity of the ν_eCC sample, with a signal selection efficiency of 59%, background rejection efficiency of 86%, and yet retaining a sample size of 425 events/year. However, other cuts are also mentioned in the table 4.8, which include combinations of multiple selection criteria, with the sole aim of improving on the purity of the sample of the "ν_eCC-like" events.

Selection Criteria	ν_e**CC**	**others**	ν_μ**CC**	ν_eCC purity %
h>15; L≤5;	68702	32953	36211	50
h>15; L≤5; rms<1.2	56254	24916	25431	53
h>15; L≤5; rms<1.2 ; max hits diff.>4	48248	20452	21241	54
h>15; L≤5; rms<1.2 ; max hits diff.>6	39610	15585	16969	55
h>10; L≥3	174192	122547	662836	18
h>10; L≥3; rms<1.2	102657	51762	58176	48
h>10; L≤4;	125321	56177	62113	51
h>10; rms<1.2	130226	59387	66843	51
h>10; L≤4; rms<1.2	111858	47961	52860	53
h>10; L≤4; rms<1.2; max hits diff.>3	86157	35115	37026	54
h>10; L≤5; rms<1.2; max hits diff.>3	99814	43409	46455	56
h>10; mean<2; rms<1.2; max hits diff.>3	83954	35130	36127	54
h>10; mean<2; rms<1.2; max hits diff.>5	60959	23063	24129	56
h>10; mean<2; rms<1.2; max hits diff.>5; hpl>4	51249	18247	18922	58

Table 4.8: Events counts after applying the hits-layers selection criteria; adding the cut on the variance of the mean of the vertical distribution of hits in layers, i.e. rms; the criteria of max hits diff. is included for a further improvement. (500 years NH data in E_ν={0.1,100} GeV.) [**"h"=#hits; "L"=#Layers; "hpl"=avg hits/layer.**]

The beauty of this selection criterion, lies in the fact, that it shows a good efficiency in selecting the signal, i.e. the ν_eCC events, while improving the purity too. The RMS cut appears quite effective in improving the ratio. In fact, the cut on the maximum difference in the hits further helps in improving the results. Therefore, one can obtain a $\sim$55% ν_eCC events purity, with a moderately large sample size.

Other Selection Criteria: The criteria described above are the most effective ones. However, a few other competent selection criteria which we devised in the process, are enlisted as follows.

4.4.7 Maximum horizontal Spread:

The energy distribution of the events selected with the hits and layers criteria, is studied using the information from NUANCE. It shows that the ν_μCC selected are due to either the low energy muons or the quite energetic near-horizontal muons. The energetic, near horizontal muons travel larger distances. This implies these events must have a larger maximum horizontal spread than the ν_eCC or the NC events.

So the maximum horizontal spread of the events may also work as a selection criteria. The horizontal spread of an event can be defined in a number of ways. Here three of such ways are described.

- **Maximum separation between two hit points in a layer:** A hit point refers to the pair of (x,y) coordinates of the hit/signal in an RPC. The signals from the detector are read as the strip numbers along the X or Y direction. Hence, the so-called hit points are devised by making all possible combinations of the signal giving X-Y strip numbers. Now, the distance between any two points are given by the standard definition:

  D = $\sqrt{((x_2 - x_1)^2 + (y_2 - y_1)^2)}$; for every hit (x_i,y_i) in a layer.

  The largest value of D in a layer is compared with the same in all the other layers.

The maximum value of D thus obtained finally is our required selection parameter.

- **Maximum distance in either x or y direction:** This refers to the distance between the farthest strips hit in an RPC. The separation between the extreme x-strip numbers is calculated in a layer. The same is done for the y direction. In mathematical terms, it is as follows:

  D = $|(x_{leftmost}\text{-}x_{rightmost})|$ or D = $|(y_{leftmost}\text{-}y_{rightmost})|$; x,y $\in$ in the same layer.

  The larger value out of these is considered the maximum separation in that layer. This value is compared with that for all the layers in an event. The final maximum value is the selection parameter.

- **Maximum x or y projection on the horizontal plane:** In the above two criteria, the x or y strip numbers were in the same layer. This criteria almost mimics the second bullet point, except the fact that the x or y strips are not restricted to the same layer. It is the farthest-most separation between either the x or the y strips among all the layers hit in an event.

  D = $|(x_{leftmost}\text{-}x_{rightmost})|$ or D = $|(y_{leftmost}\text{-}y_{rightmost})|$; x,y $\in$ in any layer.

  This can be also interpreted as the maximum x or y projection on the x-y plane.

The distributions of all the above three parameters have been observed. As expected, the horizontal spread for the ν_μCC events is slightly more than the rest of the event types considered. Corresponding upper threshold cuts are applied on the horizontal spread. There is marginal difference found between the results obtained by using the three above defined selection parameters. The third selelection criteria of x/y projection however appears slightly better than the other two. Also, it must be noted that it deals with the X or Y strip numbers exclusively.(Hence, the second and the third criteria does not include any ghost hit, i.e., any false combination of the X and Y strip numbers.) Table 4.9 shows the effectiveness of this selection criteria.

Selection Criteria	ν_e **CC (NH evts)**	**others (NH evts)**	ν_μ **CC (NH evts)**
#hits>15; #layers≤5	60613	24084	30490
#hits>15; #layers≤5; distance<100 strips	57001	23203	21105
#hits>15; #layers≤4	42576	14574	16465
#hits>15; #layers≤4; distance<110 strips	40087	11104	14068

Table 4.9: Checking the effect of the cuts on horizontal spread (x or y projection), i.e. "distance" added to the above selection criteria on the Geant output of the NH 500years data files. (500 years NH data E_ν={0.8, 20} GeV.)

However, as can be noted from the table 4.9, the cut on the horizontal spread marginally improves the ν_e CC fraction in the selected sample. In other words, this criteria does not bring any drastic improvement to add to the hits/layers selection criteria.

4.4.8 Maximum diagonal Condition:

As already stated earlier, the ν_μ CC events mostly have muons travelling comparatively larger distances than the ν_e CC or the NC events. The criteria of horizontal spread has already been discussed in the earlier section. Here, the total distance between two hits is to be calculated, irrespective of whether they are in the same layer or not. This has been done in two different perspectives.

- **Maximum total distance:** The distance calculated here is similar to the first point in the earlier section, except the fact that the (x_i,y_i) and (x_j,y_j) values may not belong to the same layer.

  D = $\sqrt{((x_2 - x_1)^2 + (y_2 - y_1)^2)}$; for every hit (x_i,y_i) in any layer.

  It can also be interpreted as the projected length of the largest diagonal between two hits in the event. The maximum value of this distance in an event serves as our selection parameter.

- **Maximum vertical (z-direction) spread:** The maximum total distance as described in the just earlier point is calculated. The difference in the z-coordinates or layer numbers corresponding to these two hit points is calculated and is called "maxz". This maxz is expected to be the maximum for the ν_μ CC events, rather hardly less than the number of layers hit. Hence, in principle, demanding events with maxz less than the number of layers, should reduce the selection of ν_μ CC events.

The effect of the above two selection cuts are tabulated in table 4.10.

Selection Criteria	ν_e **CC**	**others**	ν_μ **CC**	**Total**
NH #hits>15; #layers<=4; distance<110 strips	39763	13973	9689	63425
NH #hits>15; #layers<=5 distance<100 strips	56435	22950	17806	97191
NH #hits>15; #layers<=4; maxz<#layers	39616	13555	15287	68458

Table 4.10: Events counts after applying the hits-layers selection criteria and cuts on maximum diagonal projection as well as the z-spread of the maximally distant hit points in an event. (500 years NH data E_ν={0.8, 20} GeV.)

4.4.9 Concentration of hits in adjacent layers:

The ν_eCC events consist of EM showers, unlike the other two types of events. The em shower can hardly be identified due to the thick iron layers. Inspite of this the excess in the number of hits can still be noticed, in comparison to the NC events. This fact inspires us to check, if a selection criteria based on the concentration pattern of the hits might be effective.

A ν_eCC event is expected to have most of its hits concentrated in the first few layers. So we suppose, the number of hits in 3 adjacent layers at any of the extreme ends of the event sums up to 60% of the total number of hits in that event. Such events are to be selected by this present criteria. The effect of this cut is tabulated in table 4.11.

Selection Criteria	ν_e **CC**	**others**	ν_μ **CC**
#hits>15; #layers<=4; #hits in 3 adj.L≥60%	33214	12590	14075
#hits>15; #layers<=5; #hits in 3 adj.L≥60%	51165	22037	27951
#hits>15; #layers<=4; #hits in 3 adj.L≥60%; max. hori.spread< 100**strips**	31206	11998	8092

Table 4.11: Events counts after applying the hits-layers selection criteria and putting the condition of 60% of the hits to be confined in the extreme 3 adjacent layers. (500 years NH data E_ν={0.8, 20} GeV.)

This selection criteria slightly improves the ν_eCC counts in the selected sample. This is due to the fact that a lower threshold of 3 layers becomes mandatory in this criteria. The ν_eCC events are more concentrated in the less number of layers. In fact, adding

the cut of maximum horizontal spread adds to improving the ν_eCC signal ratio. Hence, though the criteria looks an effective one, but has a drawback of reduced ν_eCC sample.

4.5 The NC events fraction

Our primary/main focus in this paper is to obtain a ν_eCC rich sample of neutrino events at ICAL. So, the selection cuts so far have been favoring ν_eCC events. However, the NC events fraction can also be enhanced comparatively.

The cuts are based on the simplest criteria of hits and layers. However, the hardware threshold to be put in ICAL for accepting NC events must be taken into account. This requires a trigger algorithm different from that for the muon track-containing events.

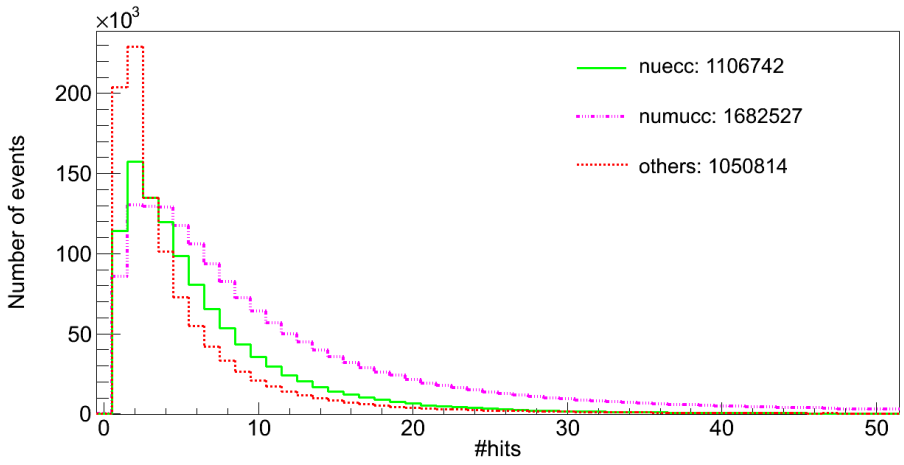

Figure 4.7: Distribution of number of hits for all non-zero hit events with E_ν = {0.1,100} GeV for 500 years of NH data.

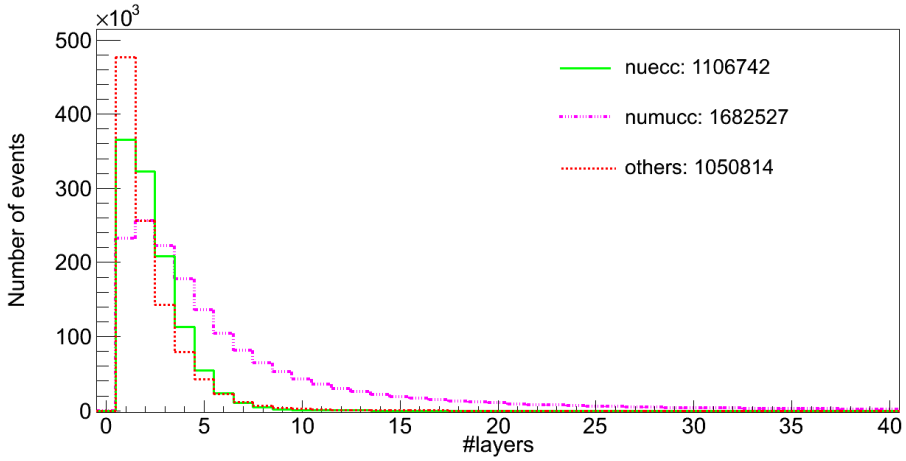

Figure 4.8: Distribution of number of layers which received one or more hits in an event, E_ν = {0.1,100} GeV for 500 years of NH data.

The NC events give mostly very few hits, and are confined in very few layers, see figures 4.7 and 4.8. So, to obtain a NC events rich sample, one might be tempted to put an upper threshold on the number of hits. But, to deal with such a small number of hits in an event, sub-GeV neutrinos should be accounted too. So, the dataset including neutrinos with E_ν = {0.1,100} GeV is the appropriate one.

Selection Criteria	ν_e**CC (NH evts)**	**others (NH evts)**	ν_μ**CC (NH evts)**	NC purity %
0<hits≤10 (only)	903904	920172	1009961	32
0<hits≤10; layers≤2	659926	724065	478480	39
0<hits<4 (only)	406705	568177	345322	43
0<hits<4; layers≤2	397895	558109	321648	44
0<hits<4; layers = 1	287799	436263	198539	47
4≤hits≤10; layers = 1	70330	38360	31046	27

Table 4.12: Enhancing NC fraction: events counts after applying the selection cuts on the Geant output of the NH 500 years data files in E_ν={0.1,100} GeV

The NC counts in the selected sample are almost equal to the sum of the selected ν_eCC and the ν_μCC events. The NC events have a very small number of hits in general. The cuts used earlier demanded a minimum of 10 hits and hence discriminated against the NC events. The dominance of the NC events can be gradually realized in case of events having 10 hits or less, as shown in Table 4.12.

If we demand number of hits $\leq$ 3 and 1 or 2 layers, we get the event samples shown in Table 4.12, which are quite rich in NC events. If the noise is kept under control, such events can be used to study mixing with sterile neutrinos. Trigger efficiency will play a major role in selecting such events. In fact, it has been checked that a sample of single hit events has more than 50% of NC events. But obviously, just one-hit is an unacceptable criteria. Therefore, the selection cuts will have to be redesigned entirely, to obtain a NC events sample with a significant purity.

4.6 Inference of the Selection Principle

The selection criteria to be finally chosen depends on the requirements of the physics study. One might insist on the maximum possible purity of the ν_eCC events, even compromising the vertical events fraction or small sample size. The effects of the most important selection cuts, based on hits and layers, are summarized below. One can visualize the status of the NC or the ν_eCC events majority in the figures 4.9 and 4.10 respectively. The neutrino energy range is {0.1,100}GeV. The selection criteria represented along the X-axis are mentioned in the tables 4.13 and 4.14.

X-axis: seln.#	hcut1	hcut2	Lcut
1	0	3	5
2	3	10	5
3	0	3	4
4	3	10	4
5	0	3	3
6	3	10	3
7	0	3	2
8	3	10	2
9	0	3	1
10	3	10	1

Table 4.13: **0-10 hits region:**List of Selection cuts in Table 15. Cuts: hcut1<#hits≤hcut2 and #Layers==Lcut. The events are from NH 500 years data files in E_ν={0.1,100} GeV

X-axis: seln.#	hcut1	hcut2	Lcut
1	10	15	5
2	15	20	5
3	20	25	5
4	25	30	5
5	30	35	5
6	35	40	5
7	40	50	5
8	50	100	5
9	10	15	4
10	15	20	4
11	20	25	4
12	25	30	4
13	30	35	4
14	35	40	4
15	40	50	4
16	50	100	4
17	10	15	3
18	15	20	3
19	20	25	3
20	25	30	3

X-axis: seln.#	hcut1	hcut2	Lcut
21	30	35	3
22	35	40	3
23	40	50	3
24	50	100	3
25	10	15	2
26	15	20	2
27	20	25	2
28	25	30	2
29	30	35	2
30	35	40	2
31	40	50	2
32	50	100	2

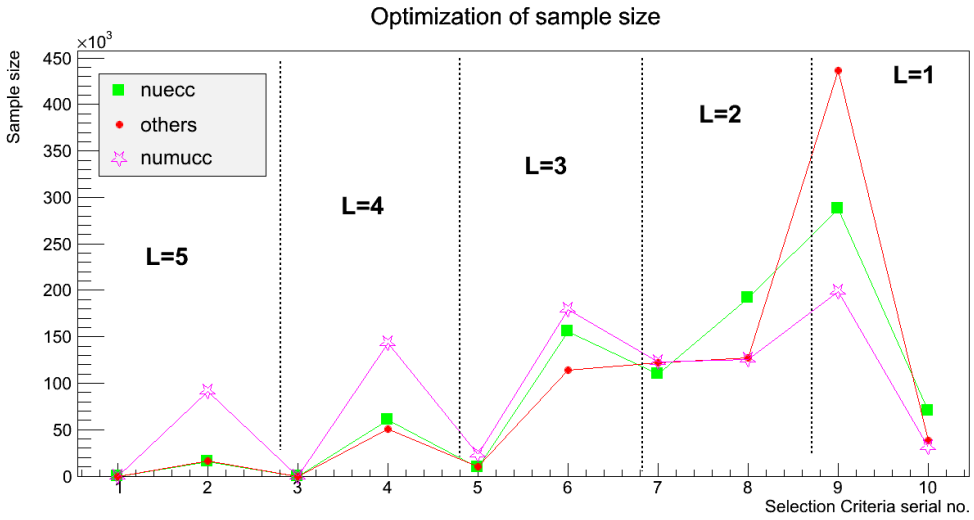

Figure 4.9: **0-10 hits region:** Surviving events-composition chart after applying varrying cuts on the number of hits and layers in the event for the 500 years NH data. E_ν={0.1,100} GeV. The serial numbers along X-axis, which are related to different hits and layers cuts, are explained in table 4.13.

Figure 4.9 shows the dominance of the NC or the ν_μCC events in the domain of 0-10 hits. Hence, a lower threshold of 10 hits has been appropriate for obtaining the ν_eCC pure sample. The figure 4.10 refers to events in the beyond-10-hits domain.

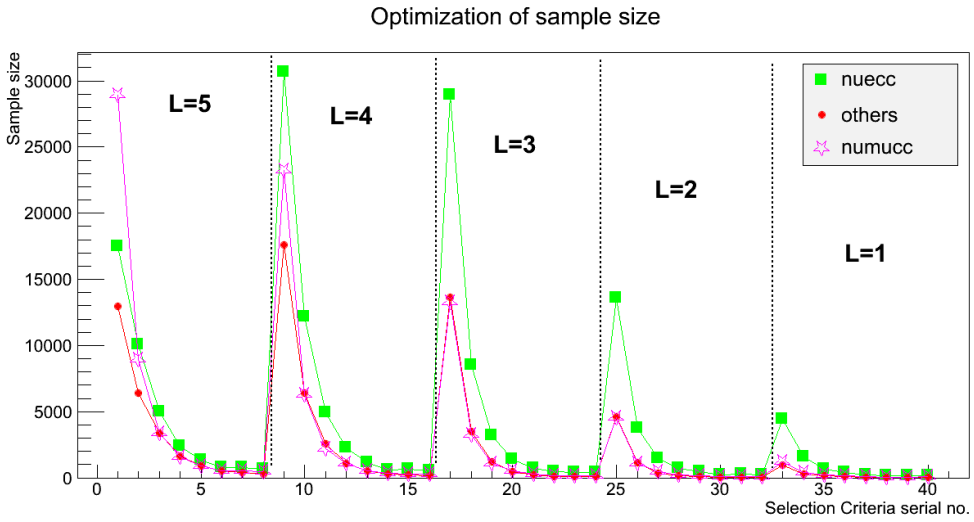

Figure 4.10: **10-100 hits region:** Surviving events-composition chart after applying varrying cuts on the number of hits and layers in the event for the 500 years NH data. E_ν={0.1,100} GeV. The serial numbers along X-axis, which are related to different hits and layer cuts, are explained in table 4.14.

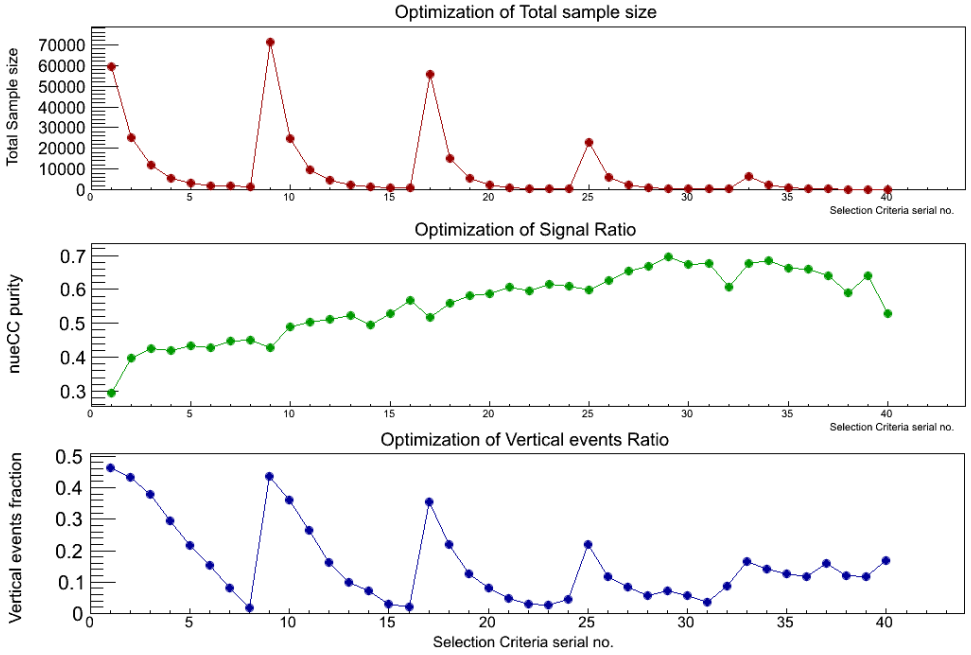

Figure 4.11: The contrasting effect of the purity of the ν_eCC events with the size of the selected sample and the fraction of vertical events in the selected sample. The serial numbers along X-axis, which are related to different hits and layer cuts, are explained in table 4.14.

The Selection cuts used in the figures are listed in table 4.13 and 4.14. The Selection criteria, as plotted along the X-axis contain a upper and lower hits cut, and a certain number of layers. Therefore, each of them are mutually exclusive to each other and one might choose a combination favorable to one's purpose of study. The hits region 0 to 10 which is an NC dominated one, is plotted in figure 4.9 and the cuts listed in table 4.13. The hits region 10 to 100 is dominated by the ν_eCC events. This is portrayed in figure 4.10 and the cuts enlisted in table 4.14 The lines in figures 4.9 and 4.10 connect events of a particular type. They just show the change in the number of events of a particular type due to a change in the cut parameters.

The cuts on the hits and the layers are the most important primary criteria. Effects of additional criteria have been mentioned in the previous subsection, and will be inferred at the end of this chapter. Figure 4.11 portrays the effect of these primary cuts. The serial numbers along X-axis are the selection cuts listed in tables 4.13 and 4.14.

4.7 ν_eCC and NC events as background to ν_μCC events

As already explained early in this chapter and the report, ICAL is mainly designed to look for ν_μCC events with reconstructable muon trajectories. This is to inspect the hierarchy dependent effects in the μ^+ and the μ^-s. In other words, events with a muon track are the primary data for the ICAL, especially those within the range E_ν={0.8,20} GeV. The ν_μCC events detected at ICAL must pass through (i.e. give hits in) a minimum number of layers (5 or 6), so that the muon track can be well reconstructed. This layer cut will undoubtedly select mostly ν_μCC events. However, some ν_eCC and NC events also will pass this cut and form potential background to the ν_μCC events sample. The present section aims to estimate the upper limit on this background.

As shown in Table 4.15, out of all the generated events, about 20% of the "others" do not give any hit in the ICAL. For ν_eCC and ν_μCC events, this fraction of "undetectable" events is about 5%. The layers distribution of each type of detectable events is shown in

figure 4.8.

Selection Criteria	ν_e**CC**	**others (NC+**ν_τ**CC)**	ν_μ**CC**
all generated events	676014	820854	1103263
#events with hits>0 in ICAL	649487	678590	1087709

Table 4.15: Events counts before applying the selection cuts on the Geant output of the NH 500 years data files in E_ν={0.8,20} GeV.

Since reconstructable ν_μCC events demand a minimum number of layers to be hit, the distributions for two different layer-cuts are shown in Table 4.16. This feature of large suppression of the ν_eCC and NC events with this cut is evident in figure 4.8.

Selection Criteria	ν_e**CC**	**others (NC+**ν_τ**CC)**	ν_μ**CC**
#events: L≥5	84115	73849	683635
	∼10%	∼9%	∼81%
#events: L≥6	35678	37031	579760
	∼5%	∼6%	∼89%

Table 4.16: Events counts after applying the selection cuts on the Geant output for the 500 years of NH data with E_ν={0.8,20}GeV.

4.8 A Comment on the purity of the ν_eCC events in the muonless sample

A Nuance based analysis of the selected events has been done to understand the compostion of the selected events. Three types of interactions are looked into. Among Quasi

Elastic (QE) interactions, the ratio of the ν_eCC to the background is 3:1. Among Resonant Scattering (RS) interactions, the ratio of the ν_eCC to the background is 2:1. Among Deep Inelastic Scattering (DIS) interactions, the ratio of the ν_eCC to the background is 1:1.

The number of QE events are very less in comparison to the other two types. Therefore, in the final sample of selected events, the ratio of the ν_eCC to the background is $\sim$3:2.

4.9 Contribution ν_eCC to determination of neutrino mass hierarchy

In this section, we search for the presence of matter effects in muonless events for hierarchy discrimination. Eventhough, muonless events are striaght forward to identify, identifying their energy or direction is a great challenge. Thus the effect of muonless events on the hierarchy is expected to be much smaller compared to that of the muon events. Nevertheless, we pursued this study with the hope of improving the hierarchy sensitivity of ICAL.

4.9.1 Physics motivation

The matter effect modifies neutrino oscillation probabilities. For long pathlengths ($L \geq$ 5000) km and moderately large energies (5GeV $\leq E_\nu \leq$ 10GeV), both $P(\nu_\mu \rightarrow \nu_\mu)$ ($P_{\mu\mu}$) and $P(\nu_e \rightarrow \nu_\mu)$ ($P_{e\mu}$) can have a change as large as 40%, leading to an observable change in the muon event rate due to matter effects. By measuring this change, it is possible to determine the neutrino mass hierarchy. The oscillation probabilities involving ν_e, $P(\nu_e \rightarrow \nu_e)$ (P_{ee}) and $P(\nu_\mu \rightarrow \nu_e)$ ($P_{\mu e}$), also undergo large changes due to matter effects. The spectrum of the electron events is given by

$$\frac{dN_e}{dE_\nu} = \left[\frac{d\Phi_e}{dE_\nu}P_{ee} + \frac{d\Phi_\mu}{dE_\nu}P_{\mu e}\right]\sigma_\nu.$$

Since muon neutrino flux $d\Phi_\mu/dE_\nu$ is twice the electron neutrino flux $d\Phi_e/dE_\nu$ and the change in $P_{\mu e}$ is half the change in P_{ee}, the effect of these large changes largely cancel each other out in the electron event sample. This fact makes finding matter effects in muonless events even more challenging.

The earlier section suggests that it is possible to have a ν_eCC events rich sample, with proper selection cuts. The background comprises of ν_μCC events and the NC events. The NC set is unafffected by oscillations. The ν_μCC events which get selected are devoid of any distinct muon track. The effect of oscillations is however averaged to nil, over wide range of energy or direction for ν_μs. So, the effect of oscillations in matter studied on this events sample, is mostly due to the ν_eCC events.

The vertical or near vertical neutrinos travel longer distance through the earth. So, the matter effects are expected to be seen to the maximum extent, in mostly vertical events, surely upward. However, unfortunately enough, the selection criteria chosen so far, as reported in section above excludes a significant percentage of the vertical events. Therefore, the following study reflects the minimum possible information that can be extracted from these muonless events.

	# ν_e**CC events**	**other events**	# ν_μ**CC events**
NO OSC.	1111704 (1248308)	1029441 (1472677)	2370977 (2499685)
NH	1106742 (1240412)	1050814 (1492906)	1682527 (1764509)
IH	1101155 (1234901)	1052781 (1494688)	1681448 (1763191)

Table 4.17: Detectable events counts from the Geant output of the Nuance data files, i.e., events with non-zero hits at the ICAL@INO detector. The total number of events generated are inside the braces. E_ν=**{0.1,100} GeV**.

Therefore, the following studies have eventually been done with neutrinos in the energy range E_ν={0.1,100} GeV.

4.9.2 The Generated Events Sample

The data files from Nuance, in the energy range E_ν={0.1,100} GeV are fed into the Geant4 INO ICAL code to get the events sample for the following studies. The neutrino oscillations have been applied using the normal and the inverted mass hierarchy parameters, which are denoted as NH and IH respectively. The oscillation parameters used are as follows: $\Delta m^2_{21} = 7.5 \times 10^{-5}$ eV^2, $\Delta m^2_{31}(NH) = 2.51 \times 10^{-3}$ eV^2, $\Delta m^2_{31}(IH) = -2.43 \times 10^{-3}$ eV^2, $\sin^2\theta_{12} = 0.31$, $\sin^2 2\theta_{13} = 0.09$, $\sin^2\theta_{23} = 0.5$ and $\delta_{CP} = 0$.

We will bin the events in terms of their hits and layers, as they indirectly give an estimate of the neutrino energy. This dependence is investigated in details in the next section. As a firsthand estimation, we checked the events counts for the NH and the IH case, by dividing the selected sample in two bins and then 15 bins, as the finest possible

and acceptable binwidth.

The 2-BIN Sampling:

The total sample is found to be best selected when done in two bins of different hits range. The criteria for the two are different and best optimized for that hits range.

The **normal mass hierarchy(NH)** oscillated set of events are in table 4.18.

Selection Criteria	ν_e**CC (NH evts)**	**others (NH evts)**	ν_μ**CC (NH evts)**
15<#hits≤25; #layers≤5	51144	25358	27232
10<#hits≤15; #layers≤4; hits/layer≥3.5	55984	24108	24667

Table 4.18: Events counts after applying the selection cuts on the Geant output of the NH 500years data files

The corresponding set for the **inverted mass hierarchy(IH)** oscillated events is in table 4.19.

Selection Criteria	ν_e**CC (IH evts)**	**others (IH evts)**	ν_μ**CC (IH evts)**
15<#hits≤25; #layers≤5	49818	25235	26975
10<#hits≤15; #layers≤4; hits/layer≥3.5	55317	23643	24510

Table 4.19: Events counts after applying the selection cuts on the Geant output of the IH 500years data files

The selection strategy appears effective enough to separate out the ν_eCC events from the NC events. The counts in the NH and the IH case also stand apart from each other in the corresponding bins.

The 15-BIN Sampling:

Particles with higher energies give more hits in the detector. Hence, we take the number of hits to be a measure of the energy. Since the oscillation probabilities are functions of energies, it makes more sense to classify the events to a larger number of energy or hits bins. The flux of atmospheric neutrinos is very high at lower energies ∼1-2 GeV, and falls rapidly with the increase in energy. So a minimal cut on the number of hits is applied.

Events with number of hits less than 20 are divided into small bins of width: 1 hit, while those above 20 to 40 are put into bins of 5 hits. The rest of the events above 40 hits account as all-in-one bin. A lower cut to exclude all events with 10 hits or less, is set as a threshold to reduce the number of NC events. Hence, the total sample is divided into

15 exclusive hits ranges. The events counts after applying the chosen selection criteria for both NH and IH cases are listed in table 4.20 and 4.21.

Selection Criteria	ν_e**CC (NH evts)**	**others (NH evts)**	ν_μ**CC (NH evts)**	**Total (NH evts)**
h=11; hpl≥3.5	15248	6496	6661	28405
h=12; hpl≥3.5	11199	4652	4566	20407
h=13; hpl≥3.5	8737	3507	3284	15528
h=14; hpl≥3.5	11552	5265	5874	22691
h=15; hpl≥4.0	5193	1990	1899	9082
h=16; hpl≥4.0	7486	3388	3305	14179
h=17; L≤4	6129	2642	2614	11385
h=18; L≤4	4903	2143	2046	9092
h=19; L≤5	5763	2826	3071	11660
h=20; L≤5	4944	2369	2509	9822
21≤h≤25; hpl>4.0	15688	8103	7866	31657
26≤h≤30; hpl>5.0	7142	3415	3546	14103
31≤h≤35; hpl≥6.0	3920	1720	1907	7547
36≤h≤40; hpl>7.0	2171	961	1177	4309
h≥40; hpl>11.5	3219	974	1994	6187

Table 4.20: Events counts after applying the selection cuts on the Geant output of the **NH** oscillated 500years data files (**h**=number of hits in an event; **L**=number of layers hit in an event; **hpl**=average hits per layer)

Selection Criteria	ν_e**CC (IH evts)**	**others (IH evts)**	ν_μ**CC (IH evts)**	**Total (IH evts)**
h=11; hpl≥3.5	15041	6395	6522	27958
h=12; hpl≥3.5	11177	4647	4567	20391
h=13; hpl≥3.5	8527	3421	3342	15290
h=14; hpl≥3.5	11537	5225	5580	22342
h=15; hpl≥4.0	5033	1857	1854	8744
h=16; hpl≥4.0	7340	3365	3216	13921
h=17; L≤4	5959	2723	2584	11266
h=18; L≤4	4862	2064	2050	8976
h=19; L≤5	5785	2833	2982	11600
h=20; L≤5	4704	2385	2465	9554
21≤h≤25; hpl>4.0	15069	7816	7846	30731
26≤h≤30; hpl>5.0	7212	3484	3508	14204
31≤h≤35; hpl≥6.0	3707	1824	1893	7424
36≤h≤40; hpl>7.0	2132	941	1106	4179
h≥40; hpl>11.5	3176	1034	2111	6321

Table 4.21: Events counts after applying the selection cuts on the Geant output of the **IH** oscillated 500years data files. (**h**=number of hits in an event; **L**=number of layers hit in an event; **hpl**=average hits per layer)

4.9.3 Calculation of the mass hierarchy χ^2 value:

The mass hierarchy χ^2 value is calculated according to the Gaussian method:

$$\chi^2 = \frac{(\#NHevts - \#IHevts)^2}{(\#NHevts)} \tag{4.1}$$

4.9.4 The Average Mass Hierarchy (MH) χ^2

Due to MC statistical fluctuations, if we simulate the NH events twice, with two different seeds, the χ^2 between these two event samples will be non-zero. In fact, this $\chi^2_{\text{true}} = \chi^2(NH1 - NH2)$ will be approximately twice the number of bins. In addition, we calculate $\chi^2_{\text{false}} = \chi^2(IH - NH)$. If the NH is the true hierarchy, then we expect χ^2_{false} to be appreciably greater than χ^2_{true}.

To minimize the overall effect of MC fluctuations, we do our calculations for very large statistics and scale them down to 10 years. Here we consider data for 500 years. We have simulated the data for NH with three different seeds and similarly for IH. Thus, we have six values of χ^2(true) and nine values of χ^2(false). We take the average of each and define the average χ^2 as:

$$< \chi^2 > = < \chi^2_{false} > - < \chi^2_{true} > \tag{4.2}$$

The numbers of the ν_eCC and the ν_μCC events generated for each of the files generated with different seeds are listed in table 4.22.

Sample ID	**NH ν_eCC**	**NH ν_μCC**	**IH ν_eCC**	**IH ν_μCC**
seed 1	676014	1103263	671309	1103667
seed 2	674971	1103879	670827	1105891
seed 3	675963	1102817	669664	1104746

Table 4.22: The ν_eCC and ν_μCC events count for 500 years of Nuance data, before interacting with the ICAL detector. Here, the counts for only the energy range E_ν={0.8,20} GeV is shown, since it makes the major contribution to the value of χ^2.

4.9.5 Calculation of Average χ^2 assuming Normal Hierarchy (NH)

The events are simulated in the energy range E_ν={0.1,100} GeV, for both NH and IH, each with three different seeds. For analysing the hierarchy information inherent in the muonless events, we need a selected sample rich in mostly vertical ν_eCC events. A further study of the above selection criteria has shown that efforts to increase the purity of the ν_eCC events result in a simultaneous depletion in the fraction of vertical events in the sample. Hence, we apply some straightforward cuts to optimize between the purity and the vertical events fraction of the ν_eCC events. We select a sample with hits (h), layers (L), and hits/layer (hpl) cuts as stated here: 11≤h≤14, hpl≥3.5; 15≤h≤16, hpl≥4; 17≤h≤18, L≤4; 19≤h≤20, L≤5; 21≤h≤25, hpl≥4; 26≤h≤30, hpl≥5; 31≤h≤35, hpl≥6; 36≤h≤40, hpl≥7; h>40, hpl≥11.5. The number of events in each bin is already tabulated in table 4.20 and 4.21.

To compare the distributions of these events, we sort them into a number of bins. We consider four different binning schemes to compare the values of $< \chi^2 >$ they finally lead to. They are briefly discussed as follows:

- 1-bin scheme: The events are all contained in one single bin. Each of these events must have a minimum of 11 hits and be confined in 4 or less layers.

- 3-bin scheme: The selected sample is divided into 3 bins, based on the number of

hits. The events in the first bin should have a minimum of 11 hits but $\leq$ 20 hits. The second bin covers the range of 21 to 40 hits, while events with 40 to 100 hits are put in the third bin.

- 10-bin scheme: The events are classified into 10 uniformly divided bins in the hits range 11 to 100.
- 15-bin scheme: The hits range 11 to 20 is divided into 10 bins. The events giving hits from 21 to 40 are grouped under 4 uniform bins. The fifteenth bin comprises the events giving more than 40 hits.

We expect the $< \chi^2 >$ to increase as the number of bins increases, until a saturation value is reached.

The values for χ^2_{true} are shown in Table 4.23. Table 4.24 contains the values of χ^2_{false}.

Sample pairs	χ^2_t (1)	χ^2_t (3)	χ^2_t (10)	χ^2_t(15)
NH2-NH1	2	6	10	30
NH3-NH1	1	3	9	27
NH3-NH2	1	9	18	17
IH2-IH1	3	9	14	44
IH3-IH2	0	14	23	22
IH3-IH1	2	7	19	47
Average	2	8	16	31

Table 4.23: Values of χ^2_{true} or χ^2_t from the three+three possible combinations of NH and IH datasets, using four different binning schemes. The number of bins is indicated in the first row.

Sample pairs	χ^2_f (1)	χ^2_f (3)	χ^2_f (10)	χ^2_f (15)
NH1-IH1	44	55	72	82
NH1-IH2	26	29	46	62
NH1-IH3	39	39	50	70
NH2-IH1	27	29	43	50
NH2-IH2	13	14	31	63
NH2-IH3	23	28	39	54
NH3-IH1	35	53	80	74
NH3-IH2	19	23	45	67
NH3-IH3	30	33	50	60
Average (all)	28	34	51	65

Table 4.24: Values of χ^2_{false} or χ^2_f from the nine possible combinations of NH and IH datasets. The number of bins is indicated in the first row.

In Table 4.25, we have listed $< \chi^2 > = < \chi^2_{false} > - < \chi^2_{true} >$ and the standard deviation in $< \chi^2 >$. This standard deviation ($\sigma(< \chi^2 >)$) is simply the sum of the standard deviations from the mean values of χ^2_{true} and χ^2_{false}.

hits binning	$< \chi^2 >$ 500 yrs	$\sigma(< \chi^2 >)$ 500 yrs	$< \chi^2 >$ 10 yrs
1	26	10	0.5
3	26	16	0.5
10	35	20	0.7
15	34	20	0.7

Table 4.25: Average χ^2 and standard deviation for different binning schemes.

A cosθ binning, following the raw hits method by Lakshmi et al. was also attempted, the final values shown in table 4.26. However it provides no additional help in the present study.

hits x cosθ binning	$<\chi^2>$ 500yrs	$\sigma <\chi^2>$500 yrs	$<\chi^2>$ in 10 yrs
10x10	37	42	0.7
15x10	35	45	0.7

Table 4.26: Values of average χ^2 with standard deviation as the error in varying number of bins. The two rows refer to (a) 10 hits bins x 10 cos θ bins; (b) 15 hits bins x 10 cos θ bins. The values are also scaled down to 10 years.

In the above calculations, we assumed that NH is true. The results for the case where IH is true are very similar.

4.9.6 Physics Confirmation from Fluctuationless Sample:

The presence of the MC fluctuations is very much evident in the event samples generated by Nuance. So, one must exclusively confirm the presence of effects due to matter oscillations in a fluctuationless sample of ν_eCC events.

Generation of the Fluctuationless Sample:

Initially, a 500 years data sample is generated using Nuance without any oscillation and a unitary mixing matrix. This gives us a 500 years unoscillated ν_μ sample and a 500 years unoscillated ν_e sample simultaneously. A duplicate of this pair is prepared, by interchanging the muon/ν_μ labels to electrons/ν_e labels and electrons/ν_e labels to muons/ν_μ labels respectively. The former is called the tagged ν_e set and the latter is called the tagged $\nu_\mu$set. Both the pairs of datasets are simulated using the GEANT4 ICAL code, to save time. Now the oscillated set of events are produced from these four

sets using acceptance/rejection method. As for example, the oscillated ν_μ events set is assembled by:

- Calling an event from the original ν_μ set and calculating its survival probability $P_{\nu_\mu \to \nu_\mu}$.
- Drawing a random number in {0,1}, say r.
- If r is less than $P_{\nu_\mu \to \nu_\mu}$, that event is accepted, otherwise rejected.
- Calling an event from the tagged ν_μ set and calculating its oscillation probability $P_{\nu_e \to \nu_\mu}$.
- Drawing again a random number in {0,1}, say r_1.
- If r_1 is less than $P_{\nu_e \to \nu_\mu}$, that event is accepted, otherwise rejected.

The oscillated set of ν_e events are also produced in the similar fashion. Thus the NH and the IH set of neutrino events are produced from the same set using oscillation parameters for Normal Hierarchy and Inverted Hierarchy respectively. This implies, the difference between the NH dataset and the IH dataset is completely due to the oscillation process and not any MC fluctuations.

Verification of the Oscillation Probability Calculating Code:

A cpp code is devised to calculate the oscillation probability for a given sign ($\nu/\bar{\nu}$), energy and direction of a neutrino. The algorithm is the same as followed by Nuance to calculate a value of oscillation probability. The well-functioning of the code is verified by generating the oscillation probability as a function of neutrino energy at different values of "L". One of them is shown in figure 4.12.

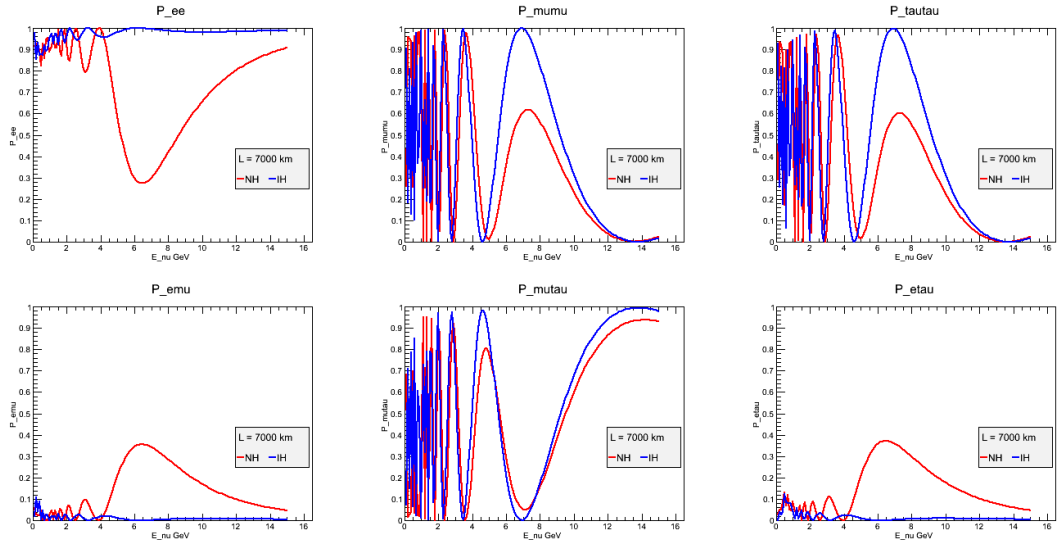

Figure 4.12: Variation of the oscillation probability $P_{\nu_e \to \nu_e}$, $P_{\nu_\mu \to \nu_\mu}$, $P_{\nu_\tau \to \nu_\tau}$, $P_{\nu_e \to \nu_\tau}$, $P_{\nu_\mu \to \nu_\tau}$, and $P_{\nu_e \to \nu_\mu}$ (clockwise from top-left) using oscillation parameters for both the Normal Hierarchy(red) and Inverted Hierarchy(blue) for L=7000km through earth for energies E_ν={0,15}GeV.

The probability values match well with the plots, three of which are present in the paper [136], to the extent of visual estimation of course.

Verification of the well working of both the Oscillation Code and Event Generation combined:

Two distinct checks have been performed to ensure the acceptability of the entire algorithm. These checks are performed before GEANT4/simulation, i.e., at Nuance level information.

- The downgoing neutrinos are devoid of matter effect oscillations. Hence the value of χ^2 calculated between the downgoing events in the NH and the IH event sets

should be ideally zero. The value so obtained by our present algorithm is 0.016 for ν_μCC events and 0.03 for ν_eCC events in 10 years for over 5000 bins (~50 E_ν×100 $\cos\theta$).

- The values of χ^2 obtained for ν_μCC events in the energy range E_ν={1,11} GeV with 20 bins and the varied cosθ bins are mentioned in table 4.27. The corresponding values reported in [7], well agree with them, as shown in the table 4.27. In fact, the characteristic saturation property of the χ^2 with increasing number of bins is clearly pronounced.

# cos θ bins	χ^2 (calculated)	χ^2 (reported in [7])
20	145	138
80	266	256
160	290	300
240	297	345
320	301	363

Table 4.27: Comparison and saturating nature of the values of Poissonian χ^2 of the devised algorithm with increasing number of bins. These are for ν_μCC events in energy range E_ν={1,11} GeV with 20 bins scaled down to 10 years.

Therefore, the algorithm devised and the oscillated files produced are good enough to be accepted/considered for further analysis.

Mass Hierarchy informations contained in fluctuationless ν_eCC events set:

The same exercise as in case of ν_μCC (the second bullet point above) is applied on the sets of NH and IH oscillated ν_eCC events. The Poissonian as well as the Gaussian method of calculating χ^2 is used and listed in table 4.28. A minimum of 5 events in 500 years

are retained in each bin. The Gaussian method has already been described earlier. The Poissonian way of calculating χ^2 is as follows:

$$\chi^2 = 2(\#IHevts - \#NHevts) + 2(\#NHevts)\ln(\frac{\#NHevts}{\#IHevts}) \tag{4.3}$$

# cos θ bins	χ^2 (Poissonian)	χ^2 (Gaussian)
20	18.8	16.3
80	29.6	24.3
160	38.6	31.0
240	47.7	37.6
320	53.4	42.4
480	58.2	47.9
960	55.3	49.9

Table 4.28: Comparison and saturating nature of the values of χ^2 of the devised algorithm with increasing number of bins. These are for ν_eCC events in energy range E_ν={1,11} GeV with 20 uniform energy bins scaled down to 10 years.

The characteristic saturating effect of χ^2 shows that the ν_eCC events set contain genuine physics effects. In fact, one can extract a MH χ^2 contribution of **$\sim$50 in 10 years** from the ICAL detector, if it is properly tapped, i.e. an ideal detector case.

Selection cuts are applied on this fluctuationless dataset. Due to the absence of the fluctuations, one can attempt the finest possible binning scheme. In such case of finest hits bins only, the maximum χ^2 available is 25.6 in 500 years, or rather scaled down to **$\sim$0.5 in 10 years**.

In the above calculations, we assumed that NH is true. The results for the case IH is true are very similar.

4.10 Conclusion

Though track containing ν_μCC events are the primary data for ICAL detector, a larger fraction (larger w.r.t. the reconstructable events) will comprise the **"muonless"** events (ref. table 4.15). Two very important and tempting event samples are contained in it: the ν_eCC events and the NC events.

4.10.1 Obtaining the ν_eCC pure sample at ICAL

The several selection criteria devised in section 4.4.2 improves the purity of ν_eCC sample with ∼40% contamination of the non-ν_eCC events.

It has also been noted that, with an increase in purity of the sample, the sample-size decreases, and so does the fraction of vertical events. So, an optimization is required between the purity and the sample size, depending on the physics we would like to extract.

Depending on the constraints used, one can obtain a neutrino data sample with the purity of ν_e events varying between 53% to 68% with 300 to 15 events per year respectively. Thus, with appropriate combinations of such cuts we can select an event sample of ν_eCC purity of $\sim 60\%$ in a sample size of ~ 100 events per year.

Application of the upper layer cut of 5 ensures that the information available from these muonless events is independent from that in the conventional analysis of ν_μCC events. Events beyond this 5-layer range comprise mostly of ν_μCC events, with just 10% background due to the muonless events.

4.10.2 Contribution of muonless events in determining neutrino mass hierarchy

The contribution of the muonless events in determining the neutrino mass hierarchy is not zero, rather ∼1 (χ^2_{10yrs}). But the statistical fluctuations in the data are too large for this contribution to have a significant effect.

5

Muonless Events in ICAL@INO - II: Kinematic Characterization of the incident neutrino

This chapter attempts to suggest a way to read the kinematics of the incoming neutrino in a muonless event. We first suggest a way of an approximate calibration of the neutrino energy with the observable parameters. Then, we also attempt to estimate the direction of the neutrino. We mostly distinguish an upgoing from a downgoing neutrino, and avertical from a horizontal neutrino, and finally combine the two to check if we can estimate the neutrino direction directly.

5.1 Introduction

The magnetised ICAL detector can easily identify the charge of the muon. The energy and direction of the muon can be estimated from muon track information [10]. In a typical ν_μCC event, there are likely to be some hadrons also. The energy of these hadrons can be estimated using the techniques described in [118]. By combining the information from the muon and the hadrons, it is possible to obtain an estimate of the neutrino energy [119] and direction.

The ν_eCC events produce electrons (positrons) which create a shower in the detector.

They lose energy very fast and are not able to travel through many layers. The ν_τCC events [54] are rather small in number because of the large mass of the τ lepton. The τ lepton decays mostly into hadrons and hence these events also look like a shower of hadrons [120]. The only visible part of an NC event consists of hadrons, because the final state neutrino escapes detection. Hence, the NC events also look like a shower of hadrons. In the sample of shower-like events, we must include those ν_μCC events for which the muon track cannot be reconstructed.

In this section, we attempt to develop methods to estimate the energy and direction of the neutrinos which produce such muonless events.

Neutrino interactions are typically described in terms of neutrino energy and direction. The direction enables us to calculate the distance the neutrino has travelled [121]. Thus an estimate of the incident atmospheric neutrino energy and direction will allow us to perform a more quantitative analysis of any physics topic, or at least let us estimate the kinematics of the incident neutrino.

Using the Nuance neutrino event generator [1], we generated 500 years data for ICAL. In generating this data, we assumed normal hierarchy and used the following values for neutrino parameters: $\Delta m^2_{21} = 7.5 \times 10^{-5}$ eV^2, $\Delta m^2_{31}(NH) = 2.51 \times 10^{-3}$ eV^2, $\Delta m^2_{31}(IH) = -2.43 \times 10^{-3}$ eV^2, $\sin^2\theta_{12}$ =0.31, $\sin^2 2\theta_{13}$ =0.09, $\sin^2\theta_{23}$=0.5 and δ_{CP}=0. The generated events are then simulated in the ICAL detector using GEANT4 [2].

5.2 Energy of the incident neutrino

A more energetic neutrino is expected to give more number of hits in the detector, distributed among more number of layers compared to a less energetic neutrino. For a given neutrino energy, an event with neutrino travelling in vertical direction will have hits in more layers compared to one travelling close to horizontal direction [17]. Also, for a given neutrino energy, the NC events have less number of hits compared to CC events. Therefore, the two quantities,

- number of hits,
- number of layers having one or more hits,

are the basic kinematical variables to be used in the determination of the neutrino energy. From these we can define additional variables such as average hits per layer (hpl), hit distribution, etc. We use combinations of these variables to obtain an estimate of the neutrino energy and direction.

We found that there is negligible correlation between the hits and the neutrino energy, as can be seen from figure 5.1 or the layers and the neutrino energy, in figure 5.2.

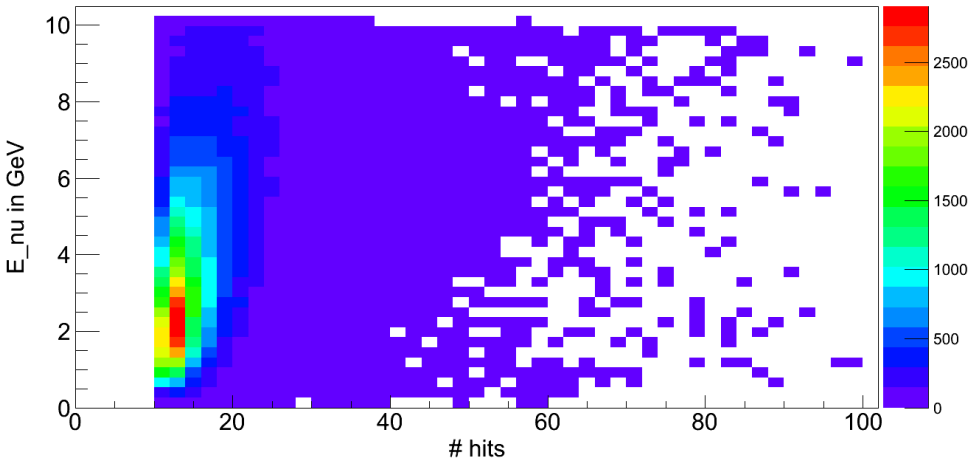

Figure 5.1: Hits vs. Energy: Correlation between the incident energy of the neutrino (here ν_eCC shown) and the number of hits in the event.

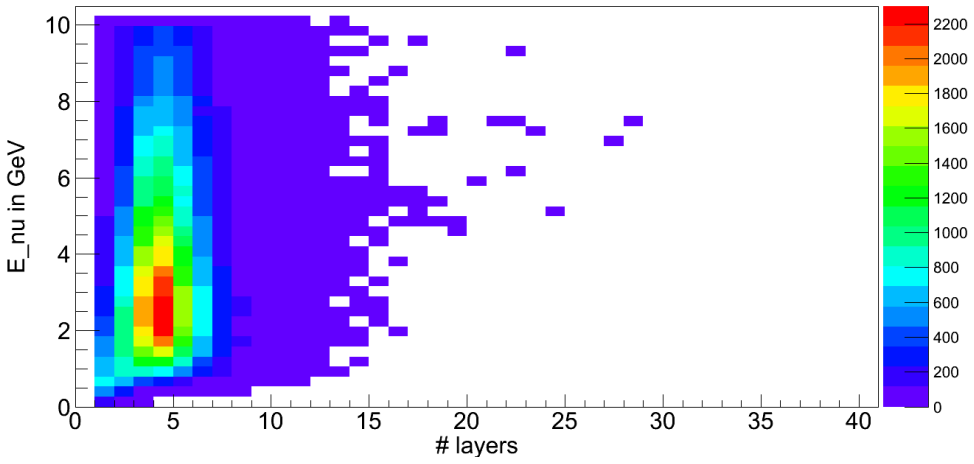

Figure 5.2: Layers vs. Energy: Correlation between the incident energy of the neutrino (here ν_eCC shown) and the number of layers hit in the event.

The variable 'hpl' does have some dependence on the neutrino energy but the correlation is too small for it to be an effective parameter for neutrino energy determination. This is depicted in figure 5.3, where we have considered all events which have number of hits greater than 10. We expect muonless events to have hits only in a few layers. Therefore, we further classify events according to the number of layers in which the hits are observed. For example, events with hits only in one layer, events with hits only in two layers etc. upto events with hits only in five layers. A majority of muonless events have hits in five layers or less. If two neutrino interactions of different energies (E_ν) give hits in same number of layers, then the more energetic neutrino should give more hits than the less energetic neutrino. That is, there should be a correlation between neutrino energy and hpl, if the number of layers is held fixed. This is illustrated in figure 5.4, for the case of hits in four layers.

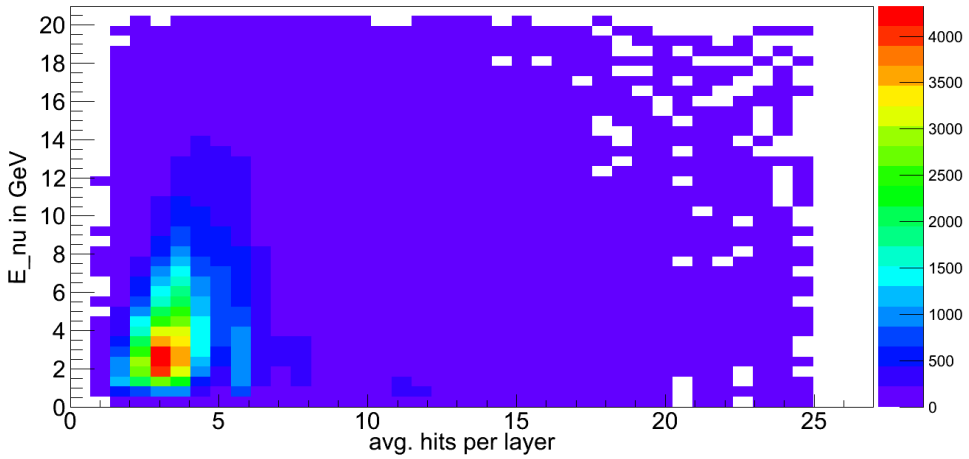

Figure 5.3: Hits/Layers vs. Energy: Correlation between the incident energy of the neutrino (here ν_eCC shown) and the average number of hits per layer in the event, after the cut #hits>10.

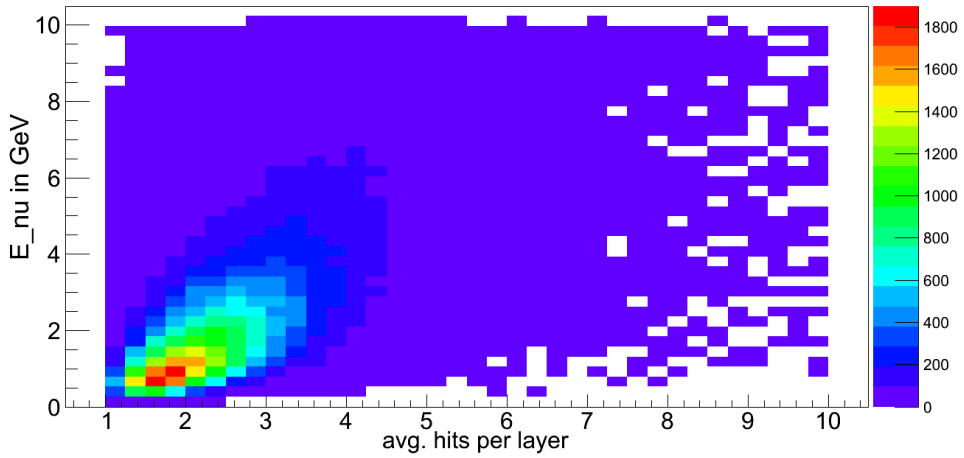

Figure 5.4: Average hits per layer vs. energy, i.e., dependence of number of hits on the neutrino energy but in a particular layer only, here L=4.

The trends observed in figure 5.4 for ν_eCC events are also evident in the case of the NC events and those ν_μCC events which are confined to a few layers.

5.2.1 Calibration of neutrino Energy

As mentioned before, we classify events according to the number of layers containing hits. We have considered values of L (number of layers with one or more hits) ={2,...,5}. For a given L, we further subdivide the events in bins of hpl (hits per layer) = {(1), (1-2), (2-3), ..., (9-10), ...}. In each of these bins, we have plotted the neutrino spectrum, with the neutrino energy taken from Nuance. A sample of these plots is shown in figure 5.5, for L=4. These spectra show a gradual shift in the peak towards the right along the energy axis, with increasing value of hits per layer. Hence, it appears to provide a reasonable calibration of the neutrino energy. One requires a distribution function to represent each of these spectra. A number of fitting functions have been attempted. Landau distribution is certainly the more obvious one, because it is related to energy loss of charged particles in any medium [122, 123].

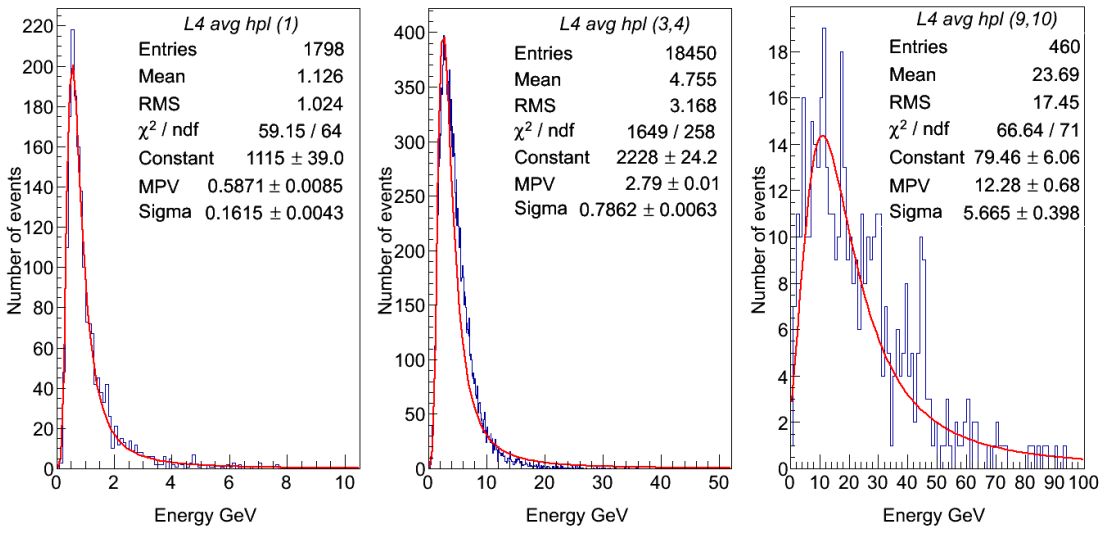

Figure 5.5: Neutrino spectra in different bins of hits per layer (from left): (1), (3,4) and (9,10), for events giving hits hits in exactly 4 layers (L=4). The spectra are fitted with Landau distribution function.

We describe the Landau distribution by its most probable value (MPV) and its sigma (σ) [4]. In our fitting procedure, we have imposed certain conditions. A fit is attempted only for those distributions which have at least a few hundred events. In addition, a fit is accepted only if the χ^2/ndf is $\leq$10.

Other distribution functions like the Vavilov and a few non-standard functional forms have also been attempted. The Vavilov distribution, which is the more general form of the Landau function, fits the spectra well in the bins with moderate values of hits per layer. In fact, the fit is slightly better than the Landau distribution. But the fit to Vavilov distribution is very sensitive to the limits on the fit parameters. Moreover, at very low values of hits per layer and at very high values, Landau distribution gives a much better fit. Here, we consider the calibration of energy over a very wide range of hits per layer. So, we prefer to use one common distribution function over the entire range.

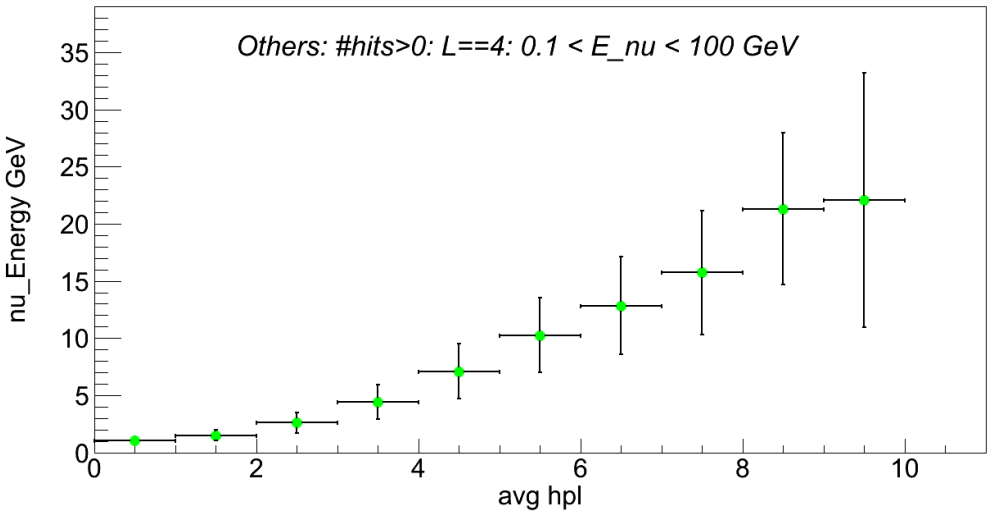

Figure 5.6: Calibration of ν-Energy vs. Average hits per layer for L=4, for the NC (+ν_τCC) events. (Points representation.) The points are given by the Landau peak positions and the 'error bars' by Landau σ in vertical scale (the horizontal bars cover the hpl bin-width).

[4] The correction -0.22 to the peak position which is recommended for fitting in ROOT at lower energies is neglected here since the error bar covers it [114].

The nature of the energy deposition is different in each of the three types of neutrino events considered here. They are grouped under the generic name "muonless" events but each type has its characteristic interaction properties. The NC events contain outgoing neutrinos which give no hits. The electrons present in the ν_eCC events give more hits, in addition to those by the hadrons. The ν_μCC events contain those muons which do not give identifiable tracks. Since the energy loss in iron is the smallest for muons, ν_μCC events are likely to have more number of hits in comparison to ν_eCC events of the same energy.

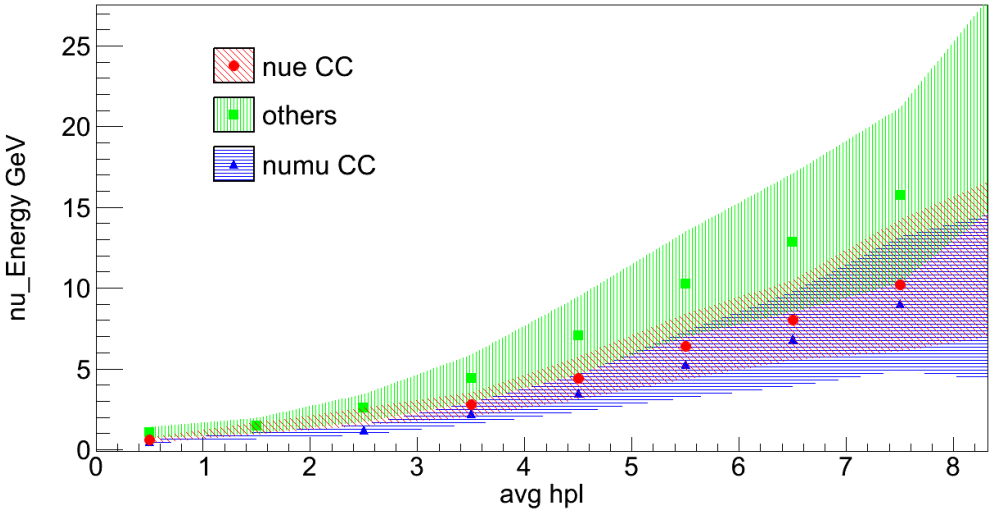

Figure 5.7: Approximate Energy calibration of the neutrinos having hits in exactly 4 layers, to visualise all the three types of muon-less neutrino events (ν_eCC in red, NC in green and ν_μCC in blue) all on a uniform scale of hits per layer.

The correlation between the neutrino energy and the hpl is shown in figure 5.6, for NC events with hits in exactly four layers. The central points are the MPVs of the corresponding Landau distributions and the error bars are $\pm\sigma$s of those distributions. Figure 5.7 shows this correlation for ν_eCC and ν_μCC events also in addition to NC events. The NC events as expected give less hits than the other two event types. A chart

of energy correlation is prepared in figure 5.8, with "number of layers" counting from 2 to 5. The curve in green is more relevant if we are dealing with an events sample rich in NC events. The curve in red is to be referred to if we have an events sample rich in ν_eCC events [3]. We have verified that a sample of pure ν_eCC events and a sample of events rich in ν_eCC events (with $\sim 60\%$ purity) both obey the same correlation plot. The curve in blue focuses on the ν_μCC events. It is worth noting that the energy scale increases with increasing L.

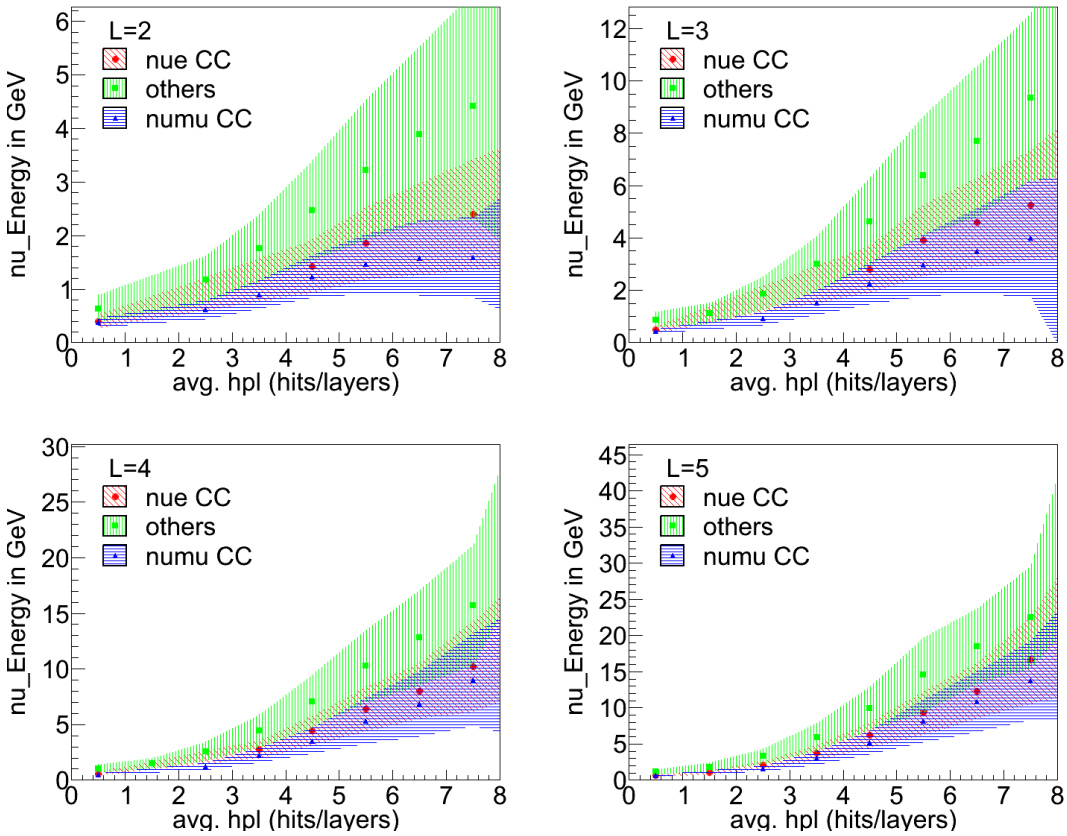

Figure 5.8: Approximate Energy calibration of the neutrinos having hits in exactly (from top) 2, 3, 4 and 5 layers. The three types of muonless neutrino events are plotted in different colours. The ν_eCC is in red, NC in green and ν_μCC in blue. Note that the scale on X-axis is the same for all plots, but the scale on Y-axis (Energy) increases with increase in L.

For Landau distribution, 68% of the events fall within the range (MPV - 1.02 σ, MPV + 4.65 σ) [124]. This leads to the definitions $\sigma_{\text{low}} = 1.02\sigma$ and $\sigma_{\text{high}} = 4.65\sigma$. The plots of σ_{low}/MPV and σ_{high}/MPV are shown in figure 5.9 for $L = 4$. The lower values are about 0.3 whereas the higher values are about 1.5 for all the cases. For given values of L and hpl, we can assign the event the most probable value of the neutrino energy. We

can also estimate the probability of the event having a given energy based on the MPV and σ of the corresponding Landau distribution.

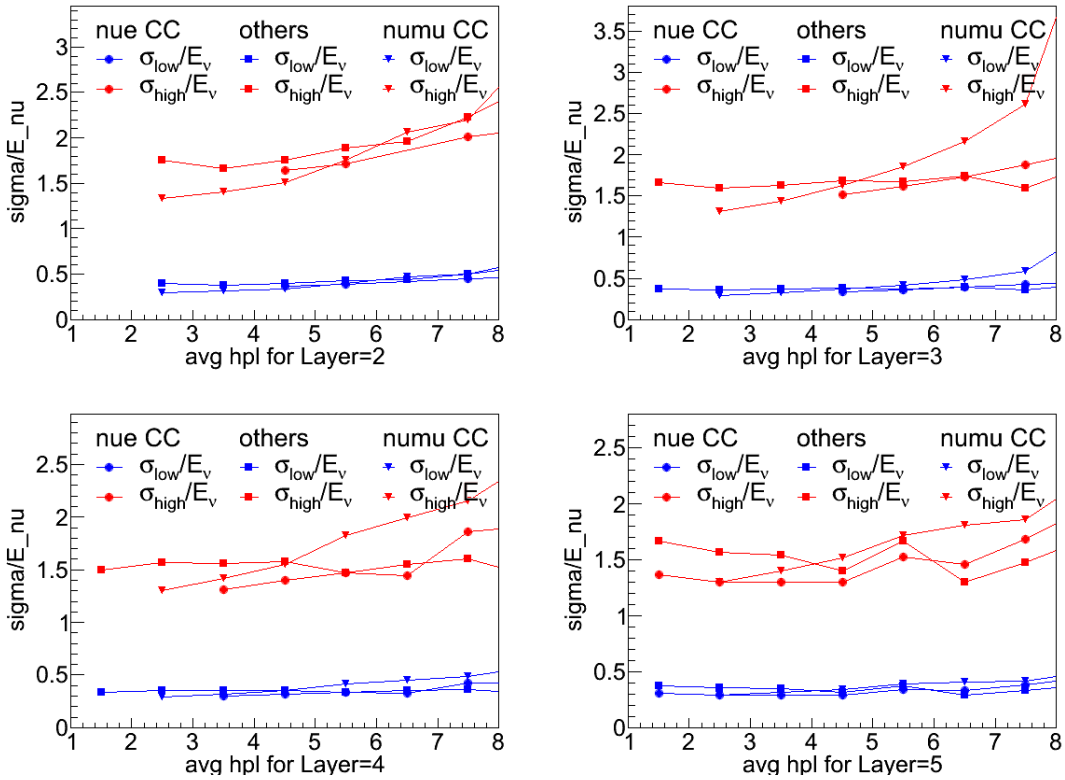

Figure 5.9: Energy Resolution: Variation of $\sigma_{\text{low}}/\text{E}_\nu$ and $\sigma_{\text{high}}/\text{E}_\nu$ with hpl, for events giving hits in L = 2, 3, 4 and 5 layers. [E_ν refers to the MPV of the Landau distribution.] The resolution plots for all three event types are shown.

5.3 Direction of the incident neutrino

The direction of a neutrino is given in terms of the polar angle θ and the azimuthal angle ϕ. The neutrino flux is expected to be symmetric in ϕ, except for a small east-west asymmetry arising due to the earth's magnetic field. The polar angle of neutrino is certainly of greater importance because it determines the distance travelled by the

neutrino, given by the expression $L = \sqrt{(R+h)^2 - (R\sin\theta)^2} - R\cos\theta$, where R is the radius of the earth and h is the atmospheric height at which the neutrino is produced [121]. We see from the above equation that $\cos\theta$=1 (-1) for the vertically up (down) going neutrinos. To do oscillation physics, we need to distinguish between upgoing neutrinos which travel thousands of km and down going neutrinos which travel only tens of km. In addition, it will be useful to distinguish between neutrino events in horizontal and vertical directions.

In muonless events, there are no tracks to serve as an easy handle in determining the neutrino direction. Since these events considered have hits in five layers or less, the timing information may not be useful in distinguishing between upward going and downward going events. Here we attempt to develop a method to find a correlation between the hit pattern and the neutrino direction. The following methods are tested with the ν_eCC events and are found to work. Both NC events and ν_μCC events without muon tracks (those for which hits are limited to five layers or less) also behave in a similar fashion. Minimal selection criteria may be used to select such event sample [3].

We have checked that the neutrino direction is not particularly correlated to the number of hits or the number of layers hit. Hence, devising criteria based on hits and layers or even hits per layer is not effective in finding a way to recognize the angular information of an incident neutrino.

Algorithms devised for neutrino angle depiction: We have considered the problem in two mutually independent steps. Firstly, we try to distinguish between the vertical to near-vertical events from the horizontal to near horizontal neutrino events. Secondly, we attempt to tell apart the up-going neutrinos from the down-going neutrinos. We have devised a number of algorithms and tested their efficacy in determining the ν direction.

5.3.1 Horizontal or Vertical Direction

The vertical or near vertical events should have shorter average horizontal spread than the horizontal or near horizontal events. Having taken this cue, the maximum total spread of a neutrino event in horizontal plane is studied. This parameter has been discussed in detail in an earlier section. The maximum horizontal distance, the variable we use here, is defined to be the maximum value of the horizontal distance of an event. It is the maximum of projected lengths, on the horizontal plane, of the distances between any two hits in the event.

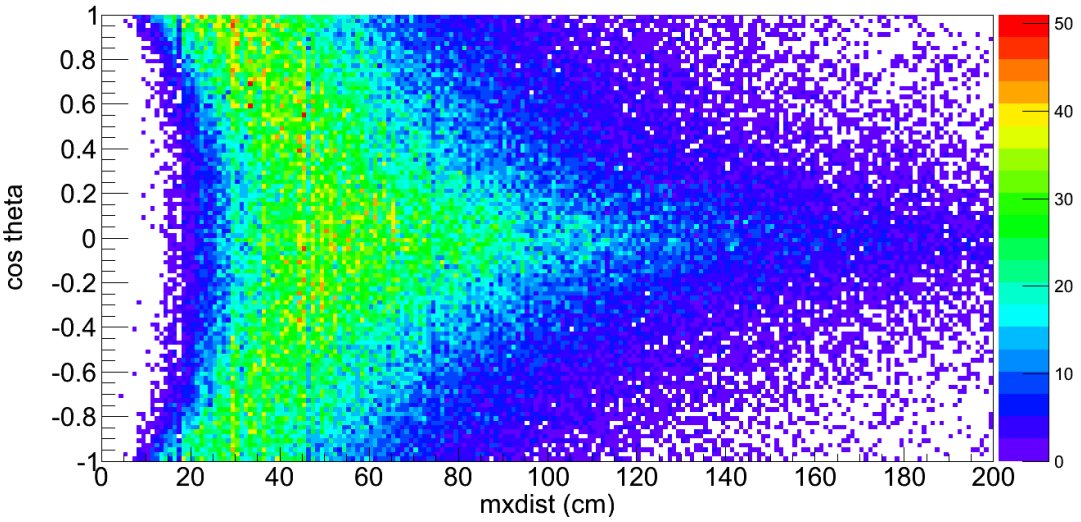

Figure 5.10: Correlation between the cosine of incident theta of the neutrino (here ν_e shown) and the maximum horizontal spread in an event for the 500years NH data. E_ν={0.8,20}GeV.

From figure 5.10, we see that there is a small correlation between direction of the neutrino (vertical or horizontal) and the maximum horizontal distance. The neutrinos incident in the vertical cone (extreme ends of the $\cos\theta$ axis) have less horizontal spread than the ones in the horizontal cone (central part of the $\cos\theta$ axis). For example, an upper cut of 30 cm on the maximum horizontal distance, gives above 75% vertical events

($|\cos\theta| > 0.4$ or those within a cone of angle 65° about the vertical direction) in the selected sample.

5.3.2 Up-going or Down-going neutrinos

The muonless events do not travel through many layers, unlike an event with a muon track. So, one needs to find a method/way to tell apart the upgoing neutrinos from the downgoing ones, in order to extract better physics information.

A number of criteria, based on the timing of the hits, were tried. But they were not very useful because most of the events in the muonless sample have all the hits contained within five layers or less. However, we describe a few such criteria as follows.

Algorithms using the timing information:

In the first case, the difference in the time stamp of hits in the topmost layer and the bottom most layer is considered. If it is positive then the event is considered downgoing whereas it is negative for upgoing events.

In the second case, the difference in the time stamp of hits between adjacent layers is classified as being positive or negative. If the number of positive differences is more than the number of negative differences, the event is called downgoing else it was called upgoing.

Both these criteria work more efficiently for events with hit layers ≥ 6. But unfortunately,the ν_eCC sample size mostly contains events with layers hit of ≤ 5. A third criterion based on the number of hits was found to be more promising. We assume hits in at least three layers and demand that the hits in the top two layers should be more (less) than the hits in the bottom two layers for the down (up) going neutrinos. It was found that 56-58% upgoing events can be identified by this criterion. But simultaneously about 34% of the downward going events also get misidentified as upward going ν_e events.

The algorithm however seems to work more efficiently for higher layer cuts, specially above 6 layers. Unfortunately, the ν_e CC sample size falls very low at such ranges of

selection.

Algorithm using the distribution pattern:

The algorithm using the hit distribution pattern can finally select upgoing neutrinos to an efficiency of 70%, and is described as follows. Assuming the number of hits across the layers as a type of distribution, their mean and the standard deviation from the mean (rms) are calculated. The details of this calculation are explained in the earlier section. These values of the mean and the rms of the layerhits distribution (figure 4.5), hardly show any dependence on the direction of the neutrino. But the ratio of layer-hits mean to layer-hits rms ("MRatio") shows a dependence on whether a neutrino is upgoing or downgoing, as seen in figure 5.11. The figure clearly shows that the lower values of this variable called MRatio selects mostly upgoing events and vice versa.

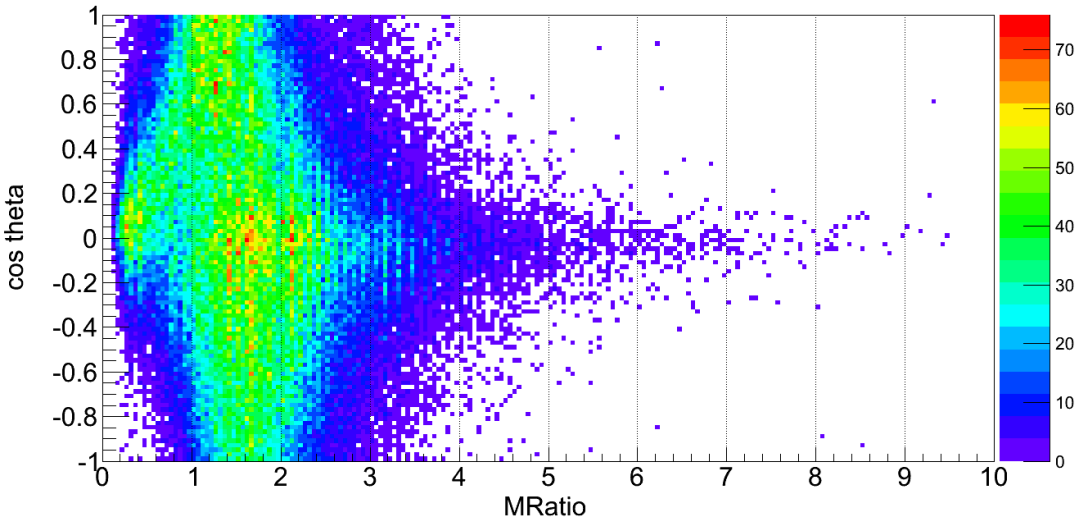

Figure 5.11: Correlation between the cosine of incident theta of the neutrino (here ν_e shown) and the ratio of layer-hits mean and rms in an event for the 500 years NH data. E_ν={0.8,20} GeV.

5.3.3 Estimation of the neutrino cos(theta):

The ratio of layer-hits mean to rms ("MRatio") gives a way to distinguish the upgoing neutrino events from the downgoing ones. The maximum horizontal distance ("mxdist") provides us with the ability to separate vertical events from the horizontal events. We have attempted to find some correlation between the two of them. 2-D histograms of these variables show gradual shifts in the peak positions of such distributions, in varying bins of neutrino direction. Figure 5.12 shows some of them. The 2D projection of the surface plot, of each of these distributions, show them to be symmetric along the MRatio-axis and asymmetric along the mxdist-axis, with a tail towards higher values of mxdist.

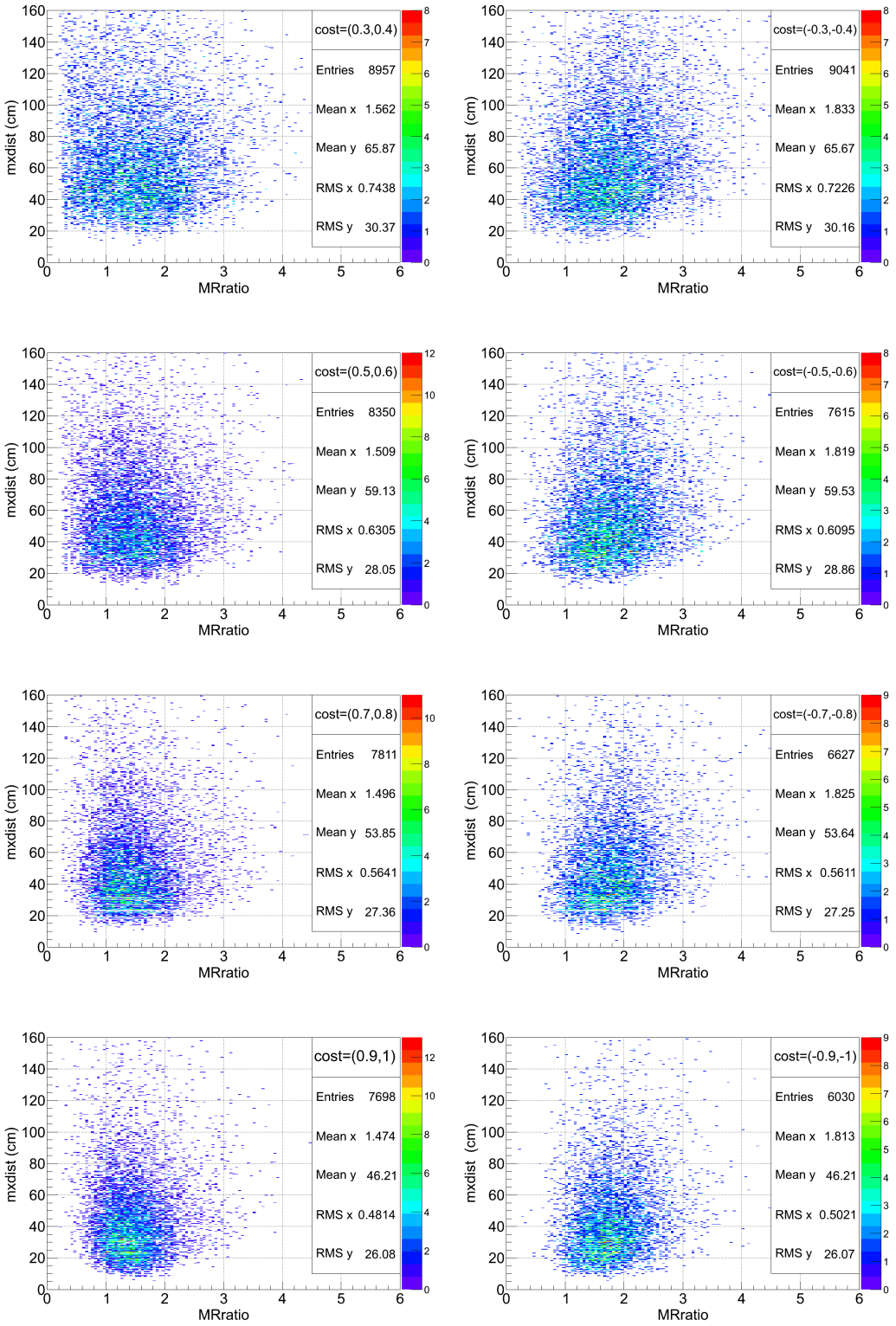

Figure 5.12: Correlation of MRatio and the mxdist, for ν_eCC events in bins of cos theta (here only some of them are shown), for the 500 years NH data. E_ν={0.8,20} GeV.

The left hand side panel in figure 5.12 shows distributions of the upgoing neutrinos in a few selected bins of cosθ. The right hand side panel shows the same for the down going neutrinos. The comet-like distribution (tail more notably) has shifted from left (in figures of the left hand side panel) to the right (in figures on the right hand side panel), along X-axis, i.e. in the direction of increasing MRatio. The head of the "comet" moves downwards (towards smaller values of mxdist), as one goes from the top to the bottom of these set of panels (as cosθ varies from vertical to horizontal) in figure 5.12.

The directional information conveyed by these two variables independently, may be combined to obtain the resultant neutrino direction. Hence, one can present a calibration of cosθ vs. MRatio and mxdist in 3-dimensions.

The 2-Dimensional histograms can be fitted with appropriate surface distribution functions. The peak of such a fitted function gives us the coordinates for the 3D-calibration plot. The errors can be quoted from the sigma of those peaks. Looking at the comet-like distribution from figure 5.12, one may propose a Gaussian distribution fit along X-axis (MRatio), and a Landau distribution fit along Y-axis (mxdist). Figure 5.13 shows such an example.

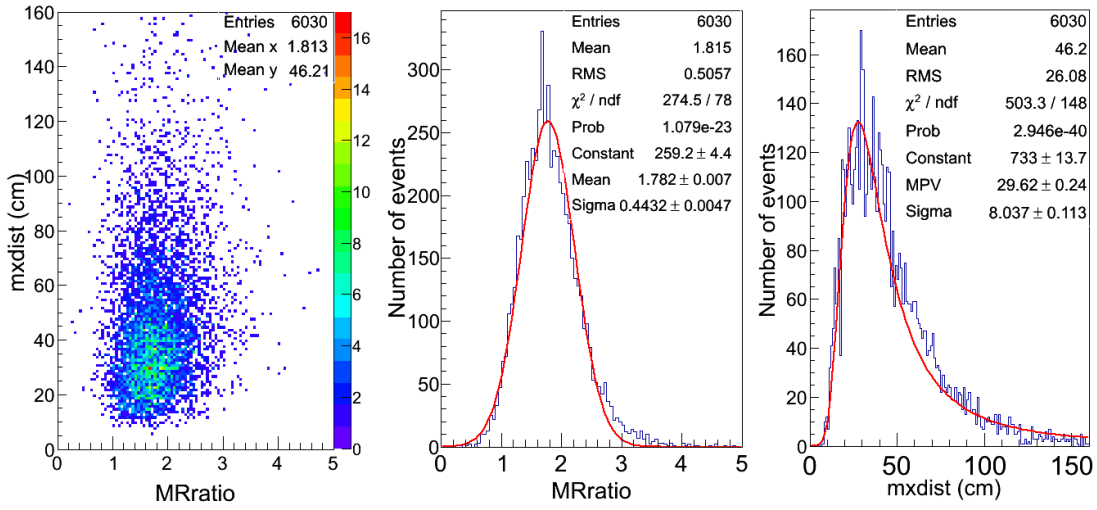

Figure 5.13: Left: 2D projection of the correlation of the MRatio and mxdist; middle: Fitting a gauss function on the XZ projection of the plot; Right: Fitting a landau function on the YZ projection of the plot.

The angular estimation can thus be done in terms of a 3D-calibration plot of MRatio along X-axis, mxdist along Y-axis and costheta along Z-axis, as in figure 5.14. The X-axis contains the Gaussian mean of the MRatio with ± Gaussian sigma as the standard deviation, in that costheta bin. The Y-axis contains the Landau peak position of the maximum spread with ± Landau sigma as the standard deviation. The costheta is along Z-axis with binwidth of 0.05.

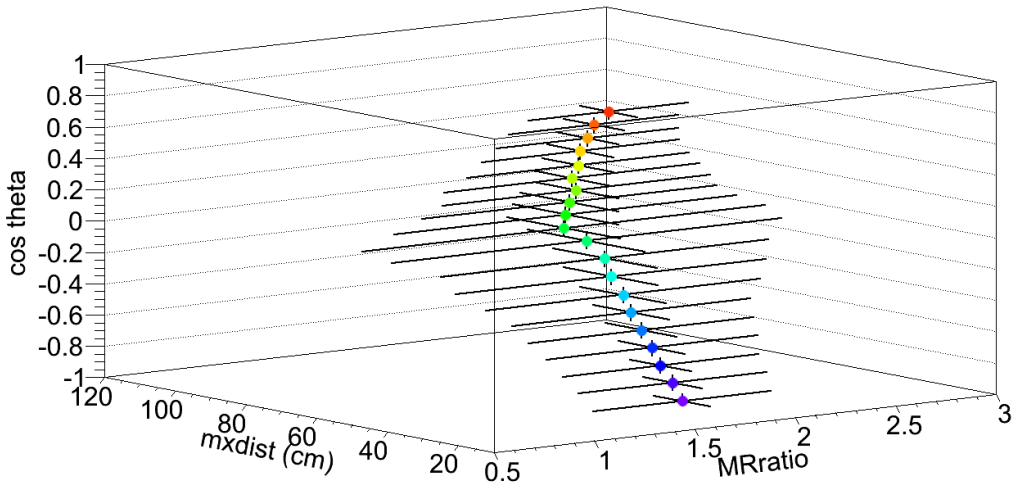

Figure 5.14: **"The Skewed-Hair-pin Structure":** Calibration of cosθ with respect to the plane spanned by the layer-hits mean to rms ratio and maximum spread, for the 500 years NH data (here ν_e shown). E_ν={0.8,20} GeV.

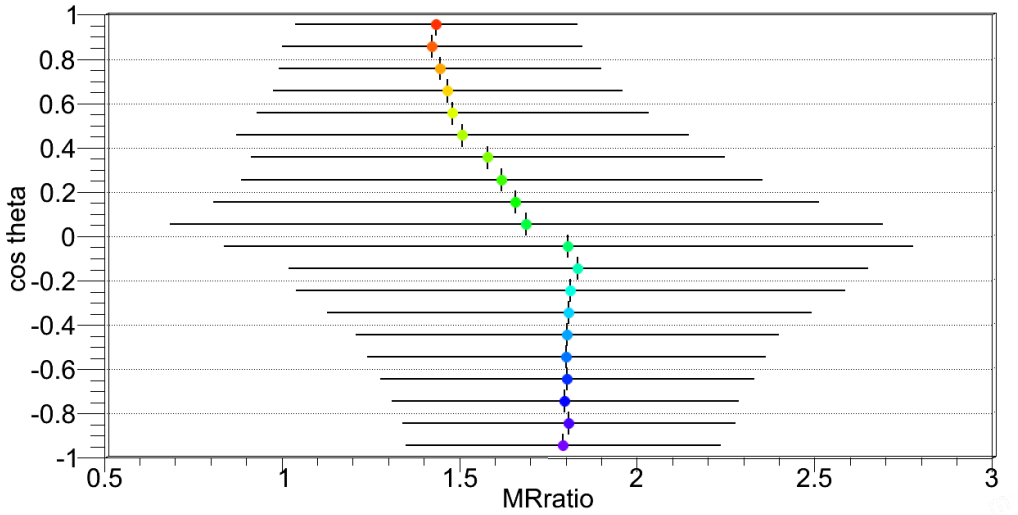

Figure 5.15: The X-Z projection of the figure 5.14, i.e. gaussian fitting of the distribution.

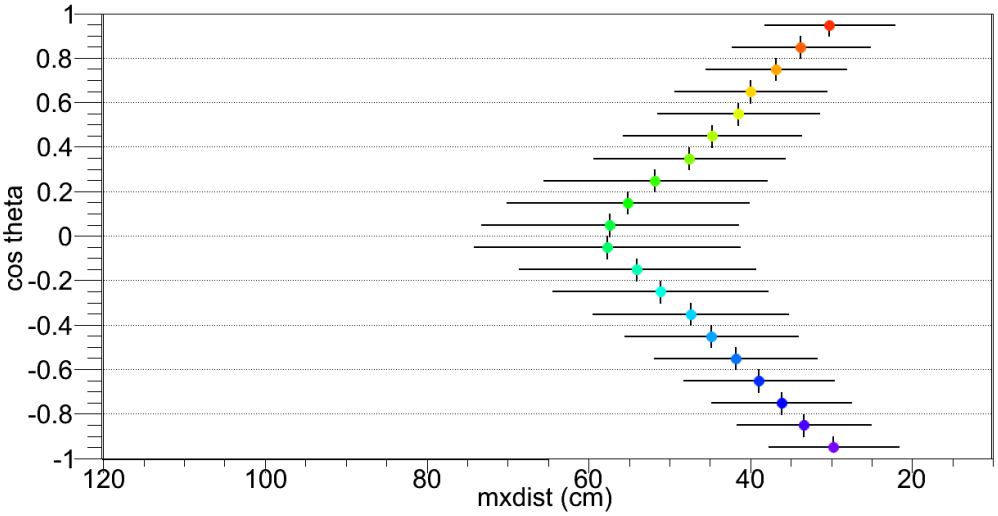

Figure 5.16: The Y-Z projection of the figure 5.14, i.e. Landau fitting of the distribution.

The XZ and YZ projections have been shown in figure 5.15 and 5.16 to help in visualising figure 5.14. But the estimation of the angle is preferably made from the 3D-Calibration Plot in figure 5.14. As we see from figure 5.16, mxdist gives a reasonable estimate of the modulus of cosθ. Then we can use MRatio to break the degeneracy between the up and down going events.

5.4 Conclusion

An effective method has been devised to estimate the energies of the neutrino events which give no clear muon track. The energy of the incident neutrino can be well estimated by following the approximate calibration curves in figure 5.8. If the event sample contains equal proportions of ν_eCC, NC and ν_μCC events, then the uncertainty in the estimated energy is rather large. However, it is possible to choose event samples which are rich in ν_eCC or in NC events [3]. For those muonless samples, it is possible to get a good energy estimate.

One of the important types of such muonless events is the NC interaction. It must

be remembered that NC events have an outgoing neutrino, which does not leave any signature. So, this method serves as an eventual solution to estimating the energy of such incident neutrinos.

The energies of the neutrinos in case of the muon-track containing events can be determined from the muon track information added to that from the hadron energy calibration. Now, with the present method, one can estimate the energies of neutrinos that do not give muon tracks, i.e., the Neutral Current interactions, ν_eCC interactions as well as ν_μCC events which lack identifiable muons. **Hence, to sum up, we can estimate the energies of all kinds of neutrinos (active) that are detected by the INO-ICAL Detector.**

We can even make a crude estimation of the angle or direction of the incident neutrino for muonless events. The two variables, mxdist and MRatio have been defined to get this estimation. Mxdist can distinguish the vertical/near-vertical events from the horizontal/near-horizontal events, which leads to a degeneracy between upgoing and downgoing events. MRatio removes this degeneracy and makes it possible to get an approximate estimate of the neutrino direction.

6

Inclusion of GENIE as Neutrino Event Generator for INO ICAL Code

This chapter aims to report the elaborate process of incorporating the GENIE Monte Carlo generator in the INO-ICAL simulation algorithm. We first state the necessity of such a step in INO, and then the various drawbacks that one will face in using the readily available version of GENIE. We finally discuss the solutions that we've included to overcome those impediments.

6.1 Introduction

Every neutrino experiment requires to analyse its probabilistic results obtainable from the real data. Monte Carlo neutrino generators are dedicated random number generating programs that mimic the interactions of the neutrinos with electrons, nucleons or nuclei [125]. These generators are essential components of an experiment, in order to be able to analyse the real data and extricate the physics information most effectively. The MC neutrino generators use the known physics processes while generating the neutrino interaction. Any deviation from the predicted results in the experiment may lead to a new physics search or required amendments in our knowledge. Hence, these generators

play a vital role not only in the analysis of the experimental data, but also bridges the difference between the theory and the experiment.

6.2 INO and GENIE

The ICAL detector at INO is dedicated to study the atmospheric neutrinos. The primary aim of ICAL is to determine the ordering of the neutrino mass hierarchy. Other physics possibilities are also important subjects of study at the ICAL. Therefore, a well suited neutrino interaction generator is necessary for the simulations of the atmospheric neutrinos in ICAL.

GENIE is a program (or a package) written in C++, using 350 classes. It makes appropriate applications of the hadronization models, the principles of nuclear physics, and various other physics phenomena in their corresponding ranges of validity, and continues to evolve while attempting to smoothen out the merging and tuning of the models, avoiding double counting or discontinuities. The applicability of GENIE extends to all nuclear targets and neutrino flavors with energies from MeV to hundreds of TeV energy scales. So, naturally it needs to take care of elementary cross-sections, which it does by accepting an external .xml file. This list of cross sections is also generated by GENIE by considering the neutrinos of different energies impinging on every possible target element present in the detector.

The GENIE event generator gives the output in a standard root file in GHEP (STDHEP-like) event record format [5]. It also provides a conversion option to convert the standard format to conventional and customised formats like the Nuance format, or the format required by T2K [131], NuMI [82] etc.

The incorporation of GENIE as neutrino event generator for INO ICAL code [2] has become a necessary task, owing to the absence of further updates in Nuance. Hence the change is required to ensure better simulation/phenomenological studies in INO.

6.3 Shortcomings for INO usage

GENIE as explained briefly in the earlier section, is itself a ready-to-go neutrino event generator software and one can use it independently. However, with the need arising to use GENIE instead of Nuance in the INO simulation algorithm, it requires to make certain modifications in the source code, preferably to make a "GENIE-INO user-friendly package", which can be used with ease, to generate neutrino events. These events can then be directly used for simulations by using the already existing ICAL code [2]. One may also use the same for analysing/studying physics, without GEANT simulations, if one wishes to.

6.3.1 Azimthal angle dependence of the flux

GENIE makes use of the two dimensional ν-flux information in E_ν and $\cos\theta$ bins (*2D*). INO flux tables by HONDA [6] show ϕ dependence also, as shown in figure 6.1 [5]. The non-uniformity in the azimuthal angle distribution is very strong in cases of E_ν ~1 GeV, and fades out for energies beyond E_ν >10 GeV. ICAL is significantly sensitive to neutrinos in this range, i.e. E_ν ~1-10 GeV. So, one must not leave the azimuthal information untapped.

[5] It must be noted that the atmospheric neutrino flux used in all other chapters is of the SK site, a convention so far followed by the INO Collaboration, apart from using Nuance. The INO flux tables are recently given by Honda et. al. This chapter involves the responsibility of not only replacing Nuance with GENIE, but also use the INO flux table in the future INO simulation/phenomenological studies. So, this chapter uses the flux tables given by Honda for the INO site.

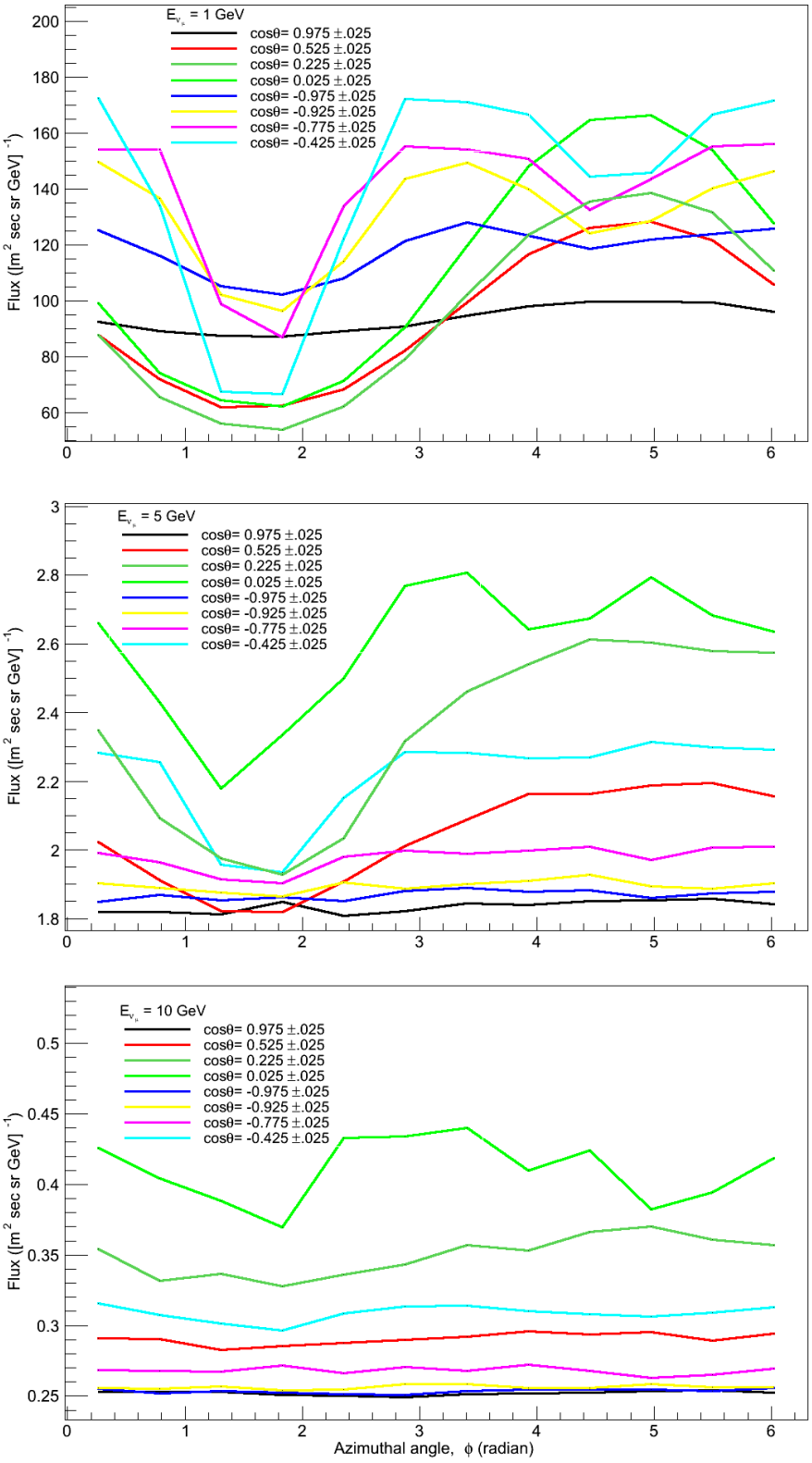

Figure 6.1: Phi-distribution of incident neutrino flux at at INO site at E_{ν_μ}=1GeV, 5GeV, 10GeV (from top) for ν_μ.

Provided ICAL reconstructs the azimuthal angle of the incident neutrinos to significant accuracy, we can attempt to observe and study the east-west effects of the flux over the periods/seasons. The low energy charged particles (mostly positive) of the cosmic origin, which enter the atmosphere, get more suppressed in the east direction due to presence of the magnetic field of the earth, than in the west. The following schematic in figure 6.2 demonstrates this fact.

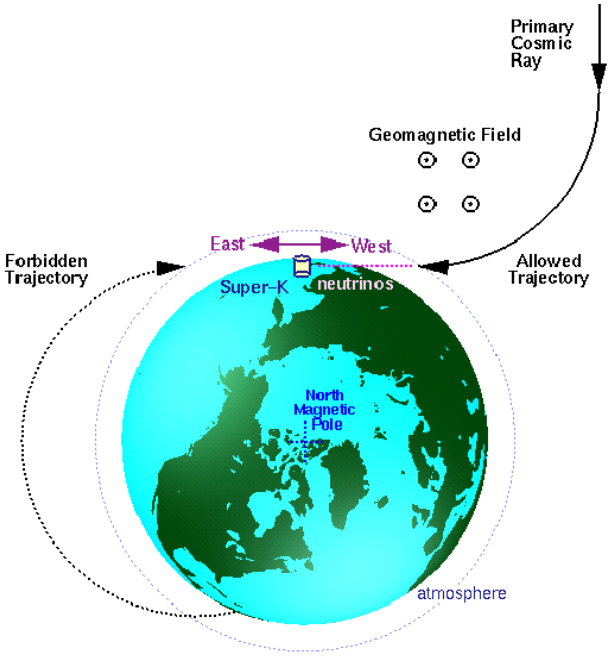

Figure 6.2: Schematic diagram of primary cosmic rays being deflected by earth's magnetic field [**?**].

The asymmetry, A can be measured hoping to reproduce the results by SK as per the definition [132]:

$$A = \frac{N_E - N_W}{N_E + N_W} \tag{6.1}$$

where, N_E (N_W)= number of events for neutrinos travelling towards east (west).

The effect of asymmetry is observed in case of low energy neutrinos from the atmospheric origin. The cosmic ray particles which enter the atmosphere and their secondary

products π/K are charged particles, and hence deviate from their original paths due to the geomagnetic field of the rotating earth. The average drift in the path of an electron/positron is generally given by [133],

$$d = \frac{qh^2 B \sin\chi}{2E_e \cos^2\theta} \tag{6.2}$$

where, χ is the angle between the field $\overrightarrow{B}$ and the original velocity of the particle v, q the electric charge, h the average vertical height of the electron path, E_e the average energy and θ the zenith angle. Similarly, drifts are experienced by the π/K and the $\mu^{\pm}$s in the earth's atmosphere. Thus, observing the azimuthal angle distribution in different bins of the neutrino energy and $\cos\theta$, one can study the changes in the earth's geomagnetic mapping, although to a crude approximation.

The orientation of the ICAL detector makes an angle ∼45° w.r.t the geographical east direction. Therefore, GENIE@INO should include all such directional information (*3D*).

6.3.2 Low flux at higher energies

The cosmic rays power spectra falls as $\frac{dN}{dE} \sim E_\nu^{-\gamma}$, where γ ∼2.7 in our concerned range. Likewise, the neutrino flux falls rapidly with energy. However ICAL is interested/sensitive to neutrinos with energies ∼1-10 GeVs. Mass hierarchy discovery potential is large for events with energy of a few GeV. The flux at these energies is rather low, as in figure 6.3.

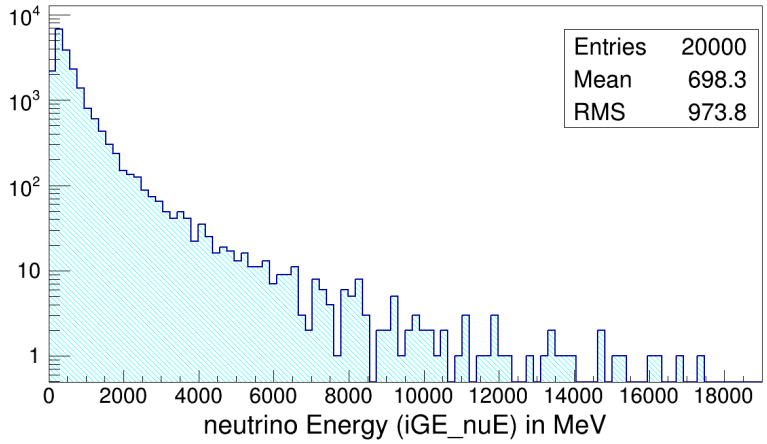

Figure 6.3: Energy-distribution of incident atmospheric neutrinos.

GENIE contains provisions for weighted event generation for the neutrino beams incident on the target. No such option has been made available for the atmospheric neutrino event generation.

6.3.3 ICAL-customised output

Every experiment has its own objective and methods of analysis. GENIE has provisions to give the output into customised formats for different experiments like T2K, NuMI, JPARC etc. Simulations for the INO experiment require the output in its own facilitating format. This demands us to develop an exclusive format for INO.

6.3.4 Event Generation for a certain Exposure Time

Atmospheric neutrino experiments like INO are required to decide their runtime, which largely (though indirectly) depends on the length of exposure of the detector to the atmospheric neutrino fluxes. GENIE has been used to generate a fixed number of ν interactions. There was no effective provision to generate the atmospheric ν events for a certain exposure time. This is a very necessary aspect for atmospheric neutrino experiments.

6.4 Solutions

In order to overcome the shortcomings mentioned in the earlier section, we modify the GENIE source code to include the following aspects. This not only results in a "ready-to-go" GENIE@INO package but also ensures a better understanding of the neutrino event generator being used at INO.

6.4.1 Accept the azimuthal angle information in flux tables

The Nuance@INO has so long been using the SK flux, which has energy (E_ν) and $\cos\theta_\nu$ dependence only, i.e. the flux is averaged over the azimuthal angle. However, the Honda flux at INO site contains the dependency of the flux on the azimuthal angles too, divided into bins of 30° each. GENIE had the provision to use the former type of flux files, be it the FLUKA [106] format or the BGLRS [134] format. So, in order to include all the available information into ICAL studies, the source code of GENIE has been modified to read such flux files which contain azimuthal angle dependencies too. It has been checked that there is an observable variation of neutrino flux along the phi direction, which is shown in the figure 6.4.

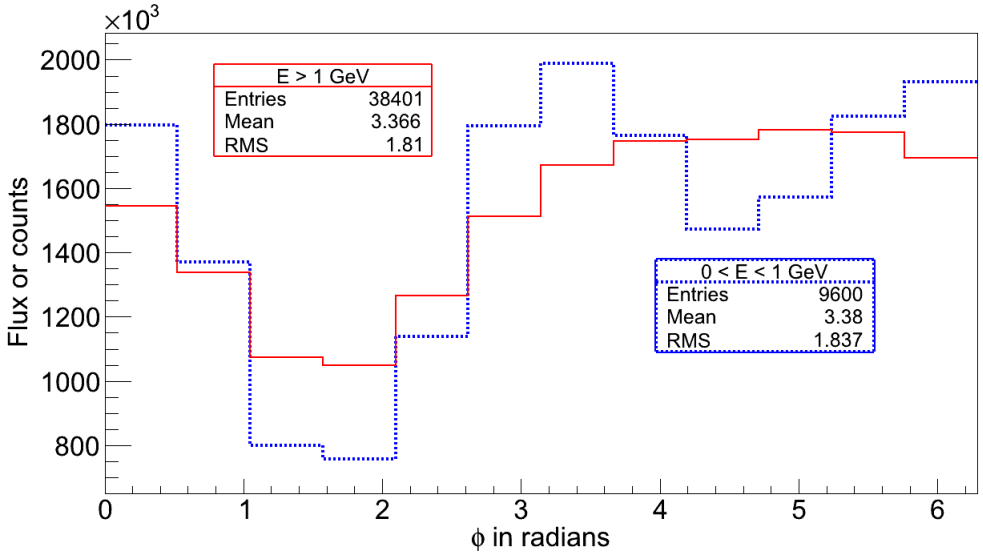

Figure 6.4: Phi-distribution of incident neutrinos at ICAL@INO with the 3D flux given by Honda at the INO site, summed over all $\cos\theta$.

The phi dependence of the flux gives a non-uniform phi-distribution at the ICAL detector, as in figure 6.5. (Please note the inversion of ϕ distribution, which is due to the convention of inverse coordinate system in ICAL with respect to HONDA coordinate system.)

Significant difference can be noted if the 3D enhanced information is used, instead of the flux averaged over phi (2D). The 2D distribution is comaparable to that of the neutrinos around or above 10 GeV for the 3D case, as shown in figure 6.6. The ICAL detector is sensitive to neutrinos above 1 GeV, where the signature of the phi is well-realisable.

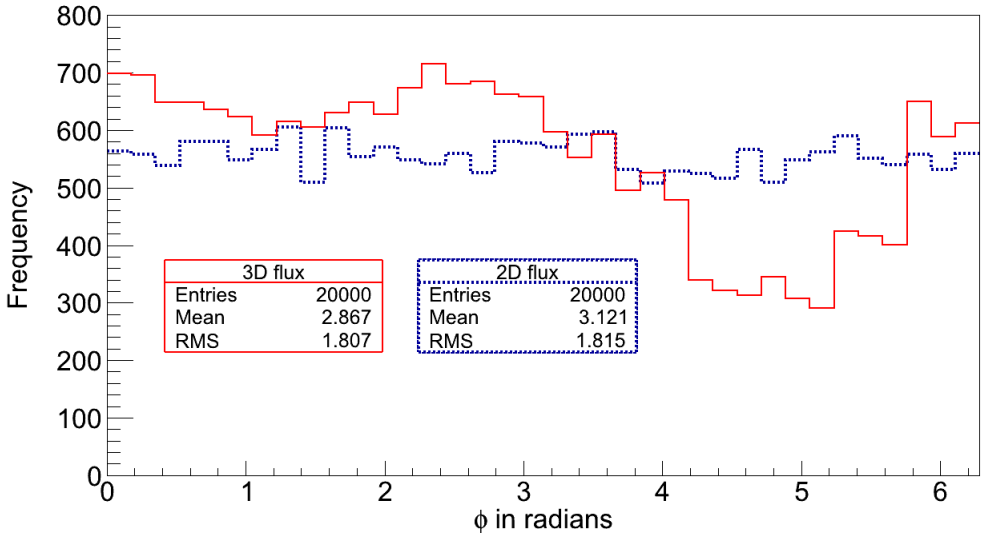

Figure 6.5: Phi-distribution at ICAL@INO with averaged over phi flux vs. the 3D flux, both by HONDA at INO site.

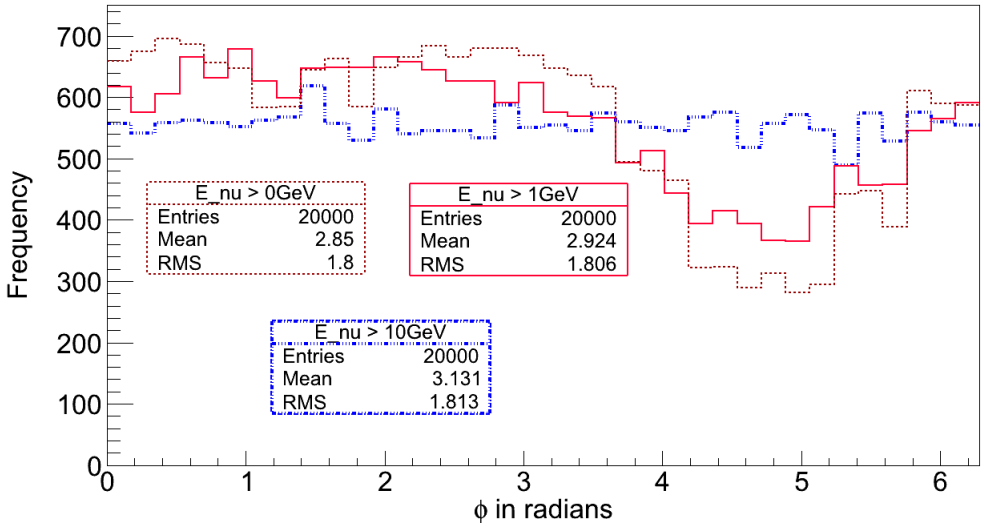

Figure 6.6: Phi-distribution at ICAL@INO with the 3D flux: Comparison of the phi-distributions for relevant energy ranges.

So, inclusion of the phi dependent flux information is absolutely necessary for the

study of atmospheric neutrinos at INO.

Besides the already available flux-file options, FLUKA and BARTOL, we introduced a third option called FLUKA3D to include this 3D flux information.

6.4.2 Weighted Event Generation of atmospheric neutrinos:

The neutrino flux being very high at low energies, the fraction of the total number of events in the high energy range is less. If one is interested in studying the effect of these high energy events, along with the lower energy ones, one faces the problem of low statistics in the higher energy region, or may tediously generate events in different energy bin and then merge them according to their cross-section. So the option of weighted atmospheric event generation is introduced. The optional tag "-w < ## >" (without quotes and braces) in the "gevgen_atmo" command [6] generates the events with the flux multiplied by the energy raised to a power "##" instead of zero. The minimum and maximum limit of the weight values have been set to be {-1.,5.}. The default is undoubtedly 0. However, it is suggested to keep the weight values limited between 0. and 2.2. If weight values above this range are considered, the number of events in the lower energy range reduces tremendously. This effect is not wanted for studying the events at the INO detector. A comparison of generated neutrino spectra with different weights is shown in figure 6.7 and the underlying algorithm used for achieving so is mentioned in steps in figure 6.8.

[6] It is the command name used in GENIE to generate atmospheric neutrino interactions.

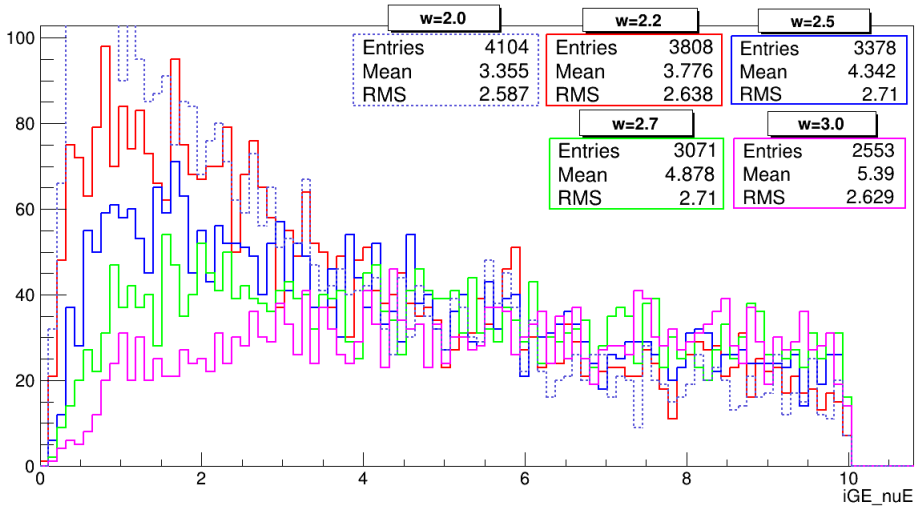

Figure 6.7: Comparison of the energy distributions of the generated neutrino events using different weight values.

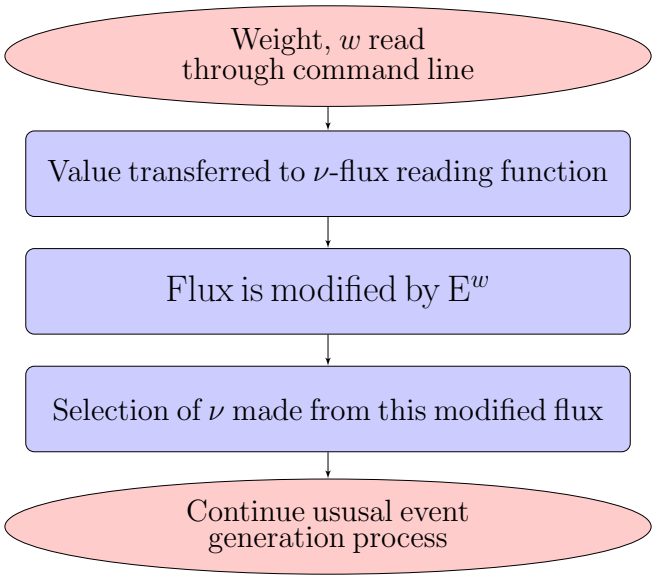

Figure 6.8: Flowchart of the changes made to ensure weighted atmospheric event generation.

The individual event weights, i.e the energy raised to the power of the weight value, as

well as the energy-weight histogram (in case one would want to calculate the implemented weight values for an energy independently) is made available in the modified GENIE output file.

6.4.3 Exclusive Output Format for INO

The GENIE output is first written in a not-so-easily-readable root file called the "ghep.root" file, and then contains the option of converting it into various generic formats like "t2k-root/txt format", "numi-format", "nuance-tracker" format etc. Every format contains parameters as per the requirement of the particular experimental studies. A new option "nu_INOGEN_rootracker" has been introduced to obtain the output in a root format customized for INO-ICAL code. Unlike the standard GENIE output in SI units, the modified output has the lengths in mm, time in ns and momenta or energy in MeV, which is the default unit of the GEANT4.

This output file can be directly fed to the ICAL code. Hence, necessary changes are also made in the ICAL code. The INO-ICAL output format is also improved alongwith, as depicted in figure 6.9. As some added advantage, the interaction identification (id) codes have been made directly available as another parameter against every event. The target nuclei pids and the the kinematics of the unstable particles have been enlisted too, in case one might be interested to look into them. (For easy identification, the unstable particle identification (pid) have been set to zero in the output for ICAL, but the pid is available in the GENIE output.)

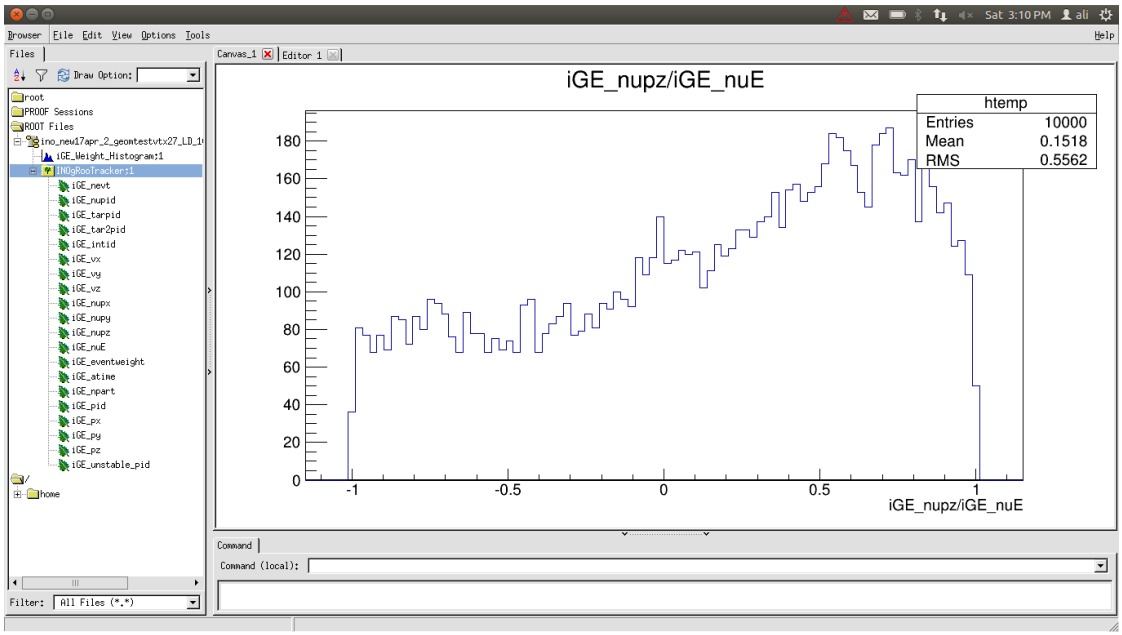

Figure 6.9: The INO compatible GENIE output root file "iGE_op.root". New variables like the particle identification numbers of the target nuclei and the unstable particle information, interaction types etc. are also enlisted in this new root version.

6.4.4 Activating the Exposure-time option

The provision to generate the atmospheric ν events for a certain exposure time has now been introduced. We can now generate the ν-interaction data for any length of exposure to the atmospheric neutrinos, using any detector geometry.

We use the following method to calculate the number of interactions. For a material with density ρ and pathlength l, atomic number A, interaction cross section σ and Avogadro's number N_A, the number of interactions is given by

$$\sigma(E_\nu) \times \frac{\rho l \times k N_A}{A}. \tag{6.3}$$

Summing over all the materials present in the detector, we get the number of interactions is given by

$$\sum_{material} [\sigma(E_\nu) \times \frac{\rho l \times k N_A}{A}]. \tag{6.4}$$

Given the incident flux of neutrino Φ has very small dependence on the $\cos\theta$ and ϕ, we take

$$\iiint \frac{d^3\Phi}{dE_\nu d\cos\theta d\phi} dE d\cos\theta d\phi = \int \frac{d\Phi}{dE_\nu}.4\pi dE, \tag{6.5}$$

and given the fact that the generator will shoot the neutrinos from a virtual disc of radius R_T, which covers the entire dimension of the detector, we shall take an average over n times of calculating this rate of interactions. The source of the neutrinos, i.e. this disc is considered in different directions, covering the full solid angle around the detector. So, this finally leads us to the following equation,

$$N = \sum_n \sum_{E_\nu} \sum_{\cos\theta} \sum_\phi \sum_{material} \left[\frac{d\Phi_\nu}{dE_\nu} \times \sigma(E_\nu) \times \frac{\rho_l \times N_A}{A} \times \Delta E\right] . \frac{1}{n} . 4\pi . \pi R_T^2 \tag{6.6}$$

where, N=Rate of interactions, n=number of iterations, R_T=Radius of the hyper surface of the neutrino gun of the generator.

As a primary check, we tally the number of events generated by Nuance and GENIE for the same exposure time in table 6.1. It must also be remembered that the Nuance event numbers shown are generated with the input of neutrino flux for the SK site, while GENIE uses that of INO.

ν-Sample	**~Nuance number**	**~GENIE number**
ν_μ **only**	5042	5684 (2D), 5504 (3D)
$\nu_\mu + \bar{\nu}_\mu + \nu_e + \bar{\nu}_e$	9947	11529 (3D)

Table 6.1: Comparing the number of events with Nuance (1 yr)

We also checked the 3D numbers (event rate for the azimuthal angle dependent flux)

against different weight values, in table 6.2. The scaled equivalent is the number of generated events weighted with the inverse scale factors, which was used to change the neutrino flux, E^{-w} for different weight factors, for one of them is also shown in table 6.2, where total number of iterations used to do this calculation is 10000. The total scaled events set is ∼3.1 times the true number for w=2.

weights	0	0.5	1.0	1.5	2.0	3.0
$\nu_\mu + \bar{\nu}_\mu + \nu_e + \bar{\nu}_e$	11529	11681	11759	11865	11746	11596

Table 6.2: Consistency check with different weight factors to obtain the number of events in one year. The scaled equivalent for the w=2 case is 35281.

We require to decide the number of iterations (in eqn. 6.6) to have an accuracy better than 1%. As can be observed from figure 6.10, the variation in the value of calculated rate of interactions is 0.3%, for number of iterations beyond n=2×10^7. So, we can use ∼ 2×10^7 iterations to calculate an acceptable value of rate of interactions.

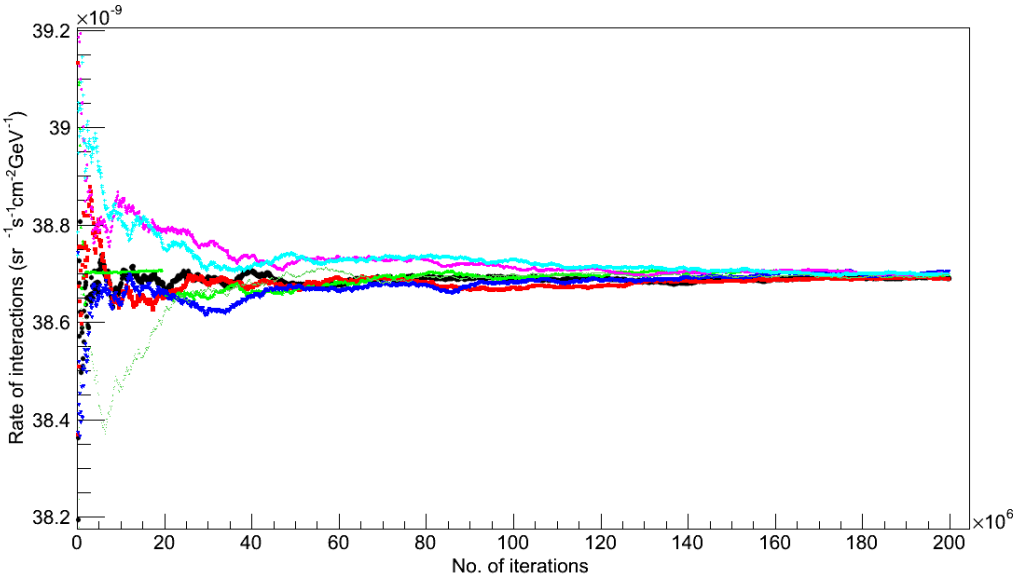

Figure 6.10: Expected flux rate for different number of iterations along the x-axis. The colors represent the execution of the program with different seeds.

6.5 Conclusion

The neutrino event generator is a vital component in the simulation studies of a neutrino experiment. INO has chosen to adopt GENIE as the neutrino event generator, after having used Nuance so far. This required us not only to make an INO-user friendly version of GENIE, but also led us to include four new options in the GENIE code, three of which may also be used for any other atmospheric neutrino experiments. So, the 4 new options in the GENIE neutrino event generation, which are available at the GENIE@INO version are:

- *FLUKA3D*: To include the 3D atmospheric neutrino flux information
- *-w <energy-weight>*: Option for weighted atmospheric event generation
- *nu_INOGEN_rootracker*: Command to get exclusive INO-customised output

- *-e <No. of years>*: To generate events for a desired exposure time of the detector.

Thus, we not only have the GENIE@INO package ready to go but also prepared to accomodate any kind of format of flux-files in GENIE.

7

Improving the hierarchy sensitivity of ICAL using neural network

7.1 Introduction

The main objective of ICAL@INO is to determine the neutrino mass hierarchy through a study of the atmospheric muon neutrinos. So, the primary data for the ICAL are the ν_μCC interactions, with identifiable muon tracks.

This chapter involves the study of these ν_μCC events in ICAL. We aim to improve the hierarchy determination sensitivity of ICAL, by the implementation of the multi-variate tools.

7.2 Physics Motivation

When a neutrino passes through a medium, its propagation gets modified due to the coherent forward scattering. All three flavours undergo this scattering due to neutral current (NC) interactions whereas only ν_e has an additional scattering amplitude due to charged current (CC) scattering off electrons [26, 27]. The scattering amplitudes give rise to potential terms in the evolution equation. Since the NC interactions of all flavours

are identical, the NC potential term does not lead to any modification of the oscillation probabilities. The CC potential term can lead to observable changes in the oscillation and survival probabilities. For the muon neutrino survival probability, $P_{\mu\mu}$, a large change is possible only if Δm^2_{31} is positive, which corresponds to normal hierarchy (NH). For Δm^2_{31} negative, called inverted hierarchy (IH), the change in $P_{\mu\mu}$ is negligible. For anti-neutrino the situation is reversed. The changes in the muon neutrino (or anti-neutrino) survival probability are significant when the following two conditions are satisfied [24]:

$$\Delta m^2_{31} \cos 2\theta_{13} \sim \pm 2EV_{CC}, \tag{7.1}$$

$$\sin^2\left(1.27\frac{\Delta m^2_{31}\sin 2\theta_{13} L}{E}\right) \sim 1, \tag{7.2}$$

where E is the energy of the neutrino, V_{CC} is the potential due to CC scattering and L is the pathlength of the neutrino. The Wolfenstein matter term $A = 2EV_{CC}$ (in eV^2) is given by $0.76 \times 10^{-4}\rho$ (in g/cc) E (in GeV), where ρ is the density of the matter through which the neutrino propagates. For $\Delta m^2_{31} \approx 2.5 \times 10^{-3}$ eV^2, eq. (7.1) is satisfied for $\rho E \approx 33$. For the density 5 gm/cc of earth's mantle, the corresponding energy is $E \approx 7$ GeV. Substituting this in eq. (7.2), we obtain a pathlength L of the order of a few thousand km. A large majority of upgoing atmospheric neutrinos pass only through earth's mantle hence the conditions mentioned above are the most relevant. Thus, we find that there is a broad range of energies around 7 GeV and a broad range of pathlengths of a few thousand kilometers for which there is an observable change in the muon neutrino survival probability [24]. However, these changes can be measured and hierarchy can be determined only if the detector has good energy and direction resolutions [135].

The plots of the muon neutrino survival probability $P_{\mu\mu}$ for atmospheric neutrinos, as a function of neutrino energy, are shown in figure 7.1 for various different values of $\cos\theta_z$, where θ_z is the zenith angle.

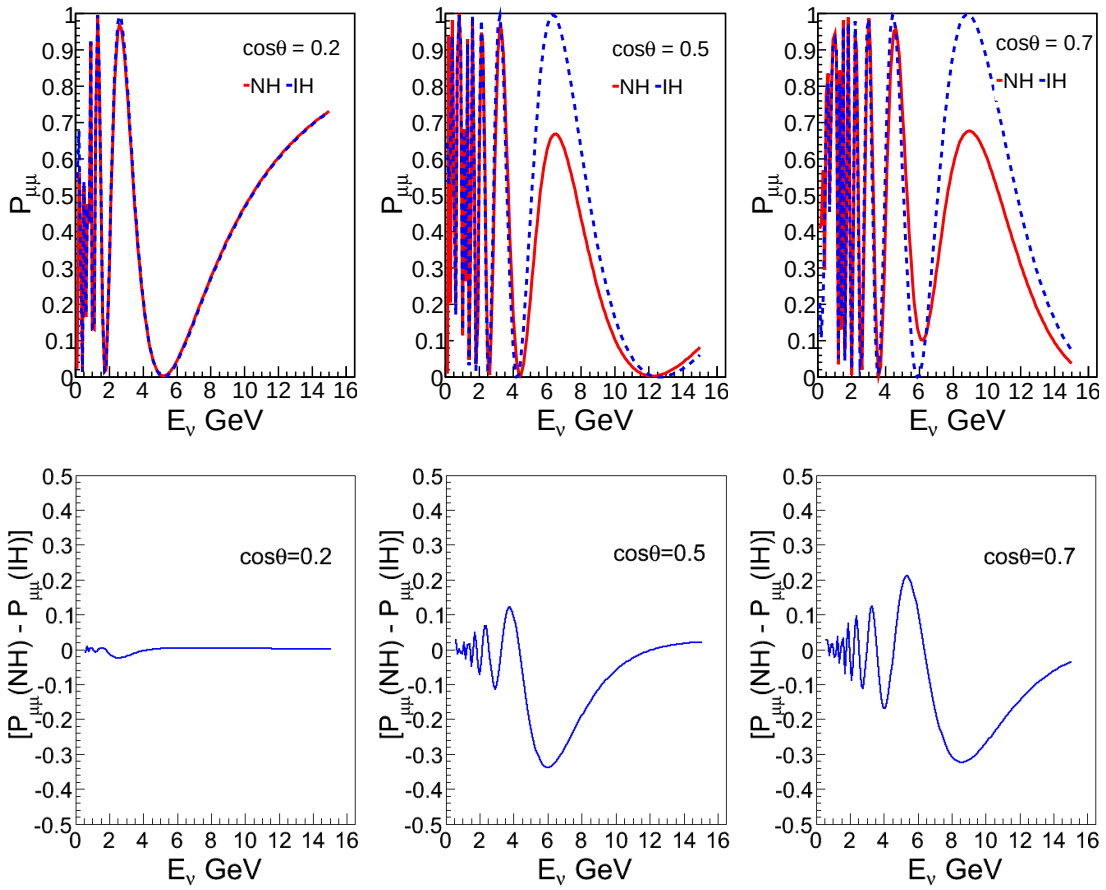

Figure 7.1: Oscillation probability plot $P_{\mu\mu}$ for neutrinos at different zenith angles for both hierarchies (top panel). Difference between the values of $P_{\mu\mu}$ in the NH and the IH conditions (bottom panel).

From these plots, we note that the signature for the neutrino mass hierarchy is most prominent in the energy range $E_\nu > 4$ GeV and for $\cos\theta_z > 0.5$. Hence, for the purpose of hierarchy determination, ν_μCC events in the *vertical cone* (i.e. with $|\cos\theta_z| > 0.5$) with $E_\nu > 4$ GeV should be considered as the signal events and all other events should be termed background. It is imperative to develop a procedure by which it is possible to select the signal events with high efficiency and purity. In this chapter, we develop such a procedure based on neural network.

ICAL has a good ability to identify muon tracks, from the pattern of hits in successive layers, and determine the energy and the direction of the muons with good precision [10]. In the present case, our **signal** events are ν_μCC events in the energy range of approx. 4-10 GeV, which are in the vertical cone. These events are expected to have long muon tracks passing through many layers. The background events come from sources: (a) low energy ν_μCC interactions, (b) ν_μCC interactions where neutrino direction is close to the horizontal, (c) ν_eCC events and a small number of ν_τCC events and finally (d) NC events. A large number of these background events do not give clear muon tracks. We aim to select a set of events which is highly rich in signal events. These events will have long muon tracks which can be recognized in a straight forward manner. We will utilize this fact to design criteria to separate the signal events from the background.

7.3 Simulations and Event Generation

We exploit the energy and the direction information of the neutrinos given to us by Nuance, in order to devise/develop the selection criteria. The selection criteria, whose development is described in detail in the next section, depend only on the visible characteristics of the ν-events in the detector, i.e. the output parameters given by GEANT4 simulation. The neural network is trained with a selected set of events. This trained network is then applied to a random set of events. It assigns a probability to the event, denoting how close it is to a perfect signal event. The signal-like events are finally chosen based on this value. The choice of the cut is such that the signal selection efficiency and the signal purity are significantly high.

In all the calculations done using the kinematic information of muons only, the following procedure is used. Atmospheric neutrino interactions for a huge exposure are generated by Nuance. The ν_μCC interactions from these simulations are isolated and binned in terms of E_μ and $\cos\theta_\mu$ values given by Nuance [11]. This data set is modulated by the following quantities which are obtained from GEANT4 simulations:

- Muon track reconstruction efficiency
- Charge identification efficiency
- Muon energy smearing
- Muon direction smearing

In all the previous analyses, the energy and direction of the muons are estimated from the Nuance simulation using the above procedure. In our analysis, we propagate every event through the GEANT4 package. The signals generated by GEANT4 simulation are input into the ICAL reconstruction code [9], which gives the "measured" energy and the direction of the muon. This study is an attempt of hierarchy determination at ICAL with full detector simulation.

In the previous section, we argued that events with $E_\nu > 4$ GeV and $\cos\theta_z > 0.5$ have the best hierarchy sensitivity. However, neutrinos over a very broad range of energy and over the full zenith angle range interact in the ICAL and produce observable events. Our job here is to develop a procedure to distinguish between the events with good hierarchy sensitivity and those without. Hence neutrino events over the full detectable range of energy must be simulated. Using NUANCE, we have generated 500 years of ICAL data in the energy range E_ν= {0.1,100} GeV, under the assumption of no oscillations (NOOSC). The data consists of all types of interactions of all active neutrino flavours. The generated events are then propagated in ICAL using a Geant4 simulation of the detector [2]. The pattern of hits thus generated are used to first identify the muon track and then reconstruct its energy E_μ and the cosine of its zenith angle $\cos\theta_\mu$ [9].

We have computed neutrino survival and oscillation probabilities for NH and for IH using the following values of neutrino parameters: $\Delta m^2_{21} = 7.5 \times 10^{-5}$ eV^2, $|\Delta m^2_{eff}| = 2.47 \times 10^{-3}$ eV^2 (i.e. Δm^2_{31}(NH) $= 2.51 \times 10^{-3}$ eV^2, Δm^2_{31}(IH) $= -2.43 \times 10^{-3}$ eV^2), $\sin^2\theta_{12} = 0.31$, $\sin^2 2\theta_{13} = 0.09$, $\sin^2\theta_{23} = 0.5$ and $\delta_{CP} = 0$. From the NOOSC data set, we construct NH data set using the accept-reject method, described in detail in section

4.9.6, with the NH probabilities as reference. The IH data set is also constructed in a similar manner.

7.4 Selection Criteria

We first select only those events with hits in more than five layers ($L > 5$). This lower limit on the number of layers is chosen to optimize the reconstruction efficiency of the muon tracks [9]. This cut also has the advantage of eliminating most of the background due to the non-ν_μCC events. About 90% of the events selected after this cut are ν_μCC events [3]. We want the neural network to select signal events with high efficiency and good purity. We need to choose appropriate input variables for the neural network to achieve this aim. We consider a number of such variables and study their ability to distinguish between signal and background among the ν_μCC events passing the $L > 5$ cut. For this study, we divide these events into four subsets based on the neutrino energy and direction, using the information from the event generator.

1. Signal events: E_ν: 4-100 GeV and $|\cos\theta_z| > 0.5$,
2. High energy horizontal events: E_ν: 4-100 GeV and $|\cos\theta_z| \leq 0.5$,
3. Low energy vertical events: E_ν: 0.1-4 GeV and $|\cos\theta_z| > 0.5$,
4. Low energy horizontal events: E_ν: 0.1-4 GeV and $|\cos\theta_z| \leq 0.5$.

We do a systematic study of the effect of various discriminating variables, listed below, on each of these subsets. We have checked that these variables discriminate against non-ν_μCC background very effectively. The counts of the signal events and background present in the sample are shown in table 7.1.

Total signal events	Total bkg. events
$\sim$1.2 $\times 10^5$	$\sim$6.3 $\times 10^5$

Table 7.1: Signal and background events in 500 years of NH dataset (generated with seed 1) in E_ν={0.1,100} GeV, with the preliminary cut of Layers>5. Signal defined: $E_\nu > 4$ GeV and $\cos\theta_z > 0.5$.

7.4.1 Hits

Low energy neutrino events give less number of hits compared to the high energy events. Hence, the number of hits is a measure of the energy of the neutrino as illustrated in figure (7.2). This variable is quite effective in distinguishing high energy events from low energy events but not for distinguishing vertical events from horizontal events.

Figure 7.2 shows that the signal-like events (top-left) give more hits than the low energy neutrino events (bottom row). The high energy horizontal events too give comparatively lower number of hits, if closely observed. This is due to the fact that the particles effectively travel through larger lengths of iron in the horizontal direction.

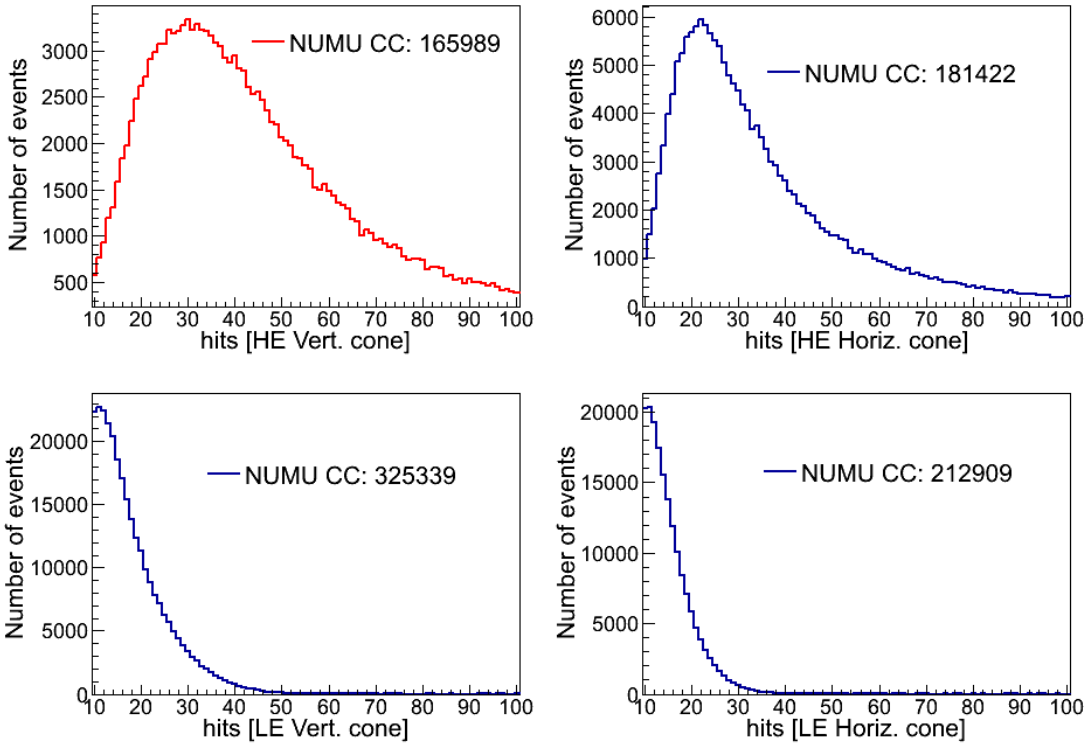

Figure 7.2: Hits Distributions for ν_μCC events with L>5, for the NOOSC 500 years dataset. The top left plot shows the distribution for the signal events (red).

7.4.2 Layers

This parameter refers to the number of layers in ICAL, which has received one or more hits in an event. The high energy vertical neutrino events give hits in more number of layers than the low energy/horizontal events. This is evident in figure 7.3. So, the vertical ν_μCC events containing high energy muon tracks give hits in a larger number of layers than the other event types.

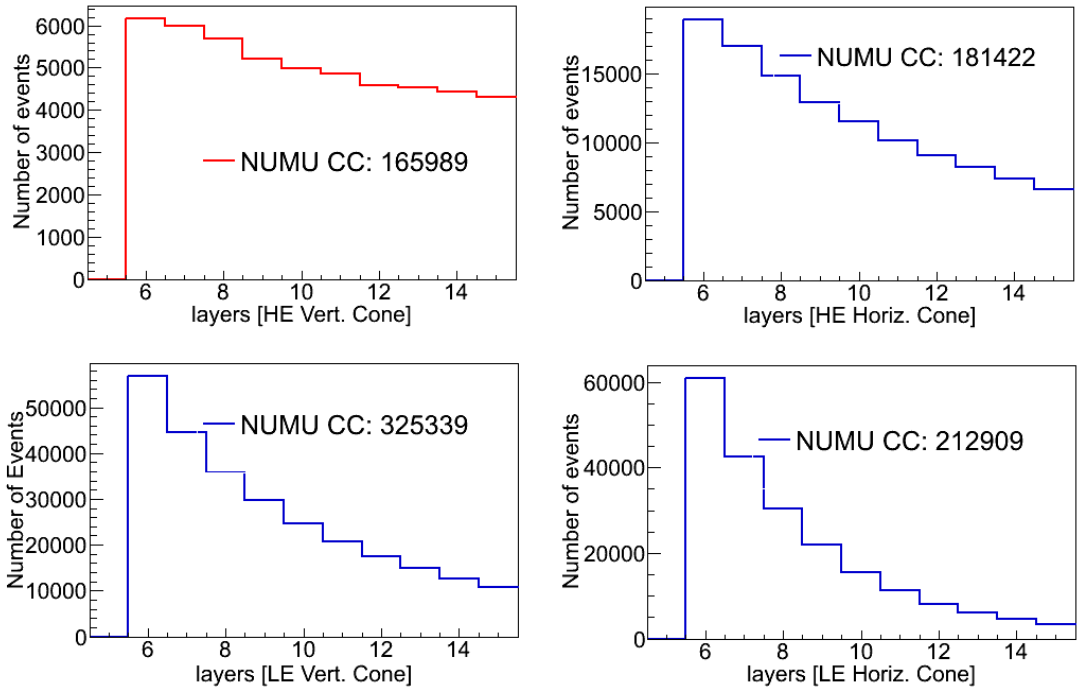

Figure 7.3: Layers Distributions for ν_μCC events with L>5, for the NOOSC 500 years dataset. The top left plot shows the distribution for the signal events (red).

7.4.3 Maximum horizontal spread of an event (maxdist)

The energetic but near horizontal muons have a larger spread on the horizontal plane than the vertical (or near-vertical) events. The horizontal spread between a pair of hits is given by $D = \sqrt{((x_2 - x_1)^2 + (y_2 - y_1)^2)}$. We calculate D for every pair of hits in an event and define its maxdist to be the maximum value of D [3]. The maxdist is quite large in case of high energy horizontal events and is moderate for the other three types of events, as can be seen in figure 7.4.

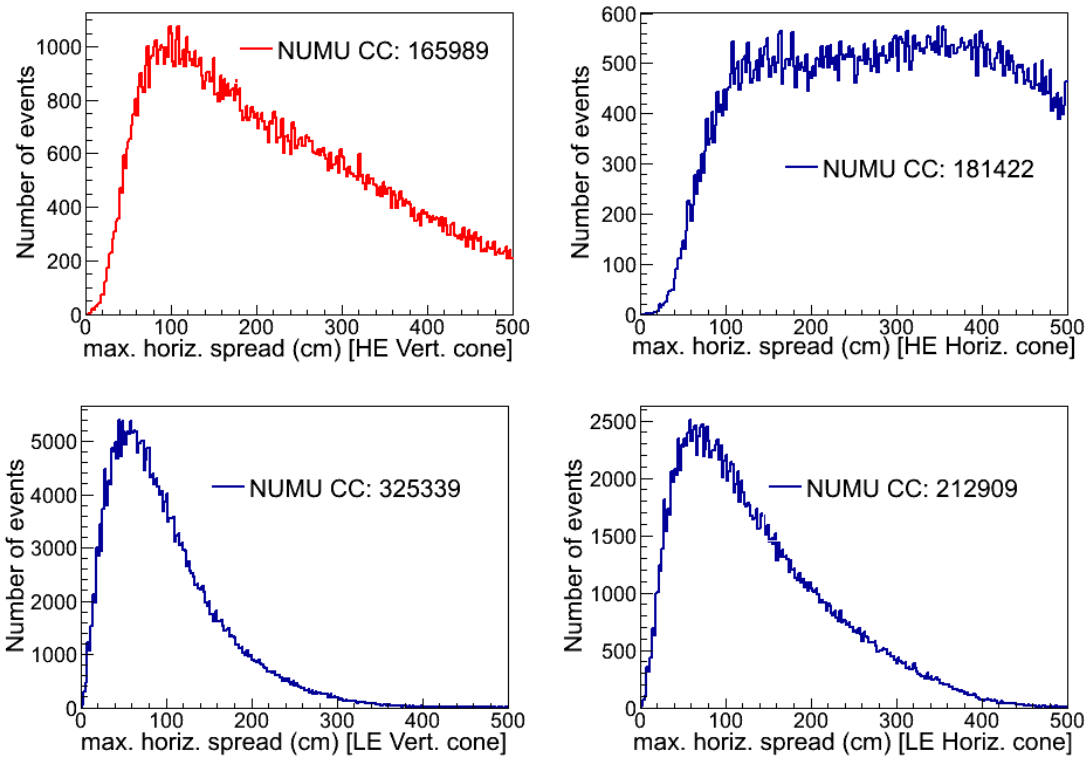

Figure 7.4: Maxdist distributions for ν_μCC events with L>5, for the NOOSC 500 years dataset. The top left plot shows the distribution for the signal events (red).

7.4.4 Singlets

A high energy vertical muon passes through a number of layers. Any hadron produced in the same event will pass through a much smaller number of layers. Therefore, in a high energy vertical event, there will be only hits due to the muon tracks after the initial few layers. For these later layers, we expect one or two hits in a layer. Almost all signal events must contain one or more layers with a single hit. The passage of a muon through an RPC can produce a hit in a single strip or hits in two adjacent strips. Therefore, we define a layer with a single hit to be one where there is only one hit or one where there are two hits in adjacent strips. *Singlets* is the number of layers in an event that contain

a single hit. A signal event is expected to contain more singlets than the low energy or the horizontal ν_μCC events. This is shown in figure 7.6.

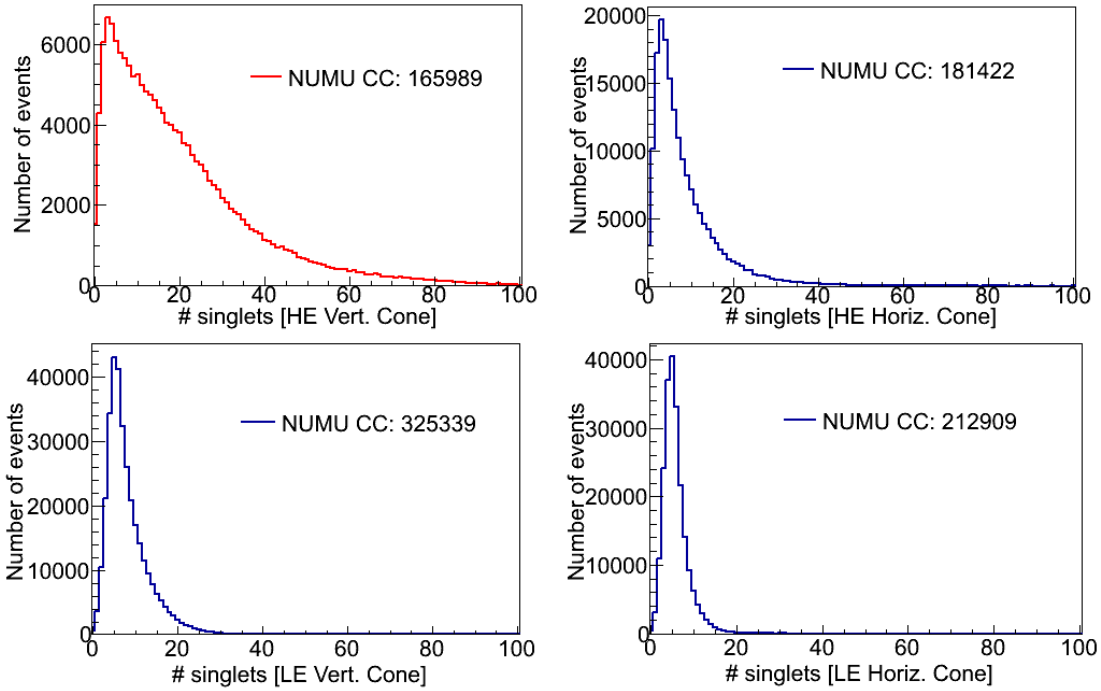

Figure 7.5: Distribution of # single-hit layers in the ν_μCC events: L>5 for the NOOSC 500 years dataset. The top left plot shows the distribution for the signal events (red).

7.4.5 Triplets

This is an extension of the previous parameter. *Triplets* is the number of 3 consecutive layers with single hits in an event. A signal event with a long muon track is expected to contain at least one such triplet. This variable gives more weightage to events with longer muon track with many consecutive single hit layers. For example, an event with five consecutive single hit layers has *three* triplets.

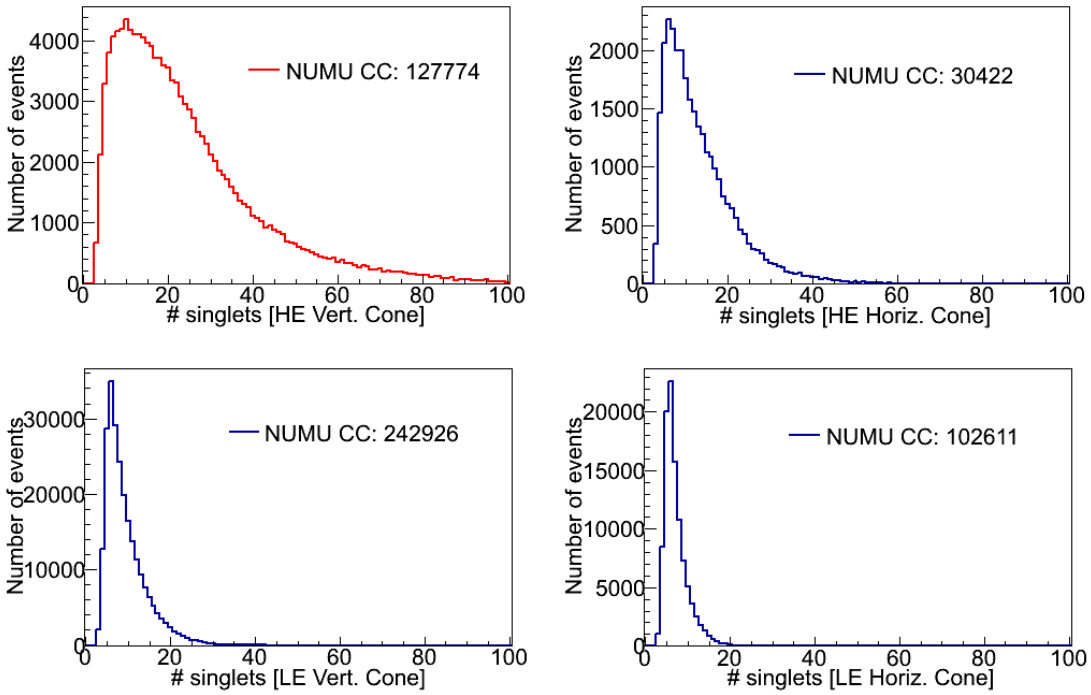

Figure 7.6: Distribution of the single-hit layers in the ν_μCC events (L>5), combined with maxdist/layers≤10 and # possible triplets>0, for the NOOSC 500 years dataset. The top left plot shows the distribution for the signal events (red).

Figure 7.6 shows an example of the efficacy of the listed parameters in selecting the signal events and in discriminating against the background events. In this figure, the singlet distribution is plotted for those satisfying the simple cuts: number of triplets non-zero and the ratio maxdist/layers $\leq$ 10. These distributions show that a cut of number of singlets $\geq$ 10 retains most of the signal events while rejecting a very large fraction of background events.

7.4.6 Summarizing the effects of the selection parameters

The effects of these carefully chosen and most crucial cuts are listed in the table 7.2.

Selection Criteria	Total $\#\nu_\mu$CC events	$\#\nu_\mu$CC events $\lvert\cos\theta\rvert$ >0.5, {4-100}GeV
L>0	23.7 $\times 10^5$	7.8 %
L>5	8.96 $\times 10^5$	18.7 %
demand min. 1 triplet	5.49 $\times 10^5$	24.2 %
#possible-Triplets>10	.559 $\times 10^5$	78.4 %
min. 1 triplet + maxdist/layers≤10	4.48 $\times 10^5$	27.3 %
min. 1 triplet + maxdist/layers≤10 + #single-hit layers≥10	1.92 $\times 10^5$	51.1 %

Table 7.2: Effect of the selection cuts on the 500 years NOOSC data at the ICAL@INO detector.

The above subsections all lead to the following inference:

- Hits or layers can distinguish the low energy from the high energy range ν events.
- Maxdist distinguishes the horizontal high energy events from the rest.
- The high energy vertical ν_μCC events contain significantly larger number of singlets than the low energy/ horizontal events.
- The hits-pattern across the layers in case of the high energy vertical ν_μCC events form more number of triplets than the the other three categories of ν_μCC events considered.

7.5 Application of Multivariate Tools

The parameters discussed in the above section indicate a reliable way to select our required signal events.

In cases of application of multiple selection criteria, varying the combination of the cuts in different ranges of the parameter values, might fetch better signal efficiency.

A selection based on neural network techniques, with these parameters as inputs, can select the signal events efficiently. So, we employ tools for multi variate analysis (TMVA), a package integrated in ROOT, for our signal selection [115].

There are a number of applicable methods that involve multivariate analysis.

7.5.1 Available Options

TMVA is a collection of classifiers, and the ones we found relevant enough to be mentioned in the process of our analysis are listed as follows [115][7].

BDT: A "decision tree" makes a sequential application of cuts to split the data into nodes, like a "tree". The final nodes ("leaf"), after "n" sequences classify an event as signal or background. Boosted decision trees combine a number of decision trees, with differently weighted events in each tree (trees can also be weighted). However, the simplicity of decision trees has the drawback that their theoretically best performance on a given problem is generally inferior to other techniques like neural networks [115].

RuleFit: This process is linear combination of rules, where a rule is a sequence of cuts:

$$y_{RF}(\overrightarrow{x}) = a_0 + \sum[a_m r_m(\overrightarrow{x})] + \sum[b_k \bar{x}_k] \tag{7.3}$$

[7] Each of the methods involve extensive sets of computational steps. Here, we state the tools/methods very briefly to save space and prevent divertion from the purpose of this study/chapter. For a proper understanding one must refer to [115].

where, y_{RF} is the RuleFit classifying parameter, the second summation term represents the sum of rules "r_m" (it refers to the status of the cuts applied during this internal/intermediate process, r_m=1 for all cuts satisfied, and 0 if none), the last term is the Linear Fischer term [115] and the $\bar{x}_k$ are the normalised event variables. The a and b are constants.

KNN (K-Nearest neighbour): The k-NN algorithm seeks k number of events which resemble the event in hand while testing. This similarity is enumerated with the help of a function, say R. The events with smallest values of this R gives the k-nearest neighbours.

SVM (Support Vector Machine): It finds a hyperplane that best separates signal from background, for the linear cases. For non-linear cases, the variables are first transformed into a higher dimensional space, so that a linear boundary can fully separate the data.

HMatrix: A covariance matrix is constructed from the values of the selection parameters during the processing of the variables at the initial stage of TMVA running (for example, a method called principle decomposition analysis [115]). The inverse of this matrix is called the H-matrix. This method calculates a χ^2 for the signal and the background events using the mean-estimators and the matrix elements. For every event, it calculates a value, y_H

$$y_H = \frac{\chi^2_S - \chi^2_B}{\chi^2_S + \chi^2_B}. \tag{7.4}$$

The higher the value of this parameter, more is the probability of an event to be a signal.

PDErs: It is basically a Probability Density Estimator, called PDE range search, which counts the number of training events which look closest similar to the test event. In other words, it is a variant of the k-NN. Eventually, it reports an estimated volume, V around the test event through a function of the number of signal events and the number of

background events closer to it.

Nonlinear Analysis: Artificial Neural Networks In cases where the variables are not linearly correlated, TMVA provides for nonlinear classifier response by "activating" output nodes using nonlinear weights. This is achieved through neural network techniques, or in other words the multilayer perceptrons.

There are three different ways of implementing Multilayer Perceptrons (MLP) in TMVA [115]:

- TMlpANN: Interface to ROOT's MLP implementation
- MLP: TMVA's own MLP implementation for increased speed and flexibility
- CFMlpANN: ALEPH's Higgs search ANN

They are all feed-forward networks, which basically do a mapping from the space of input parameters to that of the output parameters. The "mapping" certainly refers to a function, which varies from one "learning method" to another. The mapping can be done in several steps or layers, finally leading to one output value as shown in figure 7.7.

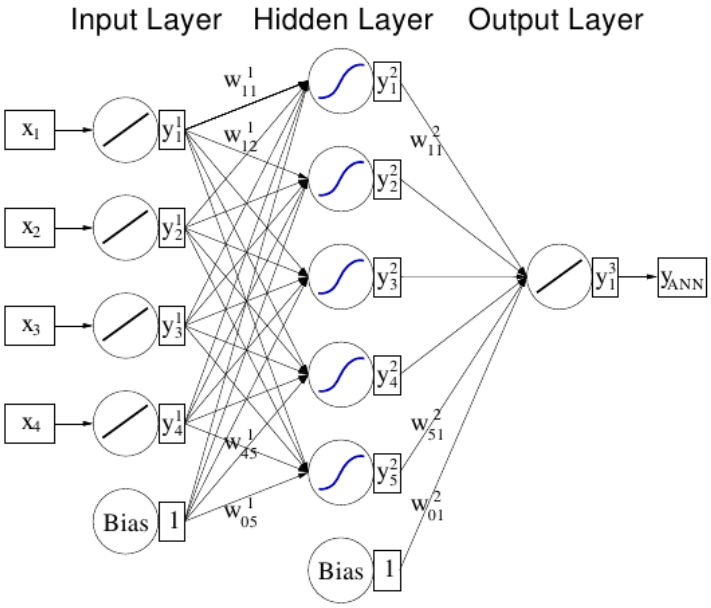

Figure 7.7: A schematic diagram of the neural network process [115]

7.5.2 Choice of a tool

The TMVA is applied on subset of the dataset (same as used for training/testing in the final tool, described later) and their comparative performance in selecting the signal events and rejecting the background events is observed in figure 7.8. The more convex the curve is, the better is its signal selection efficiency with maximum possible background rejection. If the graph for a process is linear or close to linear nature, it clearly declares that method as unacceptable. In figure 7.8, the methods shown are all closely competent with each other (we have checked few more methods whose graphs fell much lower to the ones in figure 7.8, and hence have not shown them here, to avoid unneccessary crowding). the

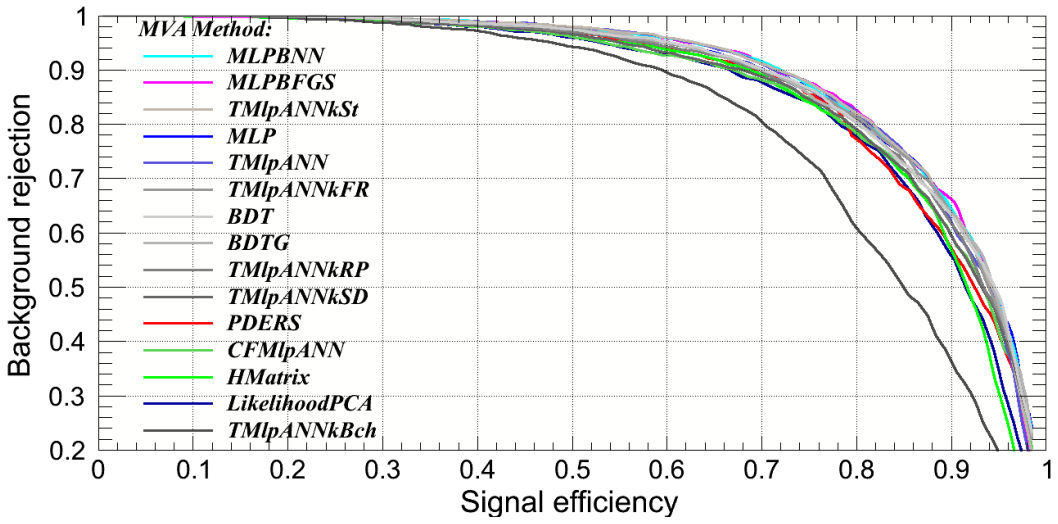

Figure 7.8: Signal selection efficiency vs. the background rejection of the various TMVA methods. There are different learning methods for training a TMlpANN and their performances are also shown.

Selection Response

Among the above methods mentioned, we must choose the one best suited for our purpose. So, we check their abilities in telling apart a signal event from the background event. We observe the distributions of the resultant values returned by every method in figure 7.9. The extreme ends of these values indicate an event identified to be a perfect signal or background. Response of the various MVA methods:

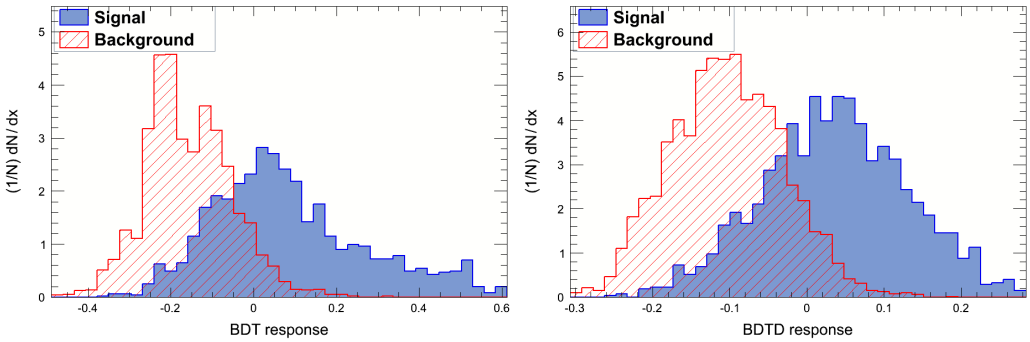

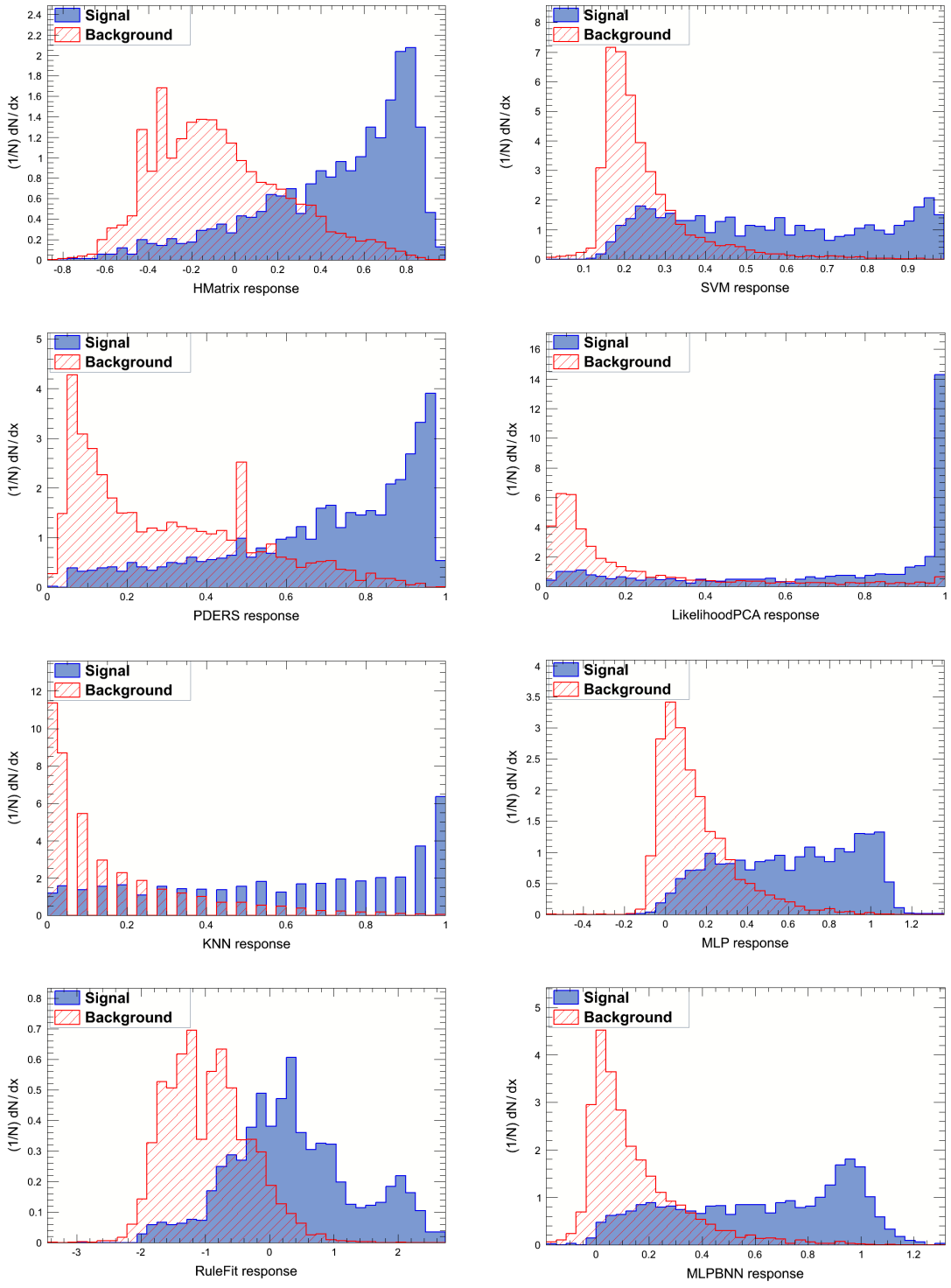
Signal
Background
(1/N) dN / dx
HMatrix response
SVM response
PDERS response
LikelihoodPCA response
KNN response
MLP response
RuleFit response
MLPBNN response

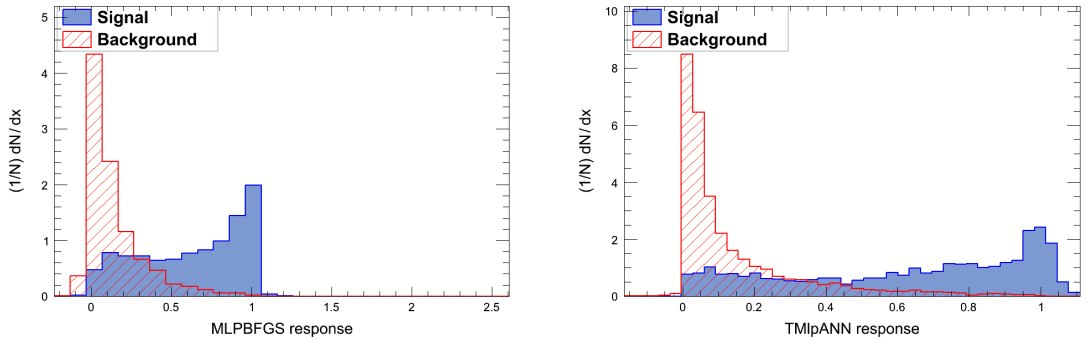

Figure 7.9: Response of the various methods to discriminate between the signal and the background in the testing sample. Row-wise from top: BDT, PDERS, BDTD (BDT with Decorrelated variables), KNN, HMatrix, RuleFit , SVM, MLPBNN, LikelihoodPCA, MLPBFGS, MLP and TMlpANN methods.

Signal efficiency and background rejection

In order to ease the user in the choice of the required tool, TMVA provides with several synthesized values which parameterise the performance of the method. For example, the contrast between the signal selection efficiency and the background efficiency or background retention, the signal significance etc. are some of them. The performance of two such methods are shown in figure 7.10 and figure 7.11.

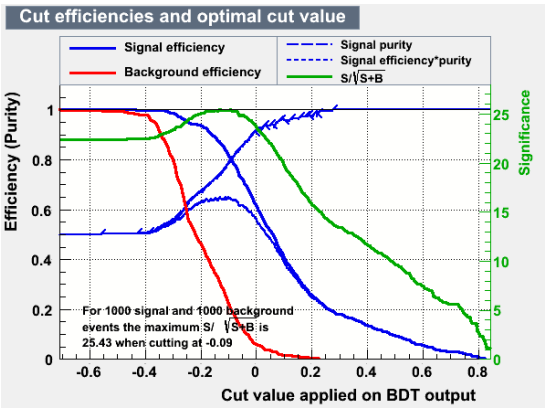

Figure 7.10: Response of the BDT in testing and training .

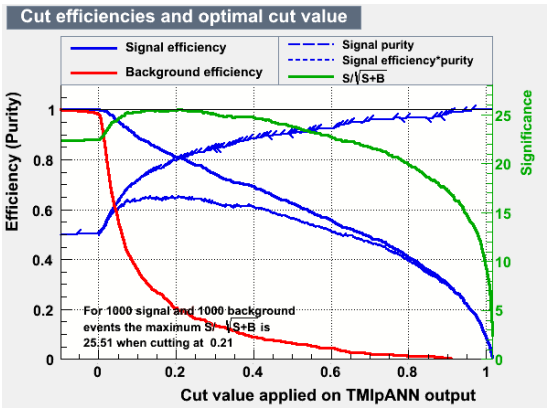

Figure 7.11: Response of the BDTD in testing and training .

Signal Significance: The signal significance is defined as

$$S_0 = \frac{Signal}{\sqrt{\text{Signal} + \text{Background}}} \tag{7.5}$$

S_0 approximately [8] peaks around the cut value when the signal selection efficiency, the purity of the signal and the background rejections are all optimized. However, for the present purpose, which is a type of multi-purpose discrimination, this value is not an adequate deciding factor [115]. This fact is evident from the tables 7.3 and 7.4.

The Signal to Background Ratio in training/testing sample The signal to background ratio may not be always unity. So, we are required to check the performance of the tools with unequal number of events for signal and background while training/testing. We considered six such cases, with varying ratio of the signal to background. The signal efficiency and purity vary most with the changing ratio.

- Set I: Signal=1000, Bkg.=1000.
- Set II: Signal=3000, Bkg.=3000
- Set III: Signal=1000, Bkg.=2000
- Set IV: Signal=3000, Bkg.=6000.
- Set V: Signal=1000, Bkg.=3000
- Set VI: Signal=3000, Bkg.=9000

The signal selection efficiency and the highest purity level obtainable by the different tools for the two of the extreme sets I and VI are listed in table 7.3 and 7.4 respectively.

[8] For exact calculation of the peak position, refer [115]

MVA method	**Cut Value**	**Signal Efficiency %**	**Bkg. Retention %**	**Signal Purity %**	**S_0**
BDT	-0.09	**80**	20	**80**	25.4
BDTD	-0.08	90	33	73	25.5
H-Matrix	0.06	86	27	77	25.5
KNN	0.15	85	28	78	25.6
LikelihoodPCA	0.22	86	28	76	25.5
MLP	0.20	86	26	78	25.7
MLPBFGS	0.18	85	27	78	25.6
MLPBNN	0.19	87	28	75	25.6
PDERS	0.38	87	32	73	25.4
RuleFit	-0.72	90	33	72	25.5
SVM	0.25	87	30	75	25.5
TMlpANN	0.21	**80**	20	**80**	25.5

Table 7.3: Set I: Comparing signal significance of the various MVA methods on a subset of the 500 years NOOSC data sample at the ICAL@INO detector, with a common cut of Layers>5.

MVA method	**Cut Value**	**Signal Efficiency %**	**Bkg. Retention %**	**Signal Purity %**	**S_0**
BDT	-0.02	**75**	8	**65**	38.3
BDTD	-0.04	75	15	63	37.7
H-Matrix	0.31	71	12	65	37.4
KNN	0.45	70	<10	65	36.9
LikelihoodPCA	0.63	70	<10	66	37.5
MLP	0.36	72	12	68	38.1
MLPBFGS	0.33	75	13	67	38.7
MLPBNN	0.35	78	13	68	38.4
PDERS	0.58	73	13	65	37.5
RuleFit	-0.23	71	12	68	37.3
SVM	0.30	78	18	68	37.6
TMlpANN	0.39	**68**	8	**72**	38.7

Table 7.4: Set VI: Comparing signal significance of the various MVA methods on a subset of the 500 years NOOSC data sample at the ICAL@INO detector, with a common cut of Layers>5.

The performances of the BDT and the TMlpANN appear better than the others in terms of signal selection efficiency and purity, as seen from Tables 7.3 and 7.4. Their performances also vary significantly with the ratio of the signal to background events. So, to save the realistic picture scenario, we decide to train the TMVA finally with a similar ratio of the signal to background, as is present in the original dataset.

Training/testing time: The time required for training or testing of the data is also a very important factor in data analysis. So, we also compare the time taken by the two tools (BDT and TMlpANN) in training and testing of sample. The comparison is shown in table 7.5.

Method	**Train. Time (s) for 11000 events [Test Time]**
BDT	8.9 [2.1]
MLPBFGS	347 [.11]
TMlpANNStch	26 [.07]
TMlpANNBFGS	51 [.07]

Table 7.5: Comparing training time taken by the different TMVA tools.

We observe from table 7.5 that the BDT takes less time to train than TMlpANN, but longer time to analyse an event (i.e. testing). Training of a sample is an offline job, and involves a very limited or small set of events. So, a longer time period may be accommodated, if so required. So, TMlpANN, once trained, will take shorter time in analysing a given data sample.

7.5.3 Comparison of TMVA Methods Results

We infer the following qualitative natures of the above selected TMVA methods:

- **Tool, Learning Process while training and Time for training/evaluating:**
  - BDT: Efficiency acceptable, training time is low, but its testing or evaluation time is at least 6 times any of the other methods mentioned here.
  - LikelihoodPCA: Efficiency acceptable, training time is very less.
  - HMatrix: Efficiency acceptable, training time is remarkably less.
  - MLPBFGS: Efficiency signifificantly good, training time is moderate.

  - TMlpANNkBFGS & TMlpANNkStch: Efficiency signifificantly good, training time is less. TMlpANNkBFGS consumes double the time that TMlpANNkStch requires.
  - On the grounds of signal selection efficiency and background rejection, the methods of BDT, LikelihoodPCA, HMatrix clearly fall behind, when compared to MLPBFGS, TMlpANNkBFGS or TMlpANNkStch methods.
  - On the grounds of training/testing time, BDT and MLPBFGS are certainly not favorable. With finer observation, TMlpANNkStch is faster than TMlpANNkBFGS. However, the methods LikelihoodPCA and HMatrix are the outstanding winners in the race of time.
  - Combining both the above aspects (efficiency/purity and time), our best optimised method is the TMlpANNkStch.

- The performance of TMlpANN method can be improved by optimising the number of nodes, layers and iteration-cycles:
  - Single layers are not preferred.
  - The nodal structure 7:5:3 (6:4:2) looks so far a favorable option.
  - Training with 200 or 300 cycles/iterations gives results comparable with that of 500 or 1000 cycles, but saves on the time simultaneously.

- Optimising the training sample size and signal fraction:
  - Large training size reduces the errors due to fluctuations/randomizations, but overtraining should also be avoided.
  - The ratio of the signal to background in the training sample is preferred to be the same as that in the real data. On the contrary, taking equal numbers of the signal and background events ensures more background rejection, at the same signal efficiency. Hence, the latter choice must be subjected to the achievement of better physics results (not discussed in this scope).

7.5.4 The final TMVA Method Chosen for this study

Our final selection after all optimizations are as follows:

- *Method*: **TMlpANN**.
- *Learning Method*: Stochastic.
- *Nodes and Cycles*: N+2:N:N-2, where N = #variables, and ∼300 iterations.
- *Training set*: Total events ≈ 20,000 with the signal to background ratio being the same as that in the actual data.

It was found that the event sample selected by TMlpANN had the best signal efficiency and purity. In addition, the time taken for the method to learn the discrimination and apply it to an event sample was also the least. In view of this the analysis was done using TMlpANN. Detailed optimization has shown that the stochastic learning method with three nodal steps and three hundred iterations gave the best performance. We applied the method on a training set of 20000 events with the signal to background ratio being the same as that in the actual data. The size of the training set was chosen after detailed optimization.

7.6 Re-Definition of our physics signal

In our initial analysis, we defined the signal events to be ν_μCC events with $E_\nu > 4$ GeV and $|\cos\theta_z| > 0.5$. But some hierarchy discrimination is present in events with lower energy and smaller $|\cos\theta_z|$. So we systematically lowered the minimum values of E_ν and $\cos\theta_z$, retrained the neural network each time, and analysed them. We found that the best hierarchy discrimination sensitivity is obtained with $E_\nu > 2$ GeV and $|\cos\theta_z| > 0.2$. The details of the calculation of this sensitivity are given in the next section. The efficiency of the neural network in distinguishing between the signal and background is shown in figure 7.12, and quantitatively in table 7.6.

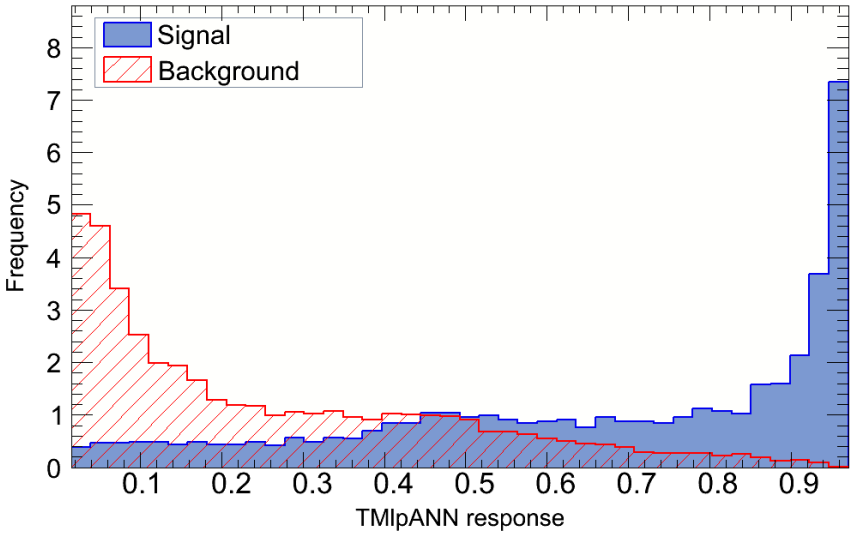

Figure 7.12: Neural network response to the signal vs. background discrimination. Here the signal definition is $E_\nu > 2$ GeV and $|\cos\theta_z| > 0.2$.

Value of ANNcut:	0.5	0.6	0.7	0.8
Efficiency %	73	64	55	46
Purity %	85	89	93	96

Table 7.6: Efficiency and purity of signal events chosen by the placing ANNcuts for the NH dataset of 500 years, assuming the signal events to be $E_\nu = \{2,100\}$ GeV and $|cos\theta| > 0.2$. and number of layers>5.

The figure 7.13 further shows very significant coincidences of the training and the test samples. So, we are further assured to use the current set of training conditions (technical grounds). of

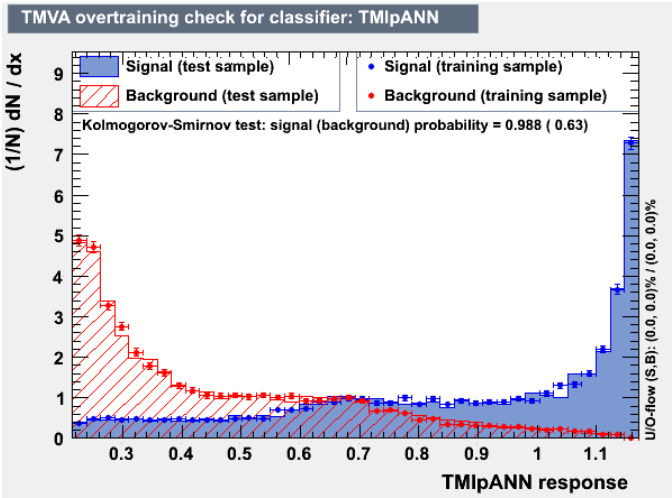

Figure 7.13: The overlapping of the test samples and the training sets for the above signal definition.

7.7 Mass Hierarchy Discrimination with ν_μCC events

Our redefined signal consists of the ν_μCC events with E_ν = {2,100} GeV and $|cos\theta| >$ 0.2. Therefore, the background comprises of all the rest of the ν_μCC events.

For the selected signal-like events, the muon energy E_μ and its direction $\cos\theta_\mu$ are reconstructed. The events are sorted into bins of the reconstructed E_μ and $\cos\theta_\mu$. A better angular resolution leads to a better hierarchy discrimination in atmospheric neutrino experiments [135, 136]. Hence the bin width in $\cos\theta_\mu$ needs to be as small as possible. The energy and $\cos\theta_\mu$ binwidths are chosen based on the energy and $\cos\theta_\mu$ resolution of the ICAL [10]. The down going events undergo no oscillation and hence there will not be any signature of matter effect in them. It is present only in the up going events. Hence in computing the $\Delta\chi^2$ for hierarchy discrimination, we will consider only the up going events, *i.e.* events with $\cos\theta_\mu \in [0, 1]$.

The effect of the ANNcut on the events sample is shown in table 7.7 and figure 7.14.

	All events	After 5 layers cut	After addn. ANNcut=0.7
upgoing signal	147734	113032	61408
upgoing background	472113	108656	5104
downgoing signal	310926	239460	133092
downgoing background	757239	196275	9994

Table 7.7: Event counts for the NH dataset of 500 years, assuming the signal events to be E_ν = {2, 100} GeV and $|cos\theta| > 0.2$. and nLayer>5. (The counts for the IH set is similar and not shown here.)

In figure 7.14, we have shown the distribution of E_μ vs. $\cos\theta_\mu$. The top panel shows the distribution for all events, i.e., without any layer or ANNcut. The middle panel shows the distribution after applying the 5-layer cut, but without any ANNcut and the bottom panel includes the ANNcut of 0.7 in addition to the layer-cut. We clearly see that low energy and horizontal events are heavily suppressed in the bottom panel.

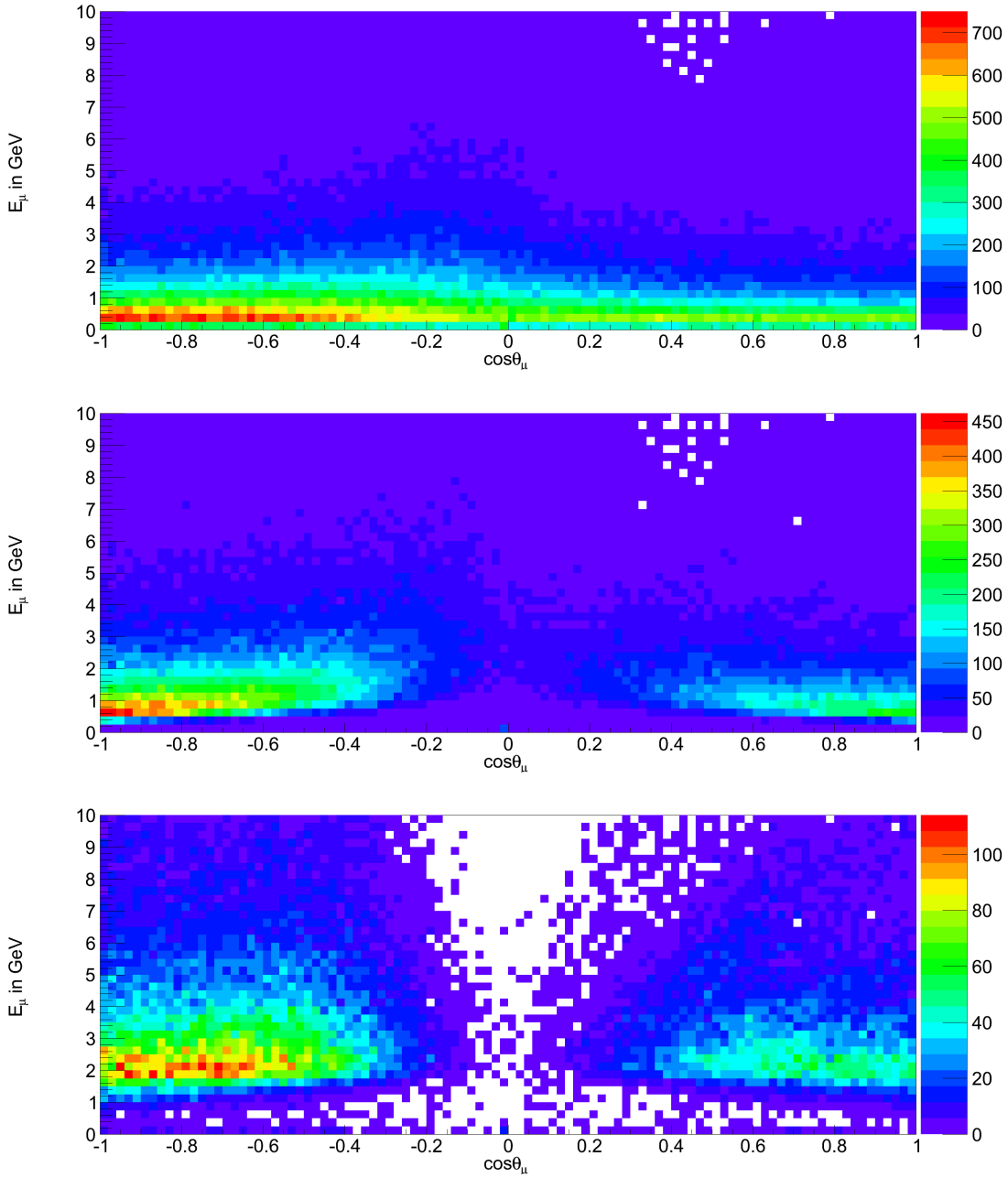

Figure 7.14: The distribution of muon energy and direction (given by NUANCE) of the ν_μCC events selected: (Top) all detectable events (without the layer-cut); (Middle) Events after the 5-layer cut only, and (Bottom) Events after 5 layer cut and the cut on the neural network probability = 0.7.

Regarding the binning in muon energy, different schemes were tested. We restricted the range of muon energies to be (0, 17) GeV. Since events with very high energy muons are rather small in number, their contribution to hierarchy discrimination is very small.

The $L > 5$ cut as well as the selection based on ANN strongly discriminate against events with $E_\mu < 1$ GeV. Therefore, our lowest energy bin is chosen to be (0, 2) GeV, so that the number of events in this bin are substantial. We found the following 10 E_μ bins to be optimal: (0, 2), (2, 3), (3, 4), (4, 5), (5, 6), (6, 7.5), (7.5, 9), (9, 11), (11, 14) and (14, 17) GeV. The binning is done separately for μ^- and μ^+ events. The chosen $\cos\theta_\mu$ binwidths, different for different E_μ ranges, are listed in table 7.11.

E_μ range	$\cos\theta_\mu$ range	$\cos\theta_\mu$ binwidth
0-6 GeV	(1-0.8, 0.8-0.2, 0.2-0)	(0.01, 0.02, 0.1)
6-17 GeV	(1-0.2, 0.2-0)	(0.01, 0.1)

Table 7.8: $\cos\theta_\mu$ binwidths in different energy ranges.

For the hierarchy discrimination analysis, the NH and the IH data of the upward going events were binned according to the scheme described above. We compute the $\Delta\chi^2$ between these two data sets using the Poissonian definition and scale it by 50 to obtain $\Delta\chi^2$ for a ten year exposure. A similar calculation of downgoing events gives a $\Delta\chi^2$ less than 1%. Thus the use of only upward going events for computing $\Delta\chi^2$ is justified. In figure 7.15, we plot $\Delta\chi^2$ vs ANNCut. We obtained a maximum $\Delta\chi^2 = 10.2 \simeq 10$ for an ANN probability cut of 0.7. Figure 7.15 also shows the comparison between the $\Delta\chi^2$ values obtained for the original signal definition and the modified one. We see from the figure that the hierarchy discrimination with the modified signal definition is better.

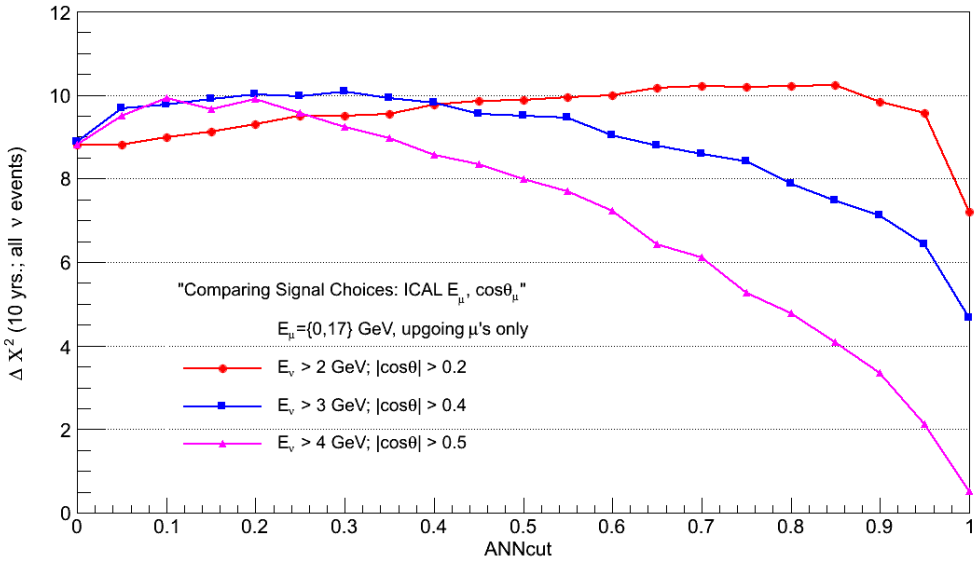

Figure 7.15: Hierarchy discrimination sensitivity for different signal definitions

7.7.1 Effect of Marginalisation

We have used the present best fit values of the oscillation parameters so far to generate the NH and IH dataset. However, the true values of these parameters can well be different from the present best fit values, but falling within the allowed range. To take into account this deviation, we need to recompute the $\Delta\chi^2$ by doing a marginalisation over these parameters. In doing the marginalisation, we have kept Δm^2_{21} and θ_{12} fixed but varied Δm^2_{eff}, θ_{13} and θ_{23} over their allowed 3 σ ranges. These ranges are listed in table 1.1. Since all these parameters are determined with reasonable precision, the effect of marginalisation is small. Without priors, the $\Delta\chi^2$ decreases to 9, whereas with priors it remains 10. The left panel in figure 7.16 shows the variation of $\Delta\chi^2$ vs θ_{13} both without and with priors. The right panel shows the $\Delta\chi^2$ vs θ_{23} both without and with priors.

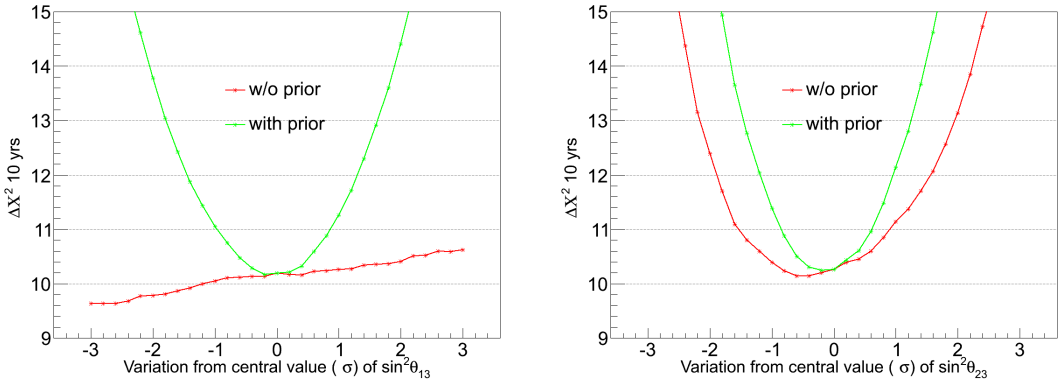

Figure 7.16: Verifying the effect of θ_{13} (left) and θ_{23} (right) on the sensitivity for normal hierarchy, from events chosen above the ANNcut, for signal definition: $E_\nu > 2$ GeV and $|\cos\theta_z| > 0.2$.

7.7.2 Effect of Systematic Uncertainties

The various inputs used in calculating the event numbers, such as the neutrino flux, the cross-section etc., have systematic errors. Taking these into account can also reduce the hierarchy discrimination sensitivity. We recalculated $\Delta\chi^2$ by including the systematic errors through the method of pulls [137, 138, 139]. In our calculation we have taken the systematic uncertainty in the flux to be 20%, in the cross-section to be 10% and in the neutrino energy and zenith angle spectrum of 5% each. In addition, we have also included an overall systematic uncertainty of 5% [7]. We have done the calculation under two different assumptions: The systematic uncertainties for neutrino and anti-neutrino events are (i) the same and (ii) unrelated. In the former case, we find that the inclusion of the systematic uncertainties has **no effect** on $\Delta\chi^2$! This occurs due to the following reason. The quantity $\Delta N_{ij} = N_{ij}(\text{NH}) - N_{ij}(\text{IH})$ (where i denotes the E_μ bin and j denotes the $\cos\theta_\mu$ bin) is mostly negative for μ^- events and is mostly positive for μ^+ events. Therefore, the pulls needed to minimize $\Delta N_{ij}(\mu^-)$ and $\Delta N_{ij}(\mu^+)$ are different. If we assume that the systematic uncertainties are the same in both cases, it is reasonable that the values of pull variables, minimizing $\Delta\chi^2$, are negligibly small. This can be

understood from the table 7.9.

Min. $\Delta\chi^2$ using	All	NH>IH	NH<IH	μ^+ only	μ^- only
Fxd. par.	10.19	4.38	5.81	4.38	5.81
Syst. w/o any prior	9.91	1.64	1.72	3.72	4.12
Syst. with prior	10.33 (10.04+0.29)	2.19 (1.99+0.20)	2.11 (1.89+0.22)	4.04 (3.79+0.25)	4.51 (4.29+0.22)

Table 7.9: The minimum values of $\Delta\chi^2$ (10 years) obtained, when certain subsets are chosen from the data (using ICAL E_μ, $\cos\theta_\mu$ with ANNcut=0.7). Here NH (IH) refers to number of events in a bin for the NH (IH) case.

When events with only positive (negative) ΔN_{ij}s are considered (ref. table 7.9), the effect of the systematics is dramatic, but the effects get neutralised, as soon as the events with negative (positive) ΔN_{ij}s are included. This gets reflected through the event counts of the μ^+ and μ^-s, as already stated above.

If the systematic uncertainties for the two cases are assumed to be different, then the pull variables for the two cases are also different. In this case, a lower $\Delta\chi^2 \simeq 8$ is obtained, if no priors on the pull variables are added. With the inclusion of the priors in the form $\sum_k \xi_k^2$ [11], the minimum $\Delta\chi^2$ is about 9.5. Combining marginalisation and systematic uncertainties, we obtain $\Delta\chi^2 \simeq 10$ for the case of equal uncertainties for μ^- and μ^+ and 9.5 for the case of unrelated uncertainties. Table 7.10 lists the values of $\Delta\chi^2$ obtained for various different cases.

Min. $\Delta\chi^2$ using	Values of $\Delta\chi^2$
Central values of osc. par.	10.2
Marg. w/o any prior	9.13
Marg. With prior	10.14 (9.75 + 0.39)
5 ξ: Syst. w/o any prior	9.91
5 ξ: Syst. With prior	10.33 (10.046+0.288)
5 ξ: Marg.+Syst. w/o prior	10.12
5 ξ: Marg.+Syst. With prior	10.84 (10.12+0.39+0.33)
10 ξ: Syst. w/o any prior	7.90 (+2.62)
10 ξ: Syst. With prior	9.45 (8.00+1.45)
10 ξ: Marg.+Syst. w/o prior	7.59 (+2.6)
10 ξ: Marg.+Syst. With prior	9.48 (7.64+0.39+1.45)

Table 7.10: Values of $\Delta\chi^2$ (10 years) with ICAL E_μ, $\cos\theta_\mu$, for central values of the oscillation parameters; including marginalisation in 3σ ranges of the Δm^2_{eff}, θ_{13} and θ_{23}; including only systematic uncertainties: "same" or 5 ξ (pull variables) and "unrelated" or 10 ξ (pull variables), and combining both marginalisation and systematic uncertainties.

7.8 Mass Hierarchy Discrimination including all ν interactions

Our signal still consists of the ν_μCC events with E_ν = {2,100} GeV and $|cos\theta| > 0.2$. The background comprises of all the rest of the ν_μCC events as well as all non-ν_μCC events

(i.e., all NCs, ν_eCC and ν_τCC).

Five different sets of data, each equivalent to 500 years of ICAL run, are generated using NUANCE in the energy range E$_\nu$= {0.1,100} GeV. Each set consists of all types of interactions of all three neutrino flavours. The first set is generated with the assumption of no neutrino oscillations (NOOSC). The next three sets are generated assuming neutrino oscillations with normal hierarchy, with 3 different seeds. The final set is generated assuming neutrino oscillations with inverted hierarchy. The generated events are then propagated in ICAL using a Geant4 simulation of the detector. The pattern of hits thus generated are used to first identify the muon track and then reconstruct its energy E_μ and the cosine of its zenith angle $\cos\theta_\mu$ [2]. In computing the oscillation probabilities, the following values of neutrino parameters were used: $\Delta{m_{21}}^2 = 7.5 \times 10^{-5}$ eV^2, $|\Delta{m_{eff}}^2| = 2.47 \times 10^{-3}$ eV^2 (i.e. $\Delta{m_{31}}^2$(NH) $= 2.51 \times 10^{-3}$ eV^2, $\Delta{m_{31}}^2$(IH) $= -2.43 \times 10^{-3}$ eV^2), $\sin^2\theta_{12} = 0.31$, $\sin^2 2\theta_{13} = 0.09$, $\sin^2\theta_{23} = 0.5$ and $\delta_{CP} = 0$.

If we impose the cut $L > 5$ on the 500 year dataset with IH oscillations, the remaining data sample has the composition shown in table 7.11. The numbers for NH oscillations are similar.

Total signal events	Total bkg. events
~350,000	~400,000

Table 7.11: Counts of the events after a cut of Layers>5, in a 500 years data sample (signal definition: $E_\nu > 2$ GeV and $|\cos\theta_z| > 0.2$).

The entire process of signal selection by neural network is repeated with this data sample. For the selected signal-like events, the muon energy E_μ and its direction $\cos\theta_\mu$ are reconstructed. The events are sorted into bins of the reconstructed E_μ and $\cos\theta_\mu$. A better angular resolution leads to a better hierarchy discrimination in atmospheric neutrino experiments [135, 136]. Hence the bin width in $\cos\theta_\mu$ needs to be as small as

possible. The down going events undergo no oscillation and hence there will not be any signature of matter effect in them. It is present only in the up going events. Hence in computing the $\Delta\chi^2$ for hierarchy signal, we will consider only the up going events, *i.e.* events with $\cos\theta_\mu \in [0, 1]$. This has the advantage of eliminating the contribution of the fluctuations in the down going events to the χ^2.

A binning scheme with uniform energy bins is not preferred. We have verified that the results are much better for a scheme with differential energy bins compared to a scheme with uniform energy bins. So, we use the same binning scheme as described and used for the study in the earlier section.

For the hierarchy discrimination analysis the four data sets $NH1, NH2, NH3$ and IH were used. Each of them was binned according to the scheme described in the earlier section. From this binned data, we compute 3 values of χ^2_{true} as $\chi^2(NH1 - NH2)$, $\chi^2(NH1 - NH3)$ and $\chi^2(NH2 - NH3)$, and take their average to obtain $< \chi^2_{true} >$. This is expected to be twice the number of bins. We also compute 3 values of χ^2_{false} as $\chi^2(NH1 - IH)$, $\chi^2(NH2 - IH)$ and $\chi^2(NH3 - IH)$, and take their average to obtain $< \chi^2_{false} >$. From these we obtain $< \Delta\chi^2 > = < \chi^2_{false} > \ - \ < \chi^2_{true} >$.

Since, the method of generating the datasets involves a slightly different path than in the earlier section, we first calculate the $< \Delta\chi^2 >$, considering the ν_μCC events alone in the present selected sample. The values of $< \Delta\chi^2 >$ against different ANN probability cuts are shown in figure 7.17. We obtained a maximum $< \Delta\chi^2 >= 9$ (assuming a 10 year run) for an ANN probability cut of 0.7, when only the ν_μCC events are considered. On inclusion of the non-ν_μCC background events, the curve of $< \Delta\chi^2 >$ is mostly lower than the former one. However, the ANNCut of 0.7 very clearly rejects all background contaminations, and the maximum $< \Delta\chi^2 >$ obtainable is restored to the value of **9**.

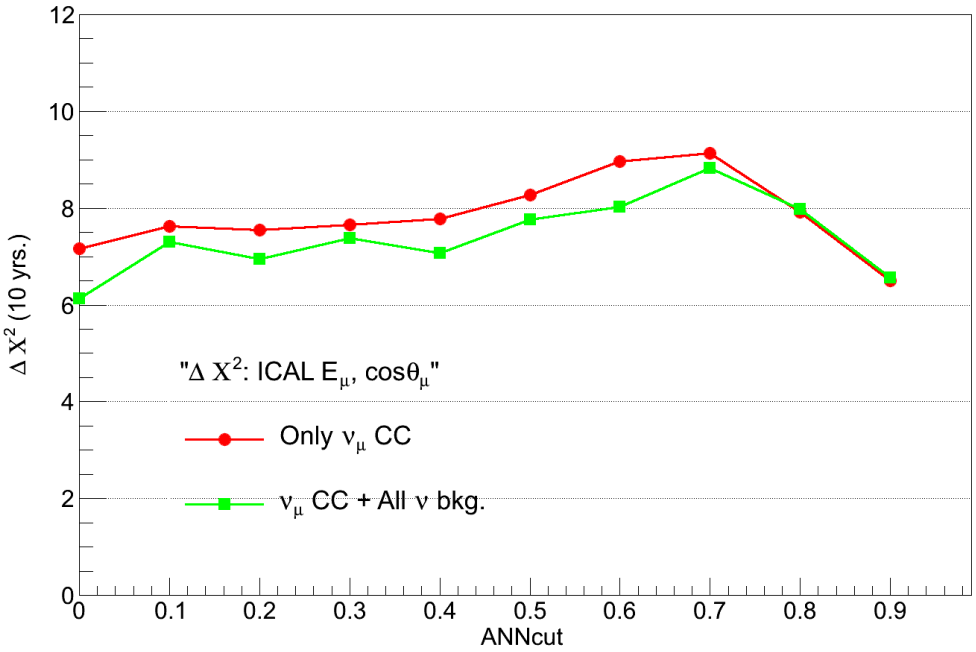

Figure 7.17: Values of $< \Delta\chi^2 >$ for 10 years, against varying cuts on the probability for the dataset containing ν_μCC events only (red) and including all neutrino interactions, i.e. ν_μCC + ν_eCC + all 3 types of NC + ν_τCC events (green).

One must remember not to make a one-to-one comparison of the results from the earlier section. In the earlier section, the NH and the IH sets were generated from a NOOSC sample, using oscillation probabilities and the accept-reject method. This results in less fluctuations due to the Monte Carlo number generation. The generation of all ν events for this section was done by the Nuance Monte Carlo neutrino event generator explicitly for the NH and the IH cases. This includes more fluctuations in the sample. Being meticulous, one may even argue that on generation of several (say thousand or more) such NH and IH datasets with Nuance will fetch us a distribution of $< \Delta\chi^2 >$, which peaks at the value of 10, like in the earlier section. This section aims to find out how much the hierarchy sensitivity might deteriorate when all ν events are considered,

i.e. in the practical scenario.

So, we infer that the obtained value of $\Delta\chi^2 = 10$ remains unaffected, when the background (non ν_μCC) are included, "*thanks to the* **neural network**" ! The value goes down to 9.5, when the marginalisation and systematic errors are also considered, as explained in the earlier section.

7.9 Results and Discussions

We have used a neural network to identify high energy ν_μCC events in the vertical direction. We defined the signal events to be those with $E_\nu > 2$ GeV and $|\cos\theta| > 0.2$. With an ANNcut of 0.7, the neural network is able to select such events with an efficiency 55% and a purity of 93%. We obtained a hierarchy discrimination $\Delta\chi^2$ of 10 for a 10 year exposure. Marginalisation and equal systematic uncertainties for neutrinos and anti-neutrinos do not reduce this value. If we assume that the systematic uncertainties for neutrinos and anti-neutrinos are unrelated, it reduces to 9.5. When the non-ν_μCC backgrounds are also included, the use of the neural network ensures no reduction in this value of $\Delta\chi^2$.

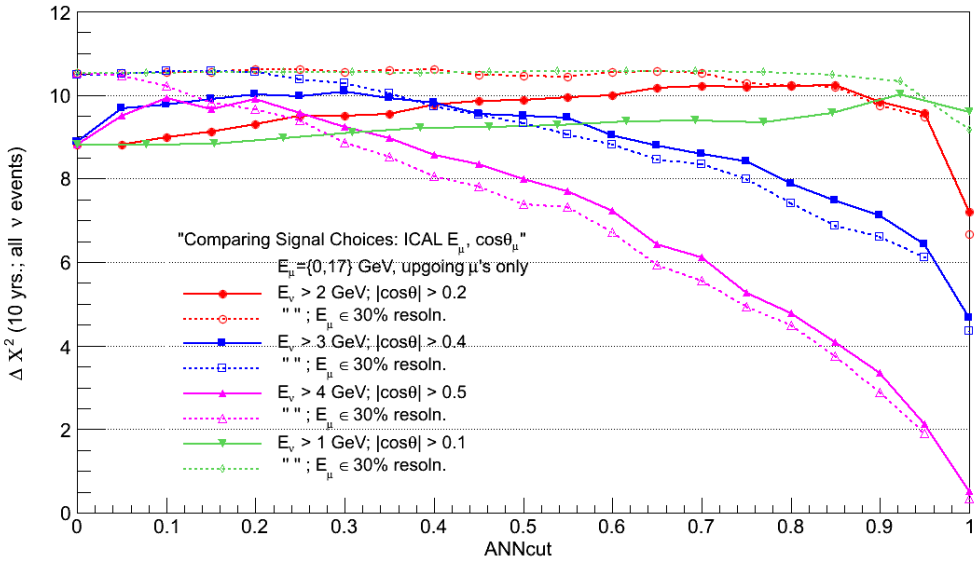

Figure 7.18: Checking the content of good events (events with their E_μ reconstructed within 30% of the true muon momenta) in the fraction of events chosen above the ANN-cut, for signal definitions: $E_\nu > 2$ GeV and $|\cos\theta_z| > 0.2$, $E_\nu > 3$ GeV and $|\cos\theta_z| > 0.4$, $E_\nu > 4$ GeV and $|\cos\theta_z| > 0.5$ and $E_\nu > 1$ GeV and $|\cos\theta_z| > 0.1$.

We considered the possibility that the fluctuations, arising due to inefficiencies in the reconstruction, are responsible for the large value of $\Delta\chi^2$. To rule out this possibility, we considered only those events which satisfied the following criterion: The reconstructed E_μ is within 30% of the NUANCE value. This restriction gives us a smaller event sample. The $\Delta\chi^2$ from this subset for the different signal definitions are shown as the dotted curves in figure 7.18. For the ANNCut of 0.7 and beyond, the curves without and with the restriction match best in case of our chosen signal, i.e. $E_\nu > 2$ GeV and $|\cos\theta_z| > 0.2$.

Therefore, the hierarchy discrimination we obtained comes mostly from vertical, high energy events, i.e. the *signal* events which are expected to be sensitive to hierarchy. In conclusion, ICAL@INO can determine the neutrino mass hierarchy at better than 3 σ sensitivity with an exposure of 10 years.

8

Summary

8.1 Muonless events

Events in ICAL at INO can be classified into events with muon tracks and those without such tracks. We refer the latter as the "muonless" events, which basically comprise of the ν_eCC events, "others" (all NC and a few ν_τCC) and the low energy or horizontal ν_μCC events.

8.1.1 ν_eCC Pure Sample

Applying certain selection cuts, we can obtain an events sample rich in atmospheric ν_eCC events. The cuts are based mostly on the number of hits and number of layers. The hits and layers criteria can alone fetch a ν_eCC sample of $\sim$50% purity. With the additional selection criteria, we can improve the purity of the sample. The most effective criteria are listed in table 8.1 along with the sample-sizes:

Selection Criteria	**Selected Sample size**	**ν_eCC Content**	**ν_eCC Purity**	**ν_eCC Net Selection Efficiency**
Maximum Hits diff.	156,000	82500	53%	50%
"+Overall Pattern: hits in layers	189,000	99814	56%	61%
Comparison: hits in layers	43,000	26006	60%	16%
Single layer hits	6,500	4420	68%	3%

Table 8.1: Examples of one of the cuts from each type of selection criteria on 500 years of NH data: Purity = ratio of ν_eCC content to selected sample size; Net Selection Efficiency = ratio of ν_eCC content in the selected sample to the same in the primary dataset i.e. with hits>10.

The purity of ν_eCC events in the total sample decreases with increasing sample size. It has also been observed that attempts to improve on the purity depletes the vertical events fraction. Appropriate selection cuts can be applied, while retaining optimum sample-sizes. This leads to a maximum **ν_eCC purity** of $\sim$ **60%** with $\sim$ 100 events per year. We can also obtain an event sample with νNC purity of $\sim$ 47% with $\sim$ 1800 events per year, provided noise is under control [3].

8.1.2 MH Contribution

The contribution of the muonless events in determining the neutrino mass hierarchy is not zero, rather $\chi^2_{10years} \sim$1. But the statistical fluctuations in the data are too large for this contribution to have a significant effect.

8.1.3 Energy and Direction

Energy and direction are the primary kinematical variables of the neutrinos. These are the essential data about the incident neutrino and are utilized in various studies. The muonless events appear merely as a bunch of hits in the detector. So, our algorithm of energy and direction estimation is mostly based on these hits and the number of layers hit in an event.

Energy:

A more energetic neutrino event gives more hits in the detector than a neutrino event of lower energy. Such a correlation becomes realizable, when the average hits per layer distribution is observed for events giving hits in a fixed number of layers. So, we observe the E_ν distribution in small bins of hits per layer, for every individual "no. of layers hit". Gradual shifts in the energy plots can be marked in the various bins, as expected. We fit the distributions with Landau distribution function. In order to be able to calibrate the neutrino energy, we recognize a parameter to represent the identity of these distributions in every such bin. Using the most probable value of the Landau distribution, "Energy-Calibration" curves can be prepared, to directly read the energies of such neutrinos. The calibration plots for events giving hits in 3-6 layers are shown in figure 5.8. It also assures that a muonless sample rich in any one of the three types of ν-events (ν_eCC, NC/ν_τCC or ν_μCC (low energy or horizontal)) has better energy resolution.

Direction:

We attempt to estimate the direction of the neutrinos using two independent kinematic variables. We use "maximum spread" in an event to resolve the horizontal neutrinos from the vertical ones. The vertical or near vertical events have shorter average horizontal spread than the horizontal or near horizontal events.

The horizontal distance between every pair of points is calculated for an event. The maximum value of this distance in an event serves as our selection parameter.

In order to distinguish between the upward and the downward going neutrinos, we define a new variable called "MRratio", which is briefly explained as follows. The hits in different layers of the ν_eCC events are non-uniform. The ν_μCC gives a broader distribution than the ν_eCC / NC. We consider the mean and the RMS (Root Mean Square or variance) value of such layerwise hits distribution of each event. The ratio of this layer-hits mean to RMS ("MRratio") shows characteristic difference for the up-going and the down-going neutrinos.

The first parameter, maximum spread ("mxdist") can select vertical events from the horizontal events. The second parameter is used to pick between the upgoing and the downgoing neutrino events. 2-D histograms of these two variables show gradual shifts in the peak positions of such distributions, in varying bins of neutrino direction. The distributions show Gaussian nature along the axis of MRratio, while Landau nature along the axis of maximum spread.

With these direction resolving techniques, the up-going ν's in the muonless sample can be selected to $\sim$70% purity. Muonless samples rich in vertical ($\lesssim 65^o$) ν's can be selected to above 80% purity. An approximate **estimation of the neutrino direction** can also be obtained, for *muonless* events, using the 3D-calibration plot in figure 5.14.

8.2 GENIE incorporation

The neutrino event generator is a vital component in the simulation studies of a neutrino experiment. So far, Nuance has been used to generate neutrino interactions for INO simulations. However, Nuance being no more updated, INO has chosen to adopt GENIE as the neutrino event generator. This required us not only to make an INO-user friendly version of GENIE, but also led us to include four new options in the GENIE code, three of which may also be used for any other atmospheric neutrino experiments. So, the 4 new options in the GENIE neutrino event generation, which are available at the GENIE@INO version are:

- *FLUKA3D*: To include the 3D atmospheric neutrino flux information
- *-w <energy-weight>*: Option for weighted atmospheric event generation
- *nu_INOGEN_rootracker*: Command to get exclusive INO-customised output
- *-e <No. of years>*: To generate events for a desired exposure time of the detector.

8.3 MH determination improved by neural network

The events containing muon track are the primary signal events of ICAL. Major contribution to determining the neutrino mass hierarchy comes from these events. We employed the technique of neural network analysis to improve the hierarchy sensitivity of the ICAL. This not only gave us the ability to effectively choose ν_μCC events in the energy range >2 GeV in the vertical cone but also led to obtaining a 3σ hierarchy sensitivity in 10 years at the ICAL.

We have used a neural network to identify high energy ν_μCC events in the vertical direction. We defined the signal events to be those with $E_\nu > 2$ GeV and $|\cos\theta| > 0.2$. With an ANNcut of 0.7, the neural network is able to select such events with an efficiency 55% and a purity of 93%. We obtained a hierarchy discrimination $\Delta\chi^2$ of 10 for a 10 year exposure. Marginalisation and equal systematic uncertainties for neutrinos and anti-neutrinos do not reduce this value. If we assume that the systematic uncertainties for neutrinos and anti-neutrinos are unrelated, it reduces to 9.5. When the non-ν_μCC backgrounds are also included, the use of the neural network ensures no reduction in this value of $\Delta\chi^2$.

8.4 Conclusion

This research work includes the study of both the kinds of the atmospheric neutrino events to be seen in the ICAL detector: the shower-like events or the **muonless** neutrino events

and also the **muon**-track-containing neutrino events. High energy ν_e ($\bar{\nu}_e$) interactions have been studied only in IMB, Kamiokande and Super-Kamiokande before. INO gives us another chance to study them in detail. We propose a method to extract the atmospheric ν_e ($\bar{\nu_e}$) data from the ICAL data. We also studied the ν_μCC events, and attempted to improve the hierarchy sensitivity of the ICAL, which is its primary objective, by applying the neural network analysis. We also showed that the use of neural network cancels the effects of the background due to other neutrino interactions. Even after including the systematic uncertainties, ICAL can still achieve a 3σ sensitivity in its main goal.

[1] D. Casper, Nucl.Phys.Proc.Suppl. **112**, 161 (2002), http://arxiv.org/abs/hep-ph/0208030 arXiv:hep-ph/0208030 [hep-ph] .

[2] G. Majumder and A. Redij (INO Collaboration), http://www.tifr.res.in/ gobinda/inosim/inosim.html "GEANT4 based INO-ICAL simulation code," (2011).

[3] A. Ajmi and S. U. Sankar, JINST **10**, P04006 (2015), http://arxiv.org/abs/1501.03252 arXiv:1501.03252 [physics.ins-det] .

[4] M. Blennow, P. Coloma, P. Huber, and T. Schwetz, JHEP **1403**, 028 (2014), arXiv:1311.1822 [hep-ph] .

[5] C. Andreopoulos *et al.*, Nucl. Instrum. Meth. **A614**, 87 (2010), arXiv:0905.2517 [hep-ph] .

[6] M. Honda, M. S. Athar, T. Kajita, K. Kasahara, and S. Midorikawa, Phys. Rev. D **92**, 023004 (2015).

[7] T. Thakore, A. Ghosh, S. Choubey, and A. Dighe, http://dx.doi.org/10.1007/JHEP05(2013)058 JHEP **1305**, 058 (2013), arXiv:1303.2534 [hep-ph] .

[8] M. M. Devi, T. Thakore, S. K. Agarwalla, and A. Dighe, http://dx.doi.org/10.1007/JHEP10(2014)189 JHEP **10**, 189 (2014), arXiv:1406.3689 [hep-ph] .

[9] K. Bhattacharya, A. K. Pal, G. Majumder, and N. K. Mondal, Comput. Phys. Commun. **185**, 3259 (2014).

[10] A. Chatterjee, K. Meghna, K. Rawat, T. Thakore, V. Bhatnagar, *et al.*, http://dx.doi.org/10.1088/1748-0221/9/07/P07001 JINST **9**, P07001 (2014), arXiv:1405.7243 [physics.ins-det] .

[11] S. Ahmed *et al.* (ICAL), (2015), arXiv:1505.07380 [physics.ins-det] .

[12] F. Reines and C. L. Cowan, Nature **178**, 446 (1956).

[13] H. Takei, *Measurement of Neutrino-Nucleon Neutral-Current Elastic Scattering Cross-section at SciBooNE*, http://lss.fnal.gov/cgi-bin/find_paper.pl?thesis-2009-19 Ph.D. thesis, Tokyo Inst. Tech. (2009).

[14] F. J. Hasert *et al.* (Gargamelle Neutrino), Nucl. Phys. **B73**, 1 (1974).

[15] A. Benvenuti *et al.*, Phys. Rev. Lett. **32**, 800 (1974).

[16] E. Perez and E. Rizvi, Rept. Prog. Phys. **76**, 046201 (2013), http://arxiv.org/abs/1208.1178 arXiv:1208.1178 [hep-ex] .

[17] F. Hasert *et al.* (Gargamelle Neutrino Collaboration), Phys.Lett. **B46**, 138 (1973).

[18] F. Hasert, H. Faissner, W. Krenz, J. Von Krogh, D. Lanske, *et al.*, http://dx.doi.org/10.1016/0370-2693(73)90494-2 Phys.Lett. **B46**, 121 (1973).

[19] S. F. King (2015) arXiv:1511.03831 [hep-ph] .

[20] B. Pontecorvo, Sov. Phys. JETP **7**, 172 (1958), [Zh. Eksp. Teor. Fiz.34,247(1957)].

[21] Z. Maki, M. Nakagawa, and S. Sakata, http://dx.doi.org/10.1143/PTP.28.870 Prog. Theor. Phys. **28**, 870 (1962).

[22] C. Giunti and C. W. Kim, *Fundamentals of Neutrino Physics and Astrophysics* (Oxford Univ. Press, Oxford, UK., 2007).

[23] D. I. Scully, *Neutrino Induced Coherent Pion Production*, Ph.D. thesis, Warwick U. (2013).

[24] R. Gandhi, P. Ghoshal, S. Goswami, P. Mehta, and S. U. Sankar, Phys. Rev. **D73**, 053001 (2006), arXiv:hep-ph/0411252 [hep-ph] .

[25] M. Blennow and A. Yu. Smirnov, Adv. High Energy Phys. **2013**, 972485 (2013), arXiv:1306.2903 [hep-ph] .

[26] L. Wolfenstein, Phys.Rev. **D17**, 2369 (1978).

[27] S. Mikheev and A. Y. Smirnov, Sov.J.Nucl.Phys. **42**, 913 (1985).

[28] C. Spiering, Eur. Phys. J. **H37**, 515 (2012), http://arxiv.org/abs/1207.4952 arXiv:1207.4952 [astro-ph.IM] .

[29] S. Weinberg, http://www-spires.fnal.gov/spires/find/books/www?cl=QC6.W431 *Gravitation and Cosmology* (John Wiley and Sons, New York, 1972).

[30] J. R. Davis, D. S. Harmer, and K. C. Hoffman, Phys. Rev. Lett. **20**, 1205 (1968).

[31] T. Araki *et al.*, Nature **436**, 499 (2005).

[32] G. Bellini *et al.* (Borexino), http://dx.doi.org/10.1016/j.physletb.2010.03.051 Phys. Lett. **B687**, 299 (2010), http://arxiv.org/abs/1003.0284 arXiv:1003.0284 [hep-ex] .

[33] V. S. Berezinsky, A. Z. Gazizov, G. T. Zatsepin, and I. L. Rozental, Sov. J. Nucl. Phys. **43**, 406 (1986), [Yad. Fiz.43,637(1986)].

[34] J. N. Bahcall, *NEUTRINO ASTROPHYSICS* (CAMBRIDGE, UK: UNIV. PR., 1989).

[35] J. N. Bahcall, A. M. Serenelli, and S. Basu, Astrophys. J. **621**, L85 (2005), http://arxiv.org/abs/astro-ph/0412440 arXiv:astro-ph/0412440 [astro-ph] .

[36] B. T. Cleveland, T. Daily, J. R. Davis, J. R. Distel, K. Lande, C. K. Lee, P. S. Wildenhain, and J. Ullman, Astrophys. J. **496**, 505 (1998).

[37] P. Anselmann *et al.* (GALLEX), http://dx.doi.org/10.1016/0370-2693(92)91521-A Phys. Lett. **B285**, 376 (1992).

[38] P. Anselmann *et al.* (GALLEX), http://dx.doi.org/10.1016/0370-2693(92)91522-B Phys. Lett. **B285**, 390 (1992).

[39] W. Hampel *et al.* (GALLEX), http://dx.doi.org/10.1016/S0370-2693(98)01579-2 Phys.Lett. **B447**, 127 (1999).

[40] A. I. Abazov *et al.*, Phys. Rev. Lett. **67**, 3332 (1991).

[41] J. Abdurashitov *et al.* (SAGE), http://dx.doi.org/10.1134/1.1506424 J.Exp.Theor.Phys. **95**, 181 (2002), http://arxiv.org/abs/astro-ph/0204245 arXiv:astro-ph/0204245 [astro-ph] .

[42] Y. Fukuda *et al.* (Super-Kamiokande), Phys.Rev.Lett. **81**, 1158 (1998), http://arxiv.org/abs/hep-ex/9805021 arXiv:hep-ex/9805021 [hep-ex] .

[43] Q. Ahmad *et al.* (SNO), Phys.Rev.Lett. **87**, 071301 (2001), http://arxiv.org/abs/nucl-ex/0106015 arXiv:nucl-ex/0106015 [nucl-ex] .

[44] T. Araki *et al.* (KamLAND), http://dx.doi.org/10.1103/PhysRevLett.94.081801 Phys.Rev.Lett. **94**, 081801 (2005), http://arxiv.org/abs/hep-ex/0406035 arXiv:hep-ex/0406035 [hep-ex] .

[45] K. Zuber, *Neutrino physics* (Boca Raton: USA: CRC Pr. 2004).

[46] D. Casper *et al.*, Phys. Rev. Lett. **66**, 2561 (1991).

[47] R. Becker-Szendy, C. Bratton, D. Casper, S. Dye, W. Gajewski, *et al.*, http://dx.doi.org/10.1103/PhysRevD.46.3720 Phys.Rev. **D46**, 3720 (1992).

[48] K. S. Hirata *et al.* (Kamiokande-II), *Proceedings: Workshop on Elementary Particle Picture of the Universe, 2nd, Tsukuba, Japan, Feb 4-6, 1988*, Phys. Lett. **B205**, 416 (1988), [,447(1988)].

[49] K. S. Hirata *et al.* (Kamiokande-II), http://dx.doi.org/10.1016/0370-2693(92)90788-6 Phys. Lett. **B280**, 146 (1992).

[50] M. Aglietta *et al.* (NUSEX), http://dx.doi.org/10.1209/0295-5075/8/7/005 Europhys. Lett. **8**, 611 (1989).

[51] K. Daum *et al.* (Frejus), Z. Phys. **C66**, 417 (1995).

[52] W. W. M. Allison *et al.* (Soudan-2), Phys. Lett. **B449**, 137 (1999), http://arxiv.org/abs/hep-ex/9901024 arXiv:hep-ex/9901024 [hep-ex] .

[53] W. W. M. Allison *et al.*, Phys. Lett. **B391**, 491 (1997), arXiv:hep-ex/9611007 [hep-ex] .

[54] Y. Fukuda *et al.* (Super-Kamiokande Collaboration), Phys.Rev.Lett. **81**, 1562 (1998), arXiv:hep-ex/9807003 [hep-ex] .

[55] Y. Ashie *et al.* (Super-Kamiokande), Phys. Rev. Lett. **93**, 101801 (2004), http://arxiv.org/abs/hep-ex/0404034 arXiv:hep-ex/0404034 [hep-ex] .

[56] M. Ambrosio *et al.* (MACRO), http://dx.doi.org/10.1016/S0370-2693(00)00267-7 Phys. Lett. **B478**, 5 (2000), http://arxiv.org/abs/hep-ex/0001044 arXiv:hep-ex/0001044 [hep-ex] .

[57] M. H. Ahn *et al.* (K2K), Phys. Rev. **D74**, 072003 (2006), arXiv:hep-ex/0606032 [hep-ex] .

[58] E. Aliu *et al.* (K2K), Phys. Rev. Lett. **94**, 081802 (2005), http://arxiv.org/abs/hep-ex/0411038 arXiv:hep-ex/0411038 [hep-ex] .

[59] D. Michael *et al.* (MINOS), http://dx.doi.org/10.1103/PhysRevLett.97.191801 Phys.Rev.Lett. **97**, 191801 (2006), http://arxiv.org/abs/hep-ex/0607088 arXiv:hep-ex/0607088 [hep-ex] .

[60] Y. Ashie *et al.* (Super-Kamiokande), Phys. Rev. **D71**, 112005 (2005), http://arxiv.org/abs/hep-ex/0501064 arXiv:hep-ex/0501064 [hep-ex] .

[61] C. K. Jung (K2K), *Weak interactions and neutrinos. Proceedings, 16th Workshop, WIN'97, Capri, Italy, June 22-28, 1997*, Nucl. Phys. Proc. Suppl. **66**, 415 (1998), [415(1998)].

[62] S. Amerio *et al.* (ICARUS), http://dx.doi.org/10.1016/j.nima.2004.02.044 Nucl. Instrum. Meth. **A527**, 329 (2004).

[63] M. Antonello *et al.* (ICARUS), http://dx.doi.org/10.1016/j.physletb.2012.05.033 Phys. Lett. **B713**, 17 (2012), http://arxiv.org/abs/1203.3433 arXiv:1203.3433 [hep-ex] .

[64] A. Di Crescenzo (OPERA), *Particle physics. Proceedings, 2nd International Conference in Memoriam Engin Arik and her Colleagues, Istanbul, Turkey, June 20-25, 2011*, J. Phys. Conf. Ser. **347**, 012009 (2012).

[65] A. Chukanov (OPERA), *Proceedings, 12th International Conference on Topics in Astroparticle and Underground Physics (TAUP 2011)*, http://dx.doi.org/10.1088/1742-6596/375/1/042074 J. Phys. Conf. Ser. **375**, 042074 (2012).

[66] K. Abe *et al.* (T2K), Phys. Rev. **D85**, 031103 (2012), http://arxiv.org/abs/1201.1386 arXiv:1201.1386 [hep-ex] .

[67] G. J. Feldman, J. Hartnell, and T. Kobayashi, http://dx.doi.org/10.1155/2013/475749 Adv. High Energy Phys. **2013**, 475749 (2013), http://arxiv.org/abs/1210.1778 arXiv:1210.1778 [hep-ex] .

[68] P. Adamson *et al.* (MINOS), http://dx.doi.org/10.1103/PhysRevLett.112.191801 Phys. Rev. Lett. **112**, 191801 (2014), http://arxiv.org/abs/1403.0867 arXiv:1403.0867 [hep-ex] .

[69] T. J. Weiler, (2013), http://arxiv.org/abs/1308.1715 arXiv:1308.1715 [hep-ph] .

[70] M. P. Decowski (KamLAND), *Particles and fields. Proceedings, Meeting of the Division of Particles and Fields of the Americal Physical Society, DPF 2004, Riverside, USA, August 26-31, 2004*, Int. J. Mod. Phys. **A20**, 3051 (2005).

[71] S. Abe *et al.* (KamLAND), Phys. Rev. Lett. **100**, 221803 (2008), arXiv:0801.4589 [hep-ex] .

[72] A. Gando *et al.* (KamLAND), http://dx.doi.org/10.1103/PhysRevD.83.052002 Phys. Rev. **D83**, 052002 (2011), arXiv:1009.4771 [hep-ex] .

[73] M. Apollonio *et al.* (CHOOZ), http://dx.doi.org/10.1016/S0370-2693(99)01072-2 Phys. Lett. **B466**, 415 (1999), http://arxiv.org/abs/hep-ex/9907037 arXiv:hep-ex/9907037 [hep-ex] .

[74] J. Wolf (Palo Verde), *Intersections of particle and nuclear physics. Proceedings, 7th Conference (CIPANP 2000), Quebec City, Quebec, Canada, 22-28 May 2000*, AIP Conf. Proc. **549**, 795 (2000), [,795(2000)].

[75] F. An *et al.* (Daya Bay), Phys.Rev.Lett. **112**, 061801 (2014), arXiv:1310.6732 [hep-ex] .

[76] J. Ahn *et al.* (RENO), Phys.Rev.Lett. **108**, 191802 (2012), arXiv:1204.0626 [hep-ex] .

[77] Y. Abe *et al.* (Double Chooz), http://dx.doi.org/10.1103/PhysRevD.86.052008 Phys. Rev. **D86**, 052008 (2012), http://arxiv.org/abs/1207.6632 arXiv:1207.6632 [hep-ex] .

[78] Y. Abe *et al.* (Double Chooz), http://dx.doi.org/10.1103/PhysRevLett.108.131801 Phys.Rev.Lett. **108**, 131801 (2012), http://arxiv.org/abs/1112.6353 arXiv:1112.6353 [hep-ex] .

[79] K. Abe *et al.* (T2K), Phys.Rev.Lett. **112**, 061802 (2014), http://arxiv.org/abs/1311.4750 arXiv:1311.4750 [hep-ex] .

[80] K. Abe *et al.* (T2K), Phys.Rev.Lett. **112**, 181801 (2014), http://arxiv.org/abs/1403.1532 arXiv:1403.1532 [hep-ex] .

[81] D. Forero, M. Tortola, and J. Valle, http://dx.doi.org/10.1103/PhysRevD.90.093006 Phys.Rev. **D90**, 093006 (2014), arXiv:1405.7540 [hep-ph] .

[82] D. Ayres *et al.* (NOvA), (2004), arXiv:hep-ex/0503053 [hep-ex] .

[83] M. S. Athar *et al.* (INO Collaboration), "India-based Neutrino Observatory: Project Report. Volume I." (2006).

[84] M. Aartsen *et al.* (IceCube PINGU), (2014), http://arxiv.org/abs/1401.2046 arXiv:1401.2046 [physics.ins-det] .

[85] K. Abe *et al.* (Hyper-Kamiokande Proto-Collaboration), PTEP (2015), http://arxiv.org/abs/1502.05199 arXiv:1502.05199 [hep-ex] .

[86] C. Adams *et al.* (LBNE), (2013), arXiv:1307.7335 [hep-ex] .

[87] F. An *et al.* (JUNO), (2015), arXiv:1507.05613 [physics.ins-det] .

[88] S.-H. S. Seo, `https://indico.cern.ch/event/356420/session/10/contribution/571/attachments/1130569/1615809/Seo_RENO_EPS2015.pdf` "New results from RENO and Future RENO-50, Talk delivered at EPS-HEP 2015, Vienna," (2015).

[89] P. Huber, M. Lindner, T. Schwetz, and W. Winter, http://dx.doi.org/10.1088/1126-6708/2009/11/044 JHEP **11**, 044 (2009), arXiv:0907.1896 [hep-ph] .

[90] S. Prakash, S. K. Raut, and S. U. Sankar, Phys. Rev. **D86**, 033012 (2012), arXiv:1201.6485 [hep-ph] .

[91] M. Sanchez, "Results and Prospects from the Nova experiment," `http://nova-docdb.fnal.gov/cgi-bin/RetrieveFile?docid=13893\&filename=nova-nufact-2015.pdf\&version=2` (2015).

[92] R. Cardarelli, G. Aielli, P. Camarri, A. Di Ciaccio, B. Liberti, *et al.*, http://dx.doi.org/10.1016/j.nima.2006.10.326 Nucl.Instrum.Meth. **A572**, 170 (2007).

[93] W. Riegler, C. Lippmann, and R. Veenhof, http://dx.doi.org/10.1016/S0168-9002(03)00337-1 Nucl.Instrum.Meth. **A500**, 144 (2003).

[94] C. Lippmann, *Detector Physics of Resistive Plate Chambers*, Ph.D. thesis.

[95] S. Behera, M. Bhatia, V. Datar, and A. Mohanty, (2014), arXiv:1406.3965 [physics.ins-det] .

[96] S. Dasgupta, N. K. Mondal, D. Samuel, M. N. Saraf, B. Satyanarayana, and S. S. Upadhya, *Proceedings, 11th Workshop on Resistive Plate Chambers and Related Detectors (RPC2012)*, PoS **RPC2012**, 068 (2012).

[97] B. Satyanarayana *et al.*, *Proceedings, 11th Workshop on Resistive Plate Chambers and Related Detectors (RPC2012)*, PoS **RPC2012**, 042 (2012).

[98] H. Gallagher, Y. Hayato, and J. Sobczyk, *Neutrino Flux Predictions for Cross Section Measurements*, AIP Conf. Proc. **1663**, 110004 (2015).

[99] Y. Hayato, `https://indico.fnal.gov/getFile.py/access?contribId=127\&sessionId=21\&resId=0\&materialId=paper\&confId=5361` .

[100] K. Hiraide *et al.* (SciBooNE), http://dx.doi.org/10.1103/PhysRevD.78.112004 Phys. Rev. **D78**, 112004 (2008), arXiv:0811.0369 [hep-ex] .

[101] A. Gazizov and M. P. Kowalski, Comput. Phys. Commun. **172**, 203 (2005), http://arxiv.org/abs/astro-ph/0406439 arXiv:astro-ph/0406439 [astro-ph] .

[102] O. Buss, T. Gaitanos, K. Gallmeister, H. van Hees, M. Kaskulov, O. Lalakulich, A. B. Larionov, T. Leitner, J. Weil, and U. Mosel, Phys. Rept. **512**, 1 (2012), http://arxiv.org/abs/1106.1344 arXiv:1106.1344 [hep-ph] .

[103] L. Alvarez-Ruso, T. Leitner, U. Mosel, and O. Buss, *Neutrino factories, superbeams, and betabeams. Proceedings, 12th International Workshop, NuFact10, Mumbai, India, October 20-25, 2010*, AIP Conf. Proc. **1382**, 170 (2011).

[104] D. Autiero, *Proceedings, 3rd International Workshop on Neutrino-nucleus interactions in the few GeV region (NUINT 04)*, Nucl. Phys. Proc. Suppl. **139**, 253 (2005), [,253(2005)].

[105] Y. Hayato, *Proceedings, 1st International Workshop on Neutrino-nucleus interactions in the few GeV region (NuInt 01)*, Nucl. Phys. Proc. Suppl. **112**, 171 (2002), [,171(2002)].

[106] G. Battistoni, A. Ferrari, T. Montaruli, and P. R. Sala, http://dx.doi.org/10.1016/S0927-6505(02)00246-3 Astropart. Phys. **19**, 269 (2003), [Erratum: Astropart. Phys.19,291(2003)], http://arxiv.org/abs/hep-ph/0207035 arXiv:hep-ph/0207035 [hep-ph] .

[107] G. Battistoni, P. R. Sala, M. Lantz, A. Ferrari, and G. Smirnov, *Neutrino interactions: From theory to Monte Carlo simulations. Proceedings, 45th Karpacz Winter School in Theoretical Physics, Ladek-Zdroj, Poland, February 2-11, 2009*, Acta Phys. Polon. **B40**, 2491 (2009).

[108] C. Juszczak, J. A. Nowak, and J. T. Sobczyk, *NuInt05, proceedings of the 4th International Workshop on Neutrino-Nucleus Interactions in the Few-GeV Region, Okayama, Japan, 26-29 September 2005*, Nucl. Phys. Proc. Suppl. **159**, 211 (2006), [,211(2005)], arXiv:hep-ph/0512365 [hep-ph] .

[109] F. Cavanna and O. Palamara, *Proceedings, 1st International Workshop on Neutrino-nucleus interactions in the few GeV region (NuInt 01)*, Nucl. Phys. Proc. Suppl. **112**, 183 (2002), [,183(2002)].

[110] H. Gallagher, *Proceedings, 1st International Workshop on Neutrino-nucleus inter-*

actions in the few GeV region (NuInt 01), Nucl. Phys. Proc. Suppl. **112**, 188 (2002), [,188(2002)].

[111] J. A. Nowak, C. Juszczak, and J. T. Sobczyk, *Proceedings, 3rd International Workshop on Neutrino-nucleus interactions in the few GeV region (NUINT 04)*, Nucl. Phys. Proc. Suppl. **139**, 272 (2005), [,272(2004)], http://arxiv.org/abs/nucl-th/0407065 arXiv:nucl-th/0407065 [nucl-th] .

[112] A. Jagannatam, http://citeseerx.ist.psu.edu/viewdoc/summary?doi=10.1.1.175.9735 .

[113] S. Agostinelli *et al.* (GEANT4), http://dx.doi.org/10.1016/S0168-9002(03)01368-8 Nucl. Instrum. Meth. **A506**, 250 (2003).

[114] R. Brun, F. Rademakers, and S. Panacek, http://root.cern.ch/ Conf.Proc. **C000917**, 11 (2000).

[115] A. Hocker, J. Stelzer, F. Tegenfeldt, H. Voss, K. Voss, *et al.*, PoS **ACAT**, 040 (2007), http://arxiv.org/abs/physics/0703039 arXiv:physics/0703039 [PHYSICS] .

[116] Y. Fukuda *et al.* (Super-Kamiokande Collaboration), Phys.Lett. **B436**, 33 (1998), arXiv:hep-ex/9805006 [hep-ex] .

[136] R. Gandhi, P. Ghoshal, S. Goswami, P. Mehta, S. U. Sankar, *et al.*, http://dx.doi.org/10.1103/PhysRevD.76.073012 Phys.Rev. **D76**, 073012 (2007), arXiv:0707.1723 [hep-ph] .

[118] M. M. Devi, A. Ghosh, D. Kaur, L. S. Mohan, S. Choubey, *et al.*, http://dx.doi.org/10.1088/1748-0221/8/11/P11003 JINST **8**, P11003 (2013), arXiv:1304.5115 [physics.ins-det] .

[119] D. Kaur, M. Naimuddin, and S. Kumar, (2014), http://arxiv.org/abs/1409.2231 arXiv:1409.2231 [hep-ex] .

[120] P. Migliozzi and F. Terranova, New J.Phys. **13**, 083016 (2011), http://arxiv.org/abs/1107.3018 arXiv:1107.3018 [hep-ex] .

[121] S. U. Sankar (INO Collaboration), Pramana **67**, 655 (2006).

[122] L. Landau, J.Phys.(USSR) **8**, 201 (1944).

[123] D. H. Wilkinson, Nucl.Instrum.Meth. **A383**, 513 (1996).

[124] N. van Eldik, P. Kluit, A. Poppleton, A. Salzburger, and S. Todorova, www.nikhef.nl/ s01/ElossTracking.ppt "Energy loss improvements and tracking," (2013).

[125] H. R. Gallagher, *Proceedings, 6th International Workshop on Neutrino-nucleus interactions in the few GeV region (NUINT 09)*, AIP Conf. Proc. **1189**, 35 (2009).

[126] T. Golan, J. T. Sobczyk, and J. Zmuda, *Proceedings, 24th International Conference on Neutrino physics and astrophysics (Neutrino 2010)*, Nucl. Phys. Proc. Suppl. **229-232**, 499 (2012).

[127] C. Juszczak, J. T. Sobczyk, and J. Zmuda, Phys. Rev. **C82**, 045502 (2010), http://arxiv.org/abs/1007.2195 arXiv:1007.2195 [nucl-th] .

[128] O. Lalakulich and U. Mosel, *Neutrino Flux Predictions for Cross Section Measurements*, AIP Conf. Proc. **1663**, 070007 (2015), arXiv:1304.2409 [nucl-th] .

[129] H. Gallagher, D. Casper, Y. Hayato, and P. Sala, *Proceedings, 3rd International Workshop on Neutrino-nucleus interactions in the few GeV region (NUINT 04)*, http://dx.doi.org/10.1016/j.nuclphysbps.2004.11.234 Nucl. Phys. Proc. Suppl. **139**, 278 (2005), [,278(2005)].

[130] H. R. Gallagher (Soudan 2), *Weak interactions and neutrinos. Proceedings, 16th Workshop, WIN'97, Capri, Italy, June 22-28, 1997*, Nucl. Phys. Proc. Suppl. **66**, 290 (1998), [,290(1998)].

[131] K. Abe *et al.* (T2K), Nucl. Instrum. Meth. **A659**, 106 (2011), arXiv:1106.1238 [physics.ins-det] .

[132] P. Lipari, Astropart. Phys. **14**, 171 (2000), http://arxiv.org/abs/hep-ph/0003013 arXiv:hep-ph/0003013 [hep-ph] .

[133] P. Bernardini, A. D'Amone, H. H. He, G. Mancarella, L. Perrone, and A. Surdo (ARGO-YBJ), in *Proceedings, 32nd International Cosmic Ray Conference (ICRC 2011)*, Vol. 1 (2011) pp. 86–89, arXiv:1110.0670 [astro-ph.IM] .

[134] G. Barr, in *Sub-dominant oscillation effects in atmospheric neutrino experiments, proceedings of the International Workshop on Sub-Dominant Oscillation Effects in Atmospheric Neutrino Experiments held on December 9-11, 2004, in Kashiwa, Japan* (2004) pp. 109–119.

[135] S. Petcov and T. Schwetz, Nucl.Phys. **B740**, 1 (2006), http://arxiv.org/abs/hep-ph/0511277 arXiv:hep-ph/0511277 [hep-ph] .

[136] R. Gandhi, P. Ghoshal, S. Goswami, P. Mehta, S. U. Sankar, *et al.*, http://dx.doi.org/10.1103/PhysRevD.76.073012 Phys.Rev. **D76**, 073012 (2007), arXiv:0707.1723 [hep-ph] .

[137] G. L. Fogli, E. Lisi, A. Marrone, and D. Montanino, http://dx.doi.org/10.1103/PhysRevD.67.093006 Phys. Rev. **D67**, 093006 (2003), http://arxiv.org/abs/hep-ph/0303064 arXiv:hep-ph/0303064 [hep-ph] .

[138] G. L. Fogli, E. Lisi, A. Marrone, D. Montanino, and A. Palazzo, Phys. Rev. **D66**, 053010 (2002), arXiv:hep-ph/0206162 [hep-ph] .

[139] M. C. Gonzalez-Garcia and M. Maltoni, Phys. Rev. **D70**, 033010 (2004), http://arxiv.org/abs/hep-ph/0404085 arXiv:hep-ph/0404085 [hep-ph] .